7-24-2018

Failure Diagnosis and Prognosis of Safety Critical Systems: Applications in Aerospace Industries

Mojtaba Kordestani
University of Windsor

Failure Diagnosis and Prognosis of Safety Critical Systems: Applications in Aerospace Industries

by

Mojtaba Kordestani

A Dissertation
Submitted to the Faculty of Graduate Studies through the
Department of Electrical and Computer Engineering in Partial Fulfillment
of the Requirements for the Degree of Doctor of Philosophy at the
University of Windsor

Windsor, Ontario, Canada
2018

Failure Diagnosis and Prognosis of Safety Critical Systems: Applications in Aerospace Industries

by

Mojtaba Kordestani

APPROVED BY:

B. Shafai, External Examiner
Northeastern University

L. Rueda
School of Computer Science

X. Chen
Department of Electrical and Computer Engineering

M. Ahmadi
Department of Electrical and Computer Engineering

M. Saif, Advisor
Department of Electrical and Computer Engineering

July 20, 2018

Declaration of Co-Authorship/ Previous Publications

I. Declaration of Co-Authorship

I hereby declare that this thesis incorporates material that is result of joint research, as follows:

Thesis Chapters	Details
Chapters 2, 4, 5 and 6	This research was supported by Thales Company of Canada under a joint Multi university project entitled Health monitoring, fault diagnosis, and prognosis with grant number DPHM702. Authors greatly appreciate Mr. Xavier Louis at Thales Company of Canada for his great technical support on this project. Furthermore, this thesis incorporates the outcome of a joint research project undertaken in collaboration with Dr. Khashayar Khorasani from Concordia University, Canada, Dr. M. Foad Samadi from University of Windsor, Canada, Dr. Roozbeh Razavi Far from University of Windsor, Canada, Dr. Marcos E. Orchard from University of Chile, Chile, and Dr. Amir Zang from Flinders University, Australia, under the supervision of Dr. Mehrdad Saif, from University of Windsor, Canada. In all cases, the author performed the key ideas, primary contributions and data analysis and interpretation, and the contribution of the co-authors was primarily through the provision of monitoring and manuscript structure checking.

I am aware of the University of Windsor Senate Policy on Authorship and I certify that I have

properly acknowledged the contribution of other researchers to my thesis, and have obtained written permission from each of the co-author(s) to include the above material(s) in my thesis.

I certify that, with the above qualification, this thesis, and the research to which it refers, is the product of my own work.

II. Declaration of Previous Publications

This thesis includes five original papers that have been previously published/submitted for publication in peer reviewed journals, as follows:

Thesis Chapters	Publication title	Publication status
Chapter 2	M. Kordestani, M. Saif, M. Orchard, R. Razavi.Far, K. Khorasani, Failure Prognosis and its Industrial Applications	to be submitted
Chapter 4	M. Kordestani, M. F. Samadi, M. Saif, K. Khorasani, A New Fault Diagnosis of Multifunctional Spoiler System Using Integrated Artificial Neural Network and Discrete Wavelet Transform methods, IEEE sensors journal. 2018	accepted and published
Chapter 4	M. Kordestani, M. F. Samadi, M. Saif, K. Khorasani, Fault Prognosis of MFS System Based on A Hybrid Approach Using Distributed Neural Networks and Adaptive Bayesian Algorithm	to be submitted
Chapter 5	M. Kordestani, A. Zand, M. Orchard, M. Saif, "A Modular Fault Diagnosis and Prognosis Method for Hydro-control Valve System based on Redundancy in Multi-Sensor Data Information"	to be submitted
Chapter 6	M. Kordestani, M. F. Samadi, M. Saif, K. Khorasani, "A New Fault Prognosis of MFS System Using Integrated Extended Kalman Filter and Bayesian Method", IEEE Transactions on Industrial Informatics. 2018	accepted and published

I certify that I have obtained a written permission from the copyright owner(s) to include the above published material(s) in my thesis. I certify that the above material describes work completed during

my registration as graduate student at the University of Windsor.

I declare that, to the best of my knowledge, my thesis does not infringe upon any ones copyright nor violate any proprietary rights and that any ideas, techniques, quotations, or any other material from the work of other people included in my thesis, published or otherwise, are fully acknowledged in accordance with the standard referencing practices. Furthermore, to the extent that I have included copyrighted material that surpasses the bounds of fair dealing within the meaning of the Canada Copyright Act, I certify that I have obtained a written permission from the copyright owner(s) to include such material(s) in my thesis.

I declare that this is a true copy of my thesis, including any final revisions, as approved by my thesis committee and the Graduate Studies office, and that this thesis has not been submitted for a higher degree to any other University or Institution.

Abstract

Many safety-critical systems such as aircraft, space crafts, and large power plants are required to operate in a reliable and efficient working condition without any performance degradation. As a result, fault diagnosis and prognosis (FDP) is a research topic of great interest in these systems.

FDP systems attempt to use historical and current data of a system, which are collected from various measurements to detect faults, diagnose the types of possible failures, predict and manage failures in advance.

This thesis deals with FDP of safety-critical systems. For this purpose, two critical systems including a multifunctional spoiler (MFS) and hydro-control value system are considered, and some challenging issues from the FDP are investigated. This research work consists of three general directions, i.e., monitoring, failure diagnosis, and prognosis. The proposed FDP methods are based on data-driven and model-based approaches.

The main aim of the data-driven methods is to utilize measurement data from the system and forecast the remaining useful life (RUL) of the faulty components accurately and efficiently. In this regard, two different methods are developed. A modular FDP method based on divide and conquer strategy is presented for MFS system. The modular structure contains three components:1) fault diagnosis unit, 2) failure parameter estimation unit and 3) RUL unit. The fault diagnosis unit identifies types of faults based on an integration of neural network (NN) method and discrete wavelet transform (DWT) technique. Failure parameter estimation unit observes the failure parameter via a distributed neural network. Afterward, the RUL of the system is predicted by an adaptive Bayesian method.

In another work, an innovative data-driven FDP method is developed for hydro-control valve systems. The idea is to use redundancy in multi-sensor data information and enhance the perfor-

mance of the FDP system. Therefore, a combination of a feature selection method and support vector machine (SVM) method is applied to select proper sensors for monitoring of the hydro-valve system and isolate types of fault. Then, adaptive neuro-fuzzy inference systems (ANFIS) method is used to estimate the failure path. Similarly, an online Bayesian algorithm is implemented for forecasting RUL.

Model-based methods employ high-fidelity physics-based model of a system for prognosis task. In this thesis, a novel model-based approach based on an integrated extended Kalman filter (EKF) and Bayesian method is introduced for the MFS system. To monitor the MFS system, a residual estimation method using EKF is performed to capture the progress of the failure. Later, a transformation is utilized to obtain a new measure to estimate degradation path (DP). Moreover, the recursive Bayesian algorithm is invoked to predict the RUL. Finally, relative accuracy (RA) measure is utilized to assess the performance of the proposed methods.

Keywords: Failure Diagnosis and Prognosis; Multifunctional spoilers; Hydro-control Valve System; Remaining Useful Life; Failure degradation.

Dedication

To my beloved wife,
who has been a constant source of support, encouragement, and inspiration.
And to my great parents,
who have blessed me with their endless love.

Acknowledgments

Praise and thanks to the beneficent God who with his boundless mercies has bestowed his favors upon me in each moment of my life. This thesis appears in its current form due to the assistance and guidance of several people. I would, therefore, like to offer my sincere thanks to all of them.

I wish to express my deepest sense of gratitude to Dr. Mehrdad Saif, for having dedicated to me his constant guidance, profound knowledge, and experience throughout my Ph.D. studies. I surely recognize that without his help and kind consideration, this work would never have come into existence. I cannot express my appreciation for his enthusiasm throughout my academic career at University of Windsor. I would also like to express my gratitude to the members of my supervisory and examination committee, Dr. Majid Ahmadi, Dr. Xiang Chen and Dr. Luis Rueda for agreeing to serve in the committee and sharing their comments to improve this work.

I much appreciate Mr. Xavier Louis at Thales Canada for his excellent technical support on this project. My sincere thanks also go to Dr. Khashayar Khorasani for sharing his immense knowledge. His guidance helped me during this research. It was particularly kind of him to allow me to have access to his research team at Concordia University. I would like to thank graduate students at Concordia University for their useful comments on this work. The efforts and insights provided by Dr. Esmaeil Naderi, Miss. Shen and Mr. Shahram Shahkar are particularly noted.

My sincere thanks also go to Dr. Marcos E. Orchard from University of Chile and Dr. Ali Akbar Safavi from Shiraz University for their continuous support during my research, for their motivation and open arms to share their knowledge. I would like to thank Dr. Foad Samadi from University of Windsor, Dr. Roozbeh Razavi Far from University of Windsor and Dr. Amir Zang from Flinders University, who as good friends, were always willing to help and give their best.

I would like to thank all my teachers and friends at University of Windsor for their invaluable

support during my graduate study.

I am genuinely thankful to my parents and my brother for all their love and encouragement. I saved the last spot for the person who deserves this degree as much as I do. I do not know how I could manage this without her. Vahideh, I thank you so much for everything.

Mojtaba Kordestani

July 2018

Contents

List of Figures

List of Tables

List of Abbreviations

AHSMM	Adaptive hidden semi-Markov model
ANFIS	Adaptive Neuro-fuzzy inference systems
AR	Autoregressive
ARMA	Auto-regressive moving average
ARIMA	Autoregressive integrated moving average
BIT	Built-In test
CBM	Condition-based maintenance
CM	Condition monitoring
CNC	Computer numerical control
DP	Degradation path
DWT	Discrete wavelet transform
EKF	Extended Kalman filter
EHSV	Electro-Hydraulic Servo Valves
EMD	Empirical mode decomposition
ETE	External test equipment
FD	Failure diagnosis
FDD	Fault detection and diagnosis
FDI	Fault detection and isolation
FDP	Failure diagnosis and prognosis
FL	Fuzzy logic
GPR	Gaussian process regression
HCV	Hydro-Control Valve
HMM	Hidden Markov model
HMS	Health management system

KF	Kalman filter
KM	Kaplan-Meier
LVDT	Linear variable displacement transducer
MFS	Multi functional spoiler
MLLR	Maximum likelihood linear regression
MLP	Multilayer perceptron
MSPO-SVM	Multi-scale parallel supported vector machine
NN	Neural network
PCU	Power control unit
PDF	Probability density function
PF	Particle filter
PHM	Prognostics and health management
PSO	Particle swarm optimization
RA	Relative accuracy
RBF	Radial basis function
RNN	Recurrent neural network
RUL	Remaining useful lifetime
RVR	Relevance vector regression
SCS	Spoiler control system
SECU	Spoiler electronic control unit
SoC	State of charge
SOV	Shut off valve
SVM	Support vector machine
TE	Tennessee Eastman
T-S	Takagi-Sugeno
TTF	Time-to-failure
UKF	Unscented kalman filter

List of Symbols

Symbols	Valves
K_v	$-1/8(mA^{-1})$
K_Q	$0.433(cis/mA) \pm 10\%$
K_{servo}	$160(mA/in)$
τ_{ehsv}	$4(msec)$
I_0	$-2 \pm 0.4(mA)$
$K_{boreext}$	$0.0848(cis/psi^{0.5})$
K_{annret}	$0.0803(cis/psi^{0.5})$
K_{annext}	$0.0833(cis/psi^{0.5})$
$K_{boreret}$	$0.0884(cis/psi^{0.5})$
V_{01}	$0.1532(in^3)$
V_{02}	$2.6429(in^3)$
A_{bore}	$2.214(in^2)$
A_{ann}	$1.7(in^2)$
β	$150(Kpsi)$
C_L	$0(cis/psi)$
K_{anti}	$1.5(cis/psi^{0.5})$
P_{CR}	$5 \pm 3(psid)$
M_P	$2.59 \times 10^{-3}(lb - sec^2/in)$
B_V	$10.18(lbf - sec/in)$
B_C	$50(lbf)$
K_{att}	$350(Klbf/in)$
J	$1.35(lbf - in - sec^2)$
B_S	$97.7(lbf - in - sec/rad)$
X_{Pmax}	$1.489 \pm 0.01(in)$

Chapter 1

Introduction

1.1 Thesis Motivation

Safety and reliability are vital issues for safety-critical systems. Fault diagnosis and prognosis (FDP) can significantly enhance the security of modern systems by isolating incipient faults and forecasting the future status of the faulty systems [12–14]. However, it is extremely hard or sometimes impossible to design an FDP system to predict an accurate behavior of the faulty systems due to complex nature of a fault or uncertainty inherited in the prediction horizon of the degradation failure.

Traditional approaches to maintenance such as corrective or preventive maintenance, which are based on a specific time schedule are conservative, and, thus they are not cost-efficient [15,16]. Furthermore, they cannot grantee safety of systems as a failure may occur between the maintenance time interval. In safety-critical systems, a real-time health management system (HMS) with detection, isolating and predicting capability of incipient failures is required [17].

Condition monitoring (CM) is a hot research area in critical infrastructures that watches processes and prevents catastrophic failures in systems. Built-in test (BIT)

and external test equipment (ETE) are two common CM techniques which are normally used for the task of fault detection and isolation (FDI). But, these techniques can only identify pre-defined and straightforward faults and may fail to recognize complicated faults or unknown faults due to the complexity of a system or multi-functionality of a fault [18].

The outcomes of the CM can be considered for condition-based maintenances (CBM) that usually save energy and reduce maintenance cost [19]. The CBM methodologies provide a higher level of reliability in comparison with traditional maintenance methods.

FDP as an essential step of CBM procedure is crucial and fundamental in successful CBM [20, 21]. The FDP information is utilized to settle a maintenance action. Besides, it is necessary to start maintenance immediately if the progress of failure grows sharply to a critical zone. Moreover, the FDP information can also be used in other sections such as performance monitoring, performance assessment, cost-benefit management, or even product recycling to earn more profit from systems [22].

Hence, monitoring, fault diagnosis, and failure prognosis play a significant role in the safe utilization of critical systems. In safety critical systems, isolating an incipient fault, and then, prediction of future behavior of faulty components has the highest priority for the system. In particular, it is required to know how much further the system can function with a proper response. Moreover, the accuracy of prediction is paramount in the optimal operation of the system. Therefore, as safety-critical systems grow in complexity, new FDP methods are needed to provide better reliability for systems.

Although there are lots of methods in the field of fault diagnosis, failure prognosis is a relatively new area of research that needs further development to deal with the safety demand of complex systems. The main objective of this thesis is to deepen the insight into the shortcomings and existing methods and also introduce new modern methods for health monitoring of safety-critical systems.

1.2 Thesis Objective

The primary research objective of this thesis is to introduce new FDP methods for safety-critical systems. For this aim, we investigate various monitoring, fault diagnosis, failure prognosis methods for health monitoring of systems to enhance current estimation, improve detectability, and increase the reliability of perdition of FDP systems. Notably, we focus on two popular FDP methodologies: 1) data-driven methods and 2) model-based methods.

1.2.1 Data-driven Methods

Data-driven methods invoke historical data and identify a black box model of systems without knowing detailed information about the mathematical model of system or degradation model of failure. In this research work, two significant industrial cases are investigated: 1) critical systems in which only a few limited sensors are available and 2) systems with multi-sensor with redundancy in measurements.

Developing data-driven FDP approach using a few measurements

We consider multifunctional spoiler (MFS) system that only has two measurements of linear variable displacement transducer (LVDT) sensor and control feedback signal available for monitoring goal. The MFS systems are control surfaces on wings of an aircraft and depending on how they are deployed change the direction of the aircraft and lead to rolling motions. As such, MFS systems are a critical part of aircraft and health monitoring of them are vital to ensure the safety of a flight. The MFS systems consist of several highly nonlinear systems with uncertainty in their structures which make monitoring task challenging, especially in case of only two measurements. In this research work, we propose a novel method via divide and conquer strategy to ease the computational complexity and improve the performance capability of FDP system. For this aim, the fault diagnosis and prognosis is split into three smaller tasks known as fault detection and diagnosis (FDD) task, failure parameter estimation

task, and remaining useful life (RUL) prediction task. An integrated methodology based on discrete wavelet transform and neural network is introduced to isolate types of failures. After identifying the failure type, a distributed system of three neural networks is developed to observe failure parameter of the MFS system. We show that the distributed structures of the networks help to improve the accuracy of estimation and lead to less error. Then, to perform RUL prediction task, an adaptive Bayesian method is developed to forecast the lifetime of the system from estimated failure parameter data. The proposed adaptive Bayesian method recursively takes the real-time data of estimated failure parameter and provides an accurate value for RUL of the system.

Developing data-driven FDP approach using a multi-sensor data information

In another research work, an innovative FDP method is developed for a hydro-control valve system. The hydro-control valve under study is a critical system of space launch vehicle propulsion systems, which is responsible for regulating the pressure in spacecraft. The structure of the valve includes four components which are nonlinear and sensitive. Hence, the complexity in construction makes the health monitoring difficult. A combination of feature selection and classification method is presented to select proper sensors and isolate types of failures in the system. For the feature selection, a pairwise incremental correlation method is considered. Then, the selected features are fitted as inputs into classifier block to classify the possible failure based on support vector machine (SVM). Similarly, a distributed system of ANFIS networks are considered to estimate failure parameter in the system. Finally, an adaptive Bayesian method is proposed to have an optimal prediction for RUL of the system. It is shown that the proper use of multi-sensor data enhances the capability of the suggested FDP system.

1.2.2 Model-based FDP approach using integrated EKF method and Bayesian algorithm

A novel FDP system based on EKF method and an adaptive Bayesian algorithm is considered using a high-fidelity model of MFS system. For this purpose, a residual estimation method via EKF method is developed to capture any nonlinearity in the failure dynamics. Then, a new measure called degradation path (DP) is introduced by a transformation formula to model the degradation patch. Finally, a recursive Bayesian algorithm is applied to the real data of the DP to predict the RUL of the system.

The proposed model-based structure improves the accuracy of the prediction and brings more reliability to the system. Moreover, the suggested failure prognosis cannot only forecast single type of failures, but also it can predict concurrent failures.

1.3 Thesis Organization

The remainder of this thesis is organized as follows. Chapter 2 illustrates definitions of the health monitoring system and provides a literature review of FDP methods. Safety-critical systems are demonstrated in Chapter 3. Then, the MFS system and hydro-control valve system are described as two popular safety-critical systems, and their mathematical models are given. Chapter 4 introduces a data-driven method based on divide and conquer for the MFS system. This FDP method is based on three significant tasks of fault diagnosis using data fusion method, failure estimation and remaining useful life prediction. An innovative data-driven method using redundancy in multi-sensor data information is developed in Chapter 5. It is shown that if redundant measurement data is accessible, they can be considered in fault diagnosis and failure estimation tasks and enhance the accuracy of classification and estimation. Chapter 6 introduces a novel model-based method for failure prognosis using a high fidelity model of the MFS system. Chapter 7 draws the conclusion of the thesis,

and it also glances over open problems and possible developments. Finally, a faulty mathematical model of the MFS system is given in Appendix A.

Chapter 2

Literature Review

Process condition monitoring (CM), fault diagnosis, and prognosis are essential capabilities in complex engineering systems with many benefits such as prevention of catastrophic failures, greater safety, and reliability, positive economic and environmental impacts, etc. A prominent benefit of a CM system is that the information obtained during the process can be used for condition-based maintenance (CBM), hence, reducing the operation and maintenance cost [23].

CBM and prognostic health management (PHM) systems always entail the following tasks: (a) fault detection, (b) fault isolation, (c) fault diagnosis, (d) predictive prognostic, (e) remaining useful life (RUL) estimation, (f) time-to-failure (TTF) predictions, (g) performance degradation, and (h) fault accommodation [24].

Diagnosis is defined as identification of characteristics of a fault including its occurrence, type, etc., whereas prognosis is the prediction of the future status of the faulty components and estimation of the remaining useful lifetime based on available information. The prognosis task allows predicting a state of damage in future, rather than diagnosing the current state of damage. It can be established by calculating the likelihood of failure as a function of future time with available information from

current and past times.

The information obtained by fault diagnosis and prognosis (FDP) may be used to monitor the system and to schedule a maintenance action. It may be necessary to start a maintenance program if degradation level reaches a critical safe operating zone [25, 26].

A proper FDP system needs accurate fault detection and diagnosis, suitable probabilistic models of the fault propagation, sufficient numbers of failure datasets. Therefore, different methods can be applied to a system based on available information. Undoubtedly, development of prognostic systems depends on the type of failure data [27].

Approaches to FDP can be divided into three main groups: 1) model-based, 2) data-driven, and 3) knowledge-based strategies. There are several works that review fault prognosis tasks [28,29]. Kan et al. [30] provide a review of prognosis methods for rotating machines in non-stationary condition. The general conditions with nonlinear models are considered, and challenges for design implementation are discussed. A literature review on prognosis methods is illustrated in [22] for statistical processes to forecast lifetime of systems. In another work, a review of design implementation of prognosis methods on machinery systems is discussed [31].

2.1 Model-based FDP methods

Model-based techniques for prognosis can be applied whenever a mathematical model of degradation is available. Obtaining model of failure requires specific knowledge about the system and its failure. This model is capable of incorporating a physical understanding of the monitored system into the design of a suitable prognosis system. Furthermore, in many cases, the parameters of the model, with the progress of failures can be employed to design a prognosis system [32–35].

After identifying a proper model, this model is considered to obtain a prediction of the future status of the faulty components and infers the remaining useful time of the system. The model-based methods result in the most precise prognosis system.

However, the challenge is that a mathematical model of a system or failure dynamic is not always available, and it is hard to obtain a proper mathematical model of failure in real time complex systems.

This group contains many methods such as Kalman filter (KF) [36], extended Kalman filter (EKF) [37], unscented Kalman filter (UKF) [38]), particle filter (PF) [39–42] and observer-based methods [43, 44].

Various types of Kalman filter such as KF, EKF, and UKF are considered for the task of prognosis. A new failure prognosis method based on EKF method is introduced in [45] for predicting RUL of bearings. They employ both experimental and computational approaches using multiple sensors to obtain a relationship between bearing current discharge events and bearing vibrations for forecasting the lifetime of bearings. Then, a model is identified based on exponential curve-fitting. Meanwhile, RUL of the bearing is recursively predicted by EKF method. The proposed method shows a satisfactory timing complexity and decent accuracy of the prognosis method over experimental data of the bearing system. A robust RUL prediction method based on constrained Kalman filter is introduced in [46] for noisy environments. The robust KF method imposes a set of inequality constraints to achieve the desired accuracy in prediction in presence of noise in the system. A model-based prognosis method via unscented Kalman filter is presented in [47]. The unscented Kalman filter assists to model nonlinear degradation path and reaches a lower computational complexity by calculating mean and variance of the nonlinear system. The RUL can be predicted by transforming the mean and covariance of the distribution into future. The proposed unscented Kalman filter is examined on a solenoid valve, and the RUL performance is accurate with lower computational complexity.

Particle filters are popular methods for determining RUL of systems. They can even be utilized in processes which are not Gaussian and have accurate estimation and prediction responses [48]. A model-based approach using particle filters is presented in [49] for predicting the RUL of the battery. For this aim, a state space of the cell is

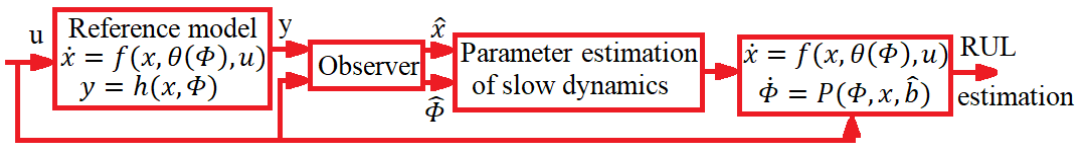

Figure 2.1: The proposed observer-based prognosis method. [1].

obtained by applying voltage and current of the system. Then, state-of-charge (SoC) of the battery is predicted by the particle filter using the state space model of the system. Finally, new risk management of battery failure is provided to evaluate the performance of the prognosis system. The proposed risk index indicates the risk of battery failure as well as a reliable measure which shows a confidence interval on prognosis algorithm. Similarly, Pola et. al. [50] developed a prognosis method using PF-based technique for predicting RUL of batteries. For estimation stage, a particle filter is developed. Then, a Markov Chain is applied to predict the RUL of the system. Experimental results using Li-Ion 26650 and two Li-Ion 18650 cells indicate a high performance of the proposed prognosis method. A new PF-based prognosis method is presented in [51]. First, multiple models of degradation system are obtained in the state space form. Then, particle filtering is utilized for estimation and prediction of RUL of the system. A partial Gibbs resample-move strategy along with a stratified sampling approach is also applied to reduce the computational complexity of the PF method. Moreover, the proposed multiple-phase modeling allows enhancing the accuracy of the prognosis system. Several numerical studies are examined to evaluate the prognosis system. Test results show high efficiency of the proposed particle filter method.

Observer-based methods are also considered for the task of prognosis. A new prognosis method using high gain observer is presented in [1] for prognosis of a battery. Figure 2.1 depicts the proposed observer-based prognosis method. It is noted from Figure 2.1 that the prognosis task is performed in three steps. In the first step, an unknown damage trajectory is estimated. Then, in the second step, a slowly varying

parameter of the system is observed using high gain observer. Finally, an RUL is predicted by Monte Carlo methodology, and a confidence interval is obtained. Test results on battery system show an excellent performance of the proposed prognosis method.

Model-based prognosis has been considered in different areas [52–54]. A model-based method using Kalman filter is considered in [55] to predict the RUL of tensioned steel. The main aim is to model the crack growth with Kalman filter. Then, this model is utilized to predict the likelihood and time of failure in the steel. As another example, in [39], a particle filter is utilized to predict the discharge time of lithium-ion batteries. They implement an empirical state-space model, inspired by battery's electrochemical model, and particle-filtering algorithms to estimate the state of charge (SoC) and other unknown model parameters in real-time. A state estimation and prediction method based on EKF is developed in [56]. They use a nonlinear stochastic model of fatigue crack dynamics and design a fault diagnosis and prognosis system to estimate the current damage state and also to predict the RUL at each sampling time. A model-based fault detection and prognosis is presented in [57] for a bearing system application. An EKF filter is considered to track the nonlinear bearing degradation model and to predict the RUL of the system. A prognosis method using a UKF and relevance vector regression (RVR) is developed in [58] to predict the RUL and short-term capacity of batteries. The RVR model is applied as a nonlinear time-series prediction model for the lithium-ion batteries. Then, the performance of the system is evaluated by the experimental data to prove its prediction accuracy. A model-based prognosis method based on particle filter is designed in [2]. Figure 2.2 depicts the proposed model-based prognosis method based on particle filter. The proposed model-based prognosis method involves two steps: First, a state-parameter estimation is developed for observation task. Second, state estimation is projected in future time to predict RUL, and End of Life (EOL) using particle filter.

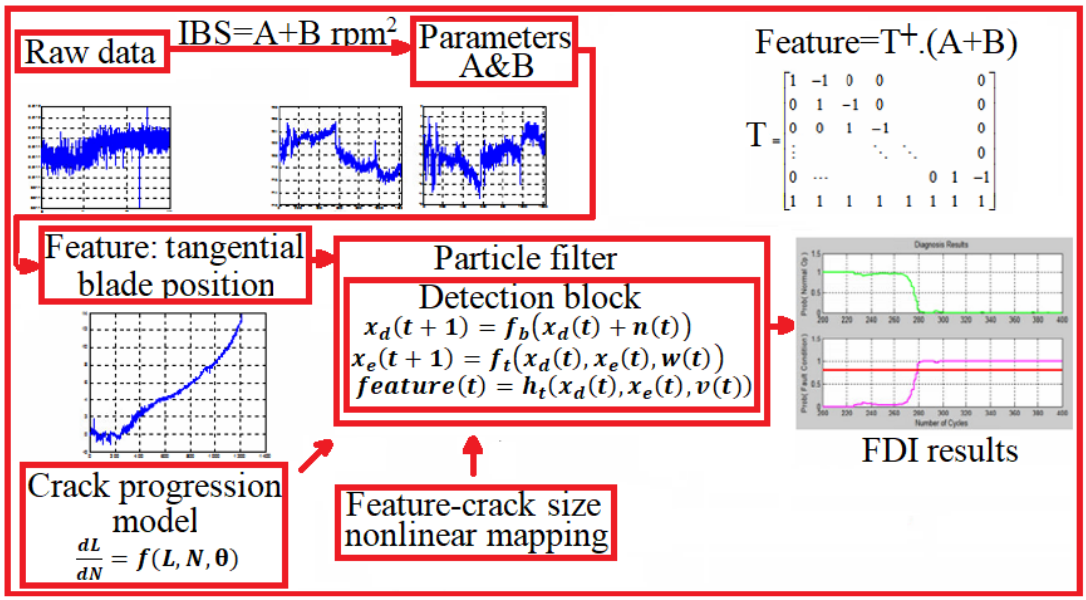

Figure 2.2: The proposed model-based prognosis method based on particle filter [2].

2.2 Data-driven methods

Data-driven methods are preferred in complex systems where a precise mathematical model is not available. The main advantage of data-driven methods is their capability to provide a mapping from high dimensional noisy data to lower dimensional information for prognosis decision. However, a significant amount of data over a wide range of operating region of the system must be provided to have a precise estimation and prediction. Moreover, some methods exist that do not apply the explicit model and utilize only process data of sensors. For instance, intelligent methods which are widely applied to prognosis task and have shown proper results in most cases.

Neural network (NN) [59–62], adaptive neuro-fuzzy inference system (ANFIS) [63–65], Markov model method [66], probability theory methods [67–69] and support vector machine (SVM) [70], regression methods [71–77] are some examples of data-driven methods. It should be noted that the accuracy of the methods relies on the historical data of the systems.

The RUL of the system can be predicted in data-driven methods by multivari-

ate pattern matching process from the data to the remaining life or via considering damage estimation followed by extrapolation to damage progression up to the failure threshold. It must be noted that the second approach requires to set up some rules for standard reasoning. The main aim is to produce an accurate prediction by considering various sources of uncertainty like process noise or measurement noise. It is noted that the uncertainty propagates in prediction horizon and creates a significant amount of uncertainty in long-term prediction, which must be addressed.

Regression-based methods have been used for the task of prognosis. An autoregressive (AR) method is developed in [78] for prediction of RUL of the lithium-ion batteries. To predict the RUL, degradation path is obtained by curve fitting and it is added to AR model to extend the AR model and forecast the lifetime of the batteries. An auto-regressive moving average (ARMA) model is presented in [79] for prediction of the RUL using historical data of the system. The ARMA method is then evaluated on an elevator door motion system. A data-driven prognosis system based on regression technique is developed in [80] for the aging problem of underground cable. First, useful features are selected which are four features of spikes. Afterwards, a regression method based on sliding window is utilized to predict the RUL of the cables. For this aim, the RUL is determined by forecasting the time for the cumulative effect of the features to reach a pre-set value known as a threshold. Field data set of current is considered which has been collected over three years from distributed power system in residential areas. The test results show a satisfactory performance of the suggested prognosis method.

Intelligent methods such as NN and ANFIS have been considered for the task of prognosis [81, 82]. The intelligent methods are powerful tools to model complex systems with high nonlinearity in their structures, where other methods may fail to provide a proper solution due to the complexity of the systems and lack of a precise mathematical model. A recurrent neural network (RNN) approach was introduced in [60] for machine condition monitoring. An appropriate clustering of input data is

used as preprocessing to enhance the accuracy of long-term prediction. Furthermore, the clustering helps the RNN system to better recognize the trend of degradation path. The RNN system with the suggested clustering shows a smaller error in comparison with common neural networks. An intelligent method using feedforward neural network is introduced in [83] for failure prognosis of pump vibration data. For this aim, a variation of KaplanMeier (KM) estimator and a degradation-based failure probability density function (PDF) is computed. Then, it is used as a training target for a feed-forward neural network. The test result using pump vibration data from Irving Pulp verifies the high performance of the prognosis method. A data-driven prognosis method is presented in [84] for bearing systems. For this aim, a neuro-fuzzy model is trained on the system failure. After this, to predict the RUL of the system, the PDF of the neuro-fuzzy residual between the system and predicted output is estimated and based on this residual, the neuro-fuzzy model is updated. Finally, the RUL is determined via Bayesian method. The experimental results from bearings of a gearbox of a helicopter are considered to validate the system. Test results indicate a high accuracy of the proposed method. A combination of empirical mode decomposition (EMD), particle swarm optimization (PSO) and support vector machine (SVM) methods is proposed in [85] for failure prognosis of an axial piston pump. The EMD method is considered to calculate the health state of the pump. Then, this health state is used to predict the RUL of the pump based on PSO and SVM methods. The parameters of SVM kernel is optimized using PSO method during the training phase. The test results show a high performance of the proposed method. Wavelet neural networks (wavenets) as intelligent methods have been also considered for fault prognosis [86]. A data-driven FDP method is introduced in [3] for an industrial chiller. The proposed FDP system includes a virtual sensor and a dynamic wavelet neural network. Figure 2.3 demonstrates the structure of the FDP system based on dynamic wavelet neural transform.

It is noted from Figure 2.3 that a wavelet neural network is used to diagnose the

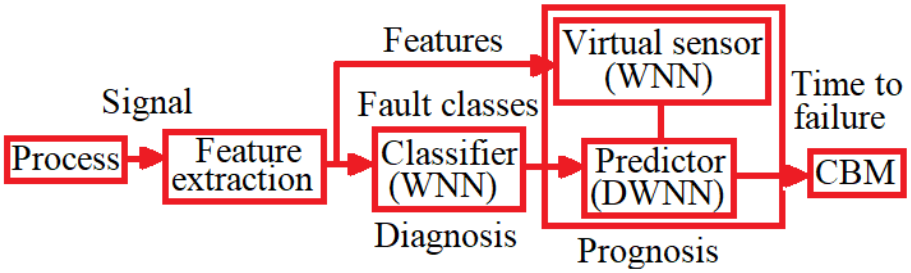

Figure 2.3: The structure of the FDP system based on dynamic wavelet neural transform [3].

type of fault. Then, virtual sensor is constructed using selected features to be used in a dynamic wavelet neural network and predict time to failure of the system.

Probability theory methods provide excellent prognosis techniques due to their suitable structures which are proper to be used for predicting RUL of systems. A prognosis method using PDF method is developed in [87]. For this aim, a state space model of the system is obtained by Markov method. Then, an algorithm is presented to calculate RUL of the system condition to some observations using a Bayesian algorithm. Simulation tests on two case studies of spring-mass system and a pneumatic valve system show a decent accuracy of the proposed prognosis method.

Markov model methods can construct an accurate model of failure using the available data. Therefore, they can be applied to prognosis methods. A new prognosis approach based on hidden Markov model (HMM) is developed in [88] for health monitoring in machinery systems. The proposed HMM method make an explicit relationship the hidden state values with actual health states to explore a model of failure path. Then, the model is used for parameter estimation and to predict the RUL of the system. To validate the performance of the proposed HMM method, several tests are performed using real data of a CNC (computer numerical control)-milling machine. Test results indicate a higher performance of the proposed method in comparison with ANN methods such as multilayer perceptron and Elman network. A new prognosis method using adaptive hidden semi-Markov model (AHSMM) is introduced in [4]. Figure 2.4 shows the proposed prognosis system using adaptive

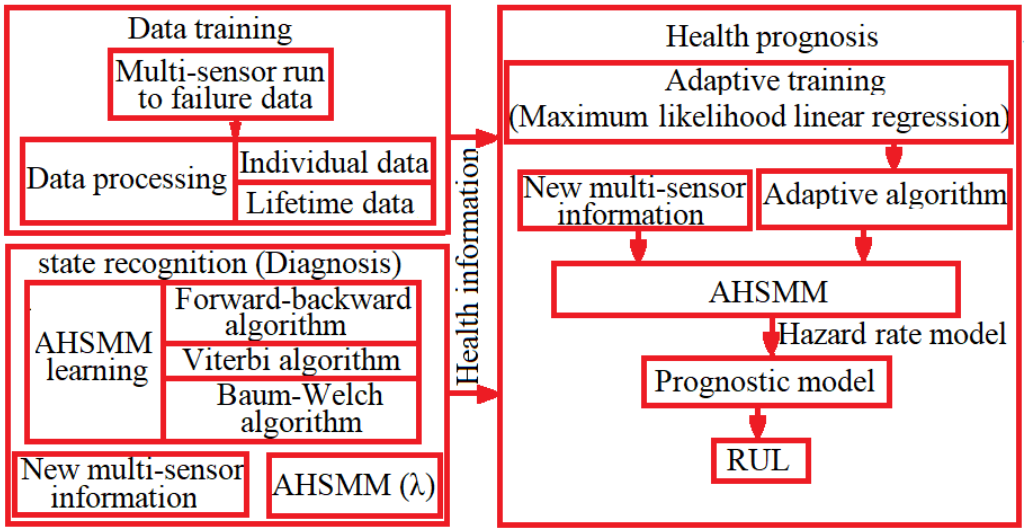

Figure 2.4: The proposed prognosis system using adaptive hidden semi-Markov model [4].

hidden semi-Markov model.

It is noted from Figure 2.4 that AHSMM algorithm is considered using multi-sensor information to reduce the computational complexity and to predict the RUL of the system. BaumWelch algorithm of AHSMM is applied. Meanwhile, maximum likelihood linear regression (MLLR) transformations technique is utilized to estimate all of the unknown parameters duration distributions. In fact, the AHSMM algorithm allows to model degradation path in the form of state space indirectly using measured data of multi-sensor array. Then, this recursive model is utilized to predict the RUL based on MLLR transformations technique. In test studies, the proposed method can accurately forecast the RUL of a hydraulic pump from Caterpillar Inc.

Data-driven methods in health monitoring have been considered for a variety of applications [89, 90]. An online prognosis method is developed in [5] for Tennessee Eastman (TE) process. For this aim, multi-scale parallel supported vector machine (MSPO-SVM) method is designed to predict the RUL of the system. Figure 2.5 shows the proposed online prognosis method.

The proposed online structure improves the prediction efficiency of the RUL method.

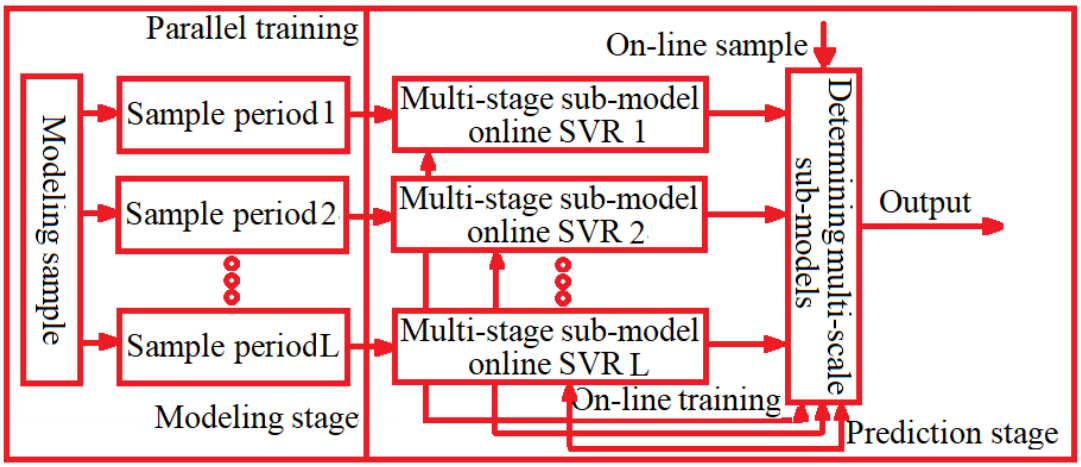

Figure 2.5: The proposed online prognosis method [5].

The experimental results on TE process show the accuracy of the technique. A data-driven fault prognosis is developed in [6] for bearings on one shaft driven by a motor and coupled by rub belts. Figure 2.6 presents the block diagram of the ANFIS prognosis method.

A variety of features are extracted by time domain and frequency domain and a mixture of time and frequency domain (wavelet transform) are used to build a rich dataset for prediction using ANFIS method. The method is implemented with Labview software on the motor. Experimental tests show a better result in comparison with RBF method for training and test of the prognosis method. A data-driven approach based on hidden Markov and grey models are presented in [91] to predict the RUL of pump systems. To obtain the hidden Markov model, features of the vibration signal are extracted via wavelet analysis. Afterwards, the wavelet coefficients are applied in the inputs of Markov model. Then, the hidden Markov method is extended using aging factor to predict the deterioration of the system. Simulation tests are performed by injecting clouds of dust in the pumps to be degraded during a period of time. Meanwhile, the proposed method forecast the lifetime of the system.

Unfortunately, often in practice, the sufficient data is scarce, especially for a complex system or newly designed system for which feedback data is non-existent [92].

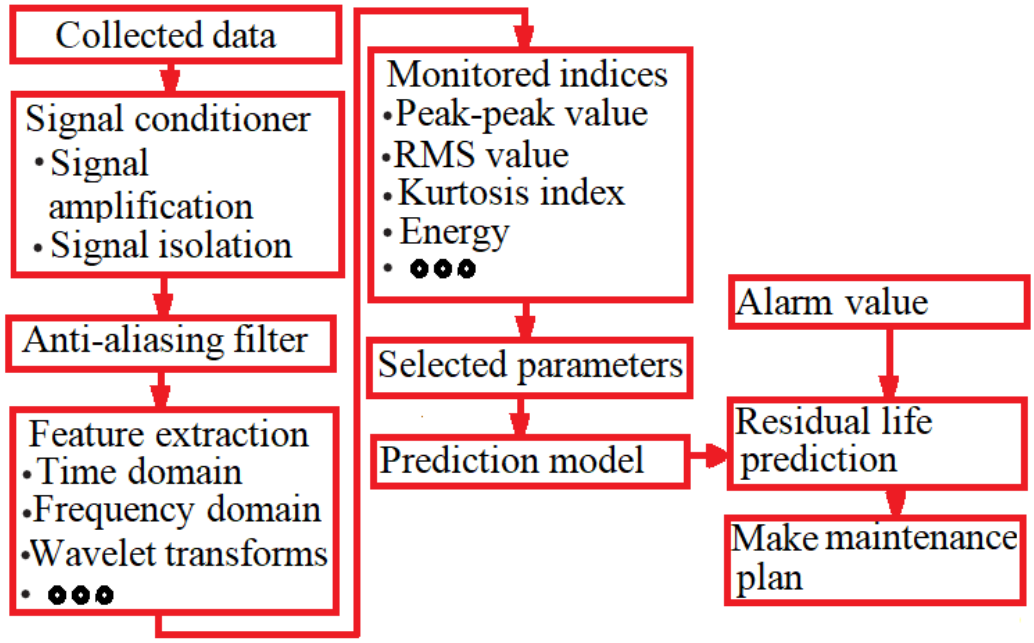

Figure 2.6: The block diagram of the ANFIS prognosis method [6].

2.3 Knowledge-based FDP methods

The knowledge-based methods can be implemented when adequate knowledge of experts are accessible. It covers a variety of methods such as fuzzy logic (FL) [93, 94], event-based methods using graph theory [95–97] and signal processing methods [98–100].

Signal processing techniques as powerful methodologies are also considered for the tasks of diagnosis and prognosis. Signal processing techniques enable analyzing signals in both time and frequency domains and enhance the accuracy of fault diagnosis. In the field of fault prognosis, although considering signal processing techniques are relatively new in comparison with fault diagnosis. However, it can lead to a more accurate prediction of the RUL by investigating the time and frequency domain properties of the faulty signal and including a precise severity of the failure [101]. Ibrahim et al. [102] present a new prognosis method using signal processing for fuel cell systems. For this aim, signals are decomposed by discrete wavelet transform

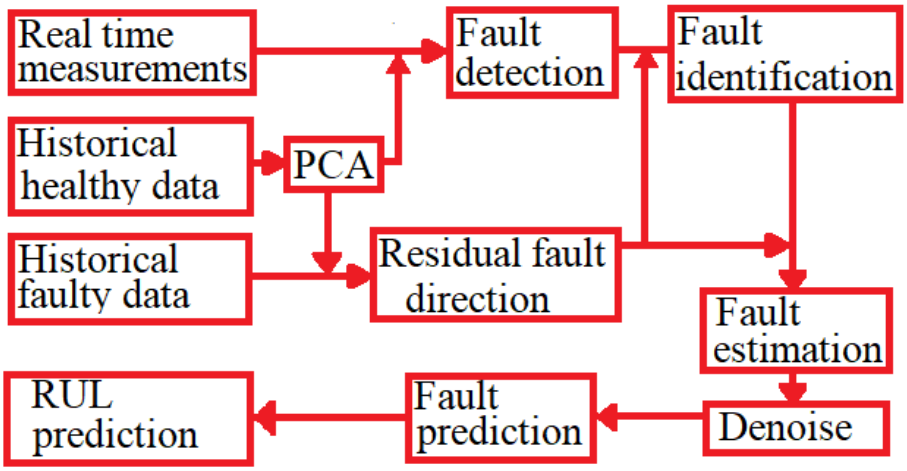

Figure 2.7: The data deriven prognosis method using signal processing method [7].

(DWT). Afterwards, appropriate coefficients are chosen to depict the original signal in a smaller number of observations. Meanwhile, the RUL of the system is predicted by well-known regression models such as autoregressive integrated moving average (ARIMA) and polynomial regression. The proposed signal processing based prognosis method provides a suitable analytical system which does not need a training part. Test results indicate an accuracy of less than 3% in prediction error for the RUL of the system. A new data-driven multivariate fault prognosis method is introduced in [7] for Tennessee Eastman process. Figure 2.7 demonstrate the proposed prognosis method based on signal processing technique. First, the magnitude of the faulty signal is reconstructed by DWT technique to de-noise the signals. Later, a vector auto-regressive (AR) model is obtained to forecast the RUL of the process.

Fuzzy logic methods as well-known knowledge-based methods are considered in prognosis system. A knowledge-based prognosis method is developed in [103]. If-then fuzzy rules are produced to isolate a fault. Then, prognosis task is performed by projecting the future status of the system using current and past values. Thumati et al. [104] develop a multiple model prognosis method based on fuzzy logic for a two-tank system. For this aim, they construct the model of the system using a class of Takagi-Sugeno (T-S) fuzzy systems. Afterwards, they design an observer to generate

the residual output. They show that the amount of this residual is proportional to the progress of the failure. Majidian and Saidi [105] develop a knowledge-based prognosis method via fuzzy logic to predict RUL of boiler reheater tubes. They set several rules with statistical properties of the wall thickness of the boiler such as minimum, initial, and the measured wall thickness to predict the lifetime of the boiler. Test results show a higher accuracy in comparison with an ANN method.

Finally, it is noted that rules defined by experts are easy to understand and results can be interpreted appropriately. However, for complex systems, obtaining a complete set of rules are hard. Notably, a failure can be caused by multiple factors. Therefore, identifying all roots of a failure sometimes are not possible. Thus, implementing knowledge-based methods are not straightforward.

Unfortunately, the knowledge of the experts are always expensive and may not be available. Therefore, developing a knowledge-based prognosis method may be very challenging, and only a few works are available in the literature.

Knowledge-based methods are widely combined with model-based and data-driven approaches to facilitate the design procedure of prognosis task and construct a hybrid structure for prognosis methods. In the following, hybrid methods for designing prognosis systems are discussed.

2.4 Hybrid methods

Several methods exist that apply a combination of model-based, data-driven and knowledge-based methods to predict RUL of systems [106–110]. Liao and Kottig [8] review hybrid methods for failure prognosis. Figure 2.8 illustrates possible hybrid methods using different combinations of prognosis tasks.

It is noted from Figure 2.8 that there are five categories for hybrid prognosis methods. For instance, H_4 prognosis method includes a combination of data-driven and model-based methods [8]. A hybrid FDP approach using a combination of knowledge-based and data-driven methods is introduced in [111] to predict RUL of a 3-tank pro-

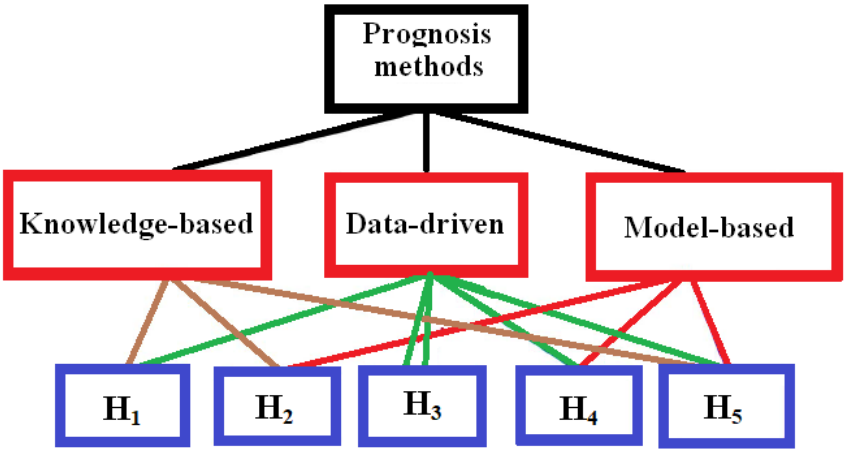

Figure 2.8: Possible hybrid methods using different combinations of prognosis tasks [8].

cess system. For this aim, a fuzzy logic system is produced based on expert knowledge to diagnose faults. Then, a dynamic wavelet neural network is developed to forecast RUL of the system.

Applying expert knowledge via fuzzy logic assists to predict the dynamics of failure in various operating conditions and results in decreasing uncertainty in the system and leads to an accurate RUL prediction. A hybrid FDP method using Kalman filter and fuzzy logic is introduced in [112] to predict a crack growth in tension steel bands. The Kalman filter is used for prediction, and fuzzy logic is considered to adjust failure threshold with respect to different operating conditions. An integrated multilayer perceptron (MLP) and radial basis function (RBF) neural networks is developed in [113] for the task of RUL forecasting. The suggested neural networks create a mapping from sensor measurements to state space. Then, a Kalman filter is applied to obtain RUL of the system.

An integration of model-based and data-driven methods are also common for constructing prognosis systems. A new hybrid prognosis method using particle filters and neural networks methods are developed in [114] for predicting the health condition of a gas turbine engine. In the suggested structure, the states and health parameters

of the system are estimated by particle filters. Meanwhile, neural networks are employed to determine the RUL of the system. The proposed neural network adaptively tracks nonergodic changes in profiles due to failure parameters. This observation is, then, considered in the particles filters to forecast the system states and health parameters. The proposed hybrid methodology allows choosing appropriate signatures that are suitable for predicting the RUL of the system based on hidden state/ parameters. The simulation study on the gas turbine indicates a high accuracy of the hybrid prognosis method. Liu et al. [115] introduce a combination of data-driven and model-based approaches for failure prognosis of lithium batteries. For this purpose, a particle filter is considered for state estimation. In addition to, a recurrent neural fuzzy model is applied to predict the future status of measurements and update the particle filter to obtain RUL of the system. A failure prognosis method based on a combination of ANFIS and high-order particle filtering is presented in [116] to track the time evolution of a crack in an epicyclic gear system. The method considers historical data of the gear system and develops hidden Markov model for the fault propagation process. Then, a particle filter is used to make a time prediction using this Markov model. The results indicate better performance in prediction accuracy compared to RNNs, or ANFIS.

Hybrid techniques can sometimes be developed by a combination of some data-driven methods (group H_3). This group is also known as ensemble methods. They can be constructed from a combination of estimations and predictions of a set of individual models. Each model is set in a region of parameter space. Then, they are integrated into a unique framework using a fusion methodology. It is noted that the performance of the ensemble methods is superior to that of the single individual methods. An ensemble data-driven prognosis method is developed in [117] to predict RUL of an electric cooling fan system. They integrate multiple algorithms using a weighted sum formula. Then, k-fold cross validation is utilized to obtain the weighting factors of summation. The experimental test results show a higher performance of

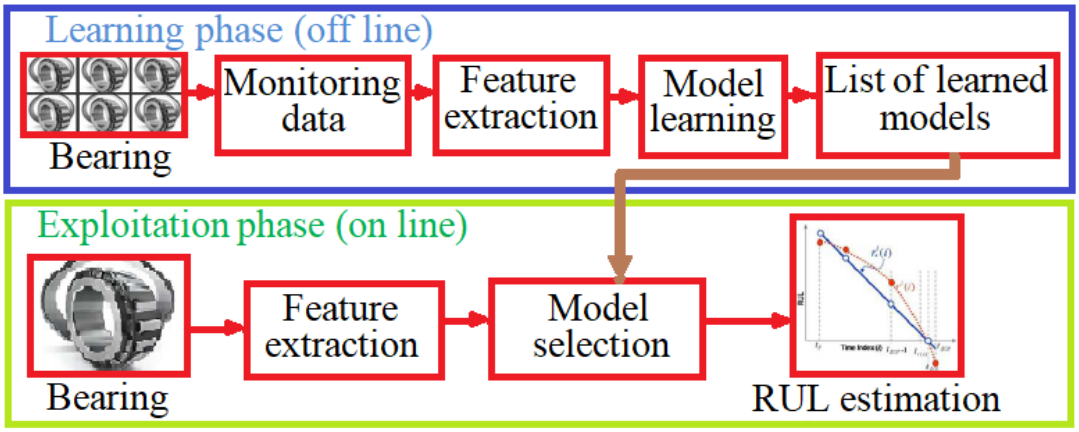

Figure 2.9: The procedure for predicting the RUL of the bearing [9].

the fusion method in comparison with other methods like SVM or RNN. A hybrid fault prognosis method using a mixture of Gaussians hidden Markov models and a Bayesian algorithm is introduced in [9] to predict the RUL of bearings. For this aim, the proper features of the monitoring data are extracted. Then, the mixture of Gaussian hidden Markov models is obtained by transforming extracted features to a relevant physical model of degradation failure path. Figure 2.9 explains the procedure for predicting the RUL of the bearing [9].

It is noted from Figure 2.9 that the prognosis method includes two phases: 1) a learning phase, and 2) an exploitation phase. During the learning phase, the parameters of the Gaussian hidden Markov models are trained. Then, in the second phase, the trained model of the Gaussian hidden Markov models are utilized to forecast the RUL of a new bearing. The performance of the prognosis method is verified by prognostic metrics like accuracy, precision, and prediction horizon, and test results show high efficiency of the prognosis method. A hybrid FDP method using a combination of the model-based and data-based method is introduced in [118] to predict RUL of a battery system. Firstly, a fault is identified by estimating the state of charge (SOC). Then, RUL of the battery is predicted by a Bayesian algorithm. Simulation test study is performed, and test results show a high performance of the proposed method.

2.5 FDP methods for safety-critical systems

Safety-critical systems (SCSs) such as aircraft or spacecraft often have several mechanical and electrical components that play a crucial role in the functionality of the entire system. Actuators are the most critical mechanical component of SCSs which are highly vulnerable to failure. The actuator failure could lead to total failure in SCSs.

There are only a few works available in the literature for fault prognosis of safety-critical systems [119, 120]. A linear regression prognosis method is presented in [121] for forecasting the RUL of an aircraft engine fuel pumping system. The regression method is easy to implement. However, this method may not be a proper option in noisy conditions or a time-varying system in which operating condition rapidly changes over time. In these conditions, the performance of the RUL predictor may decline in long-term prediction horizon. A fault prognosis method based on particle filters is presented in [122] to predict the degradation of fault for electromechanical actuators. They develop a particle filter for fault prognosis using a nonlinear mathematical model of the electromechanical actuator. A fault prognosis method is introduced for the electromechanical actuator system to determine the RUL of the actuator in aircraft [123]. For this purpose, an NN is considered to identify the fault in the system. Then, a regression method is utilized to predict the RUL of the system. A model-based prognosis method via Kalman filter is used in [124]. The model parameter of the system is constructed using regression method. Afterwards, the identified model is employed to develop a prognosis system. A prognosis method is presented in [125] for actuator system of aircraft. They develop a two-step approach to determine RUL of the system. At the first step, a particle filter is developed to monitor the system and diagnose any faults. Then, at the second step, the RUL is predicted by Monte Carlo simulation. A data-driven fault prognosis method is presented in [119] for the actuator of A/F-18 aircraft. The proposed data fusion method is a combination of neural network, along with fuzzy logic classifier and Kalman filter state

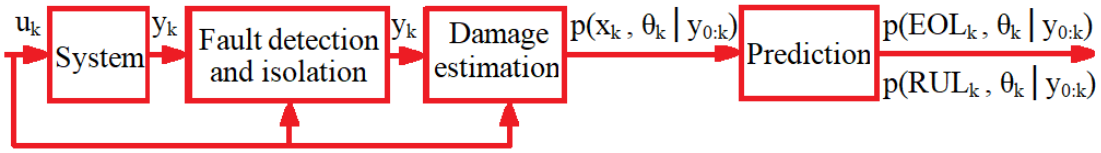

Figure 2.10: The proposed prognosis method based on unscented Kalman filter [10].

space predictor. The developed data fusion method is tested using electro-hydraulic servo valve data (EHSV), and results are very accurate. A model-based method using particle filters is introduced in [10] to predict the RUL of a pneumatic valve. Figure 2.10 explains the proposed prognosis method based on based on unscented Kalman filter.

The model of the system is obtained using a joint state-parameter estimation. Then, this state parameter is propagated in the future time to predict the RUL of the system. Simulation test results show the accuracy of the system under a limited number of sensors.

Chapter 3

Safety critical systems

3.1 Introduction

There has been a dramatic shift to monitoring and maintenance of safety-critical systems such as aircraft in recent years. Many complex engineering systems, including safety-critical systems, need to perform reliably, efficiently, safely and securely for extended periods of time without any interruption or degradation in their performance. As a result, FDP in complex systems is a critical area of study that has attracted much attention in recent years [13].

Safety-critical systems are vital systems whose malfunctions or failure may lead to, at least, one of the following catastrophes:

- Severe damage to the system
- Serious injury to people
- Environmental disaster

In this project, two safety-critical systems including a multifunctional spoiler (MFS) and hydro-control valve (HCV) systems are investigated in the following sec-

tions.

3.2 Multifunctional spoiler (MFS) system

This section briefly outlines the MFS system and its components. It also illustrates the mathematical model of the main components [126, 127].

3.2.1 Description of the MFS System

There is one MFS system per wing of the aircraft, and for each MFS, there is a hydraulically powered and electronically controlled power control unit (PCU) that actuates the surface of the MFS system. Finally, a spoiler electronic control unit (SECU) controls and monitors the operation of the MFS system. The MFS system consists of five main components which are highly nonlinear with uncertainty in their model parameters. Figure 3.1 shows the SECU and its components including the MFS systems and communication between the SECU and the MFS.

The MFS's PCU is a servo actuator and consists of the following components [126]:

1. Electro-Hydraulic Servo Valves (EHSV):

   The MFS actuator is controlled by the EHSV. It takes its commands from the SECU and constructs a control signal which is proportional to the command and finally applies the control signal to the actuator. The EHSV dynamics consists of a dead zone, a hysteresis, a first-order dynamic system, and saturation.

2. MFS actuator or power control unit (PCU):

   The actuator structure includes a cylinder and a piston. The actuator converts the hydraulic pressure in its input to the mechanical movement of its piston. It can be represented by a second-order nonlinear dynamic system for the movement of the piston plus two first order dynamic systems for the pressure equations. Furthermore, the impact of the aerodynamic on pressure is represented by a feedback path. It can be represented by a nonlinear static gain which is

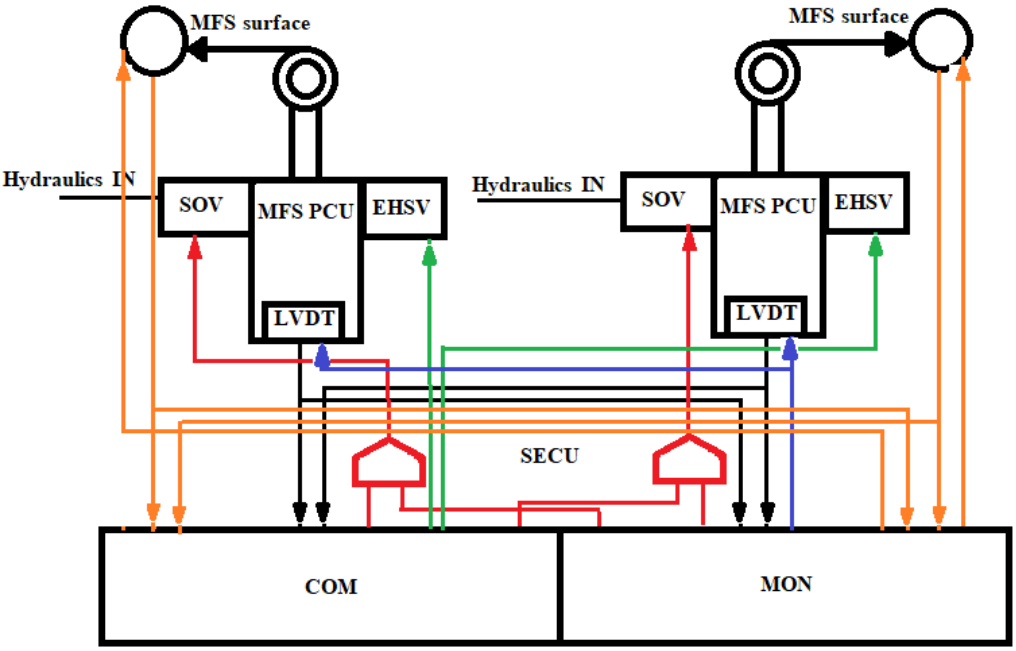

Figure 3.1: The SECU and the MFS system.

implemented by a look-up table. It should be noted that the actuator is driven by the EHSV.

3. Shut off valve (SOV):

   The SOV triggers the EHSV and allows the hydraulic pressure to reach the EHSV. The operation mechanism of the SOV can be modeled by an on/off valve which can be presented by a threshold, rate limiter and a relay. The SOV leads the hydraulic pressure to the EHSV and is activated by the SECU.

4. Linear variable displacement transducer (LVDT) sensor:

   The LVDT sensor is installed on the actuator, and it measures the linear piston position of the MFS.

5. Anti-cavitation check valve:

   The Anti-cavitation check valve is installed between the EHSV and the PCU actuator bore port to suck in the flow from return line in case of sudden assisted

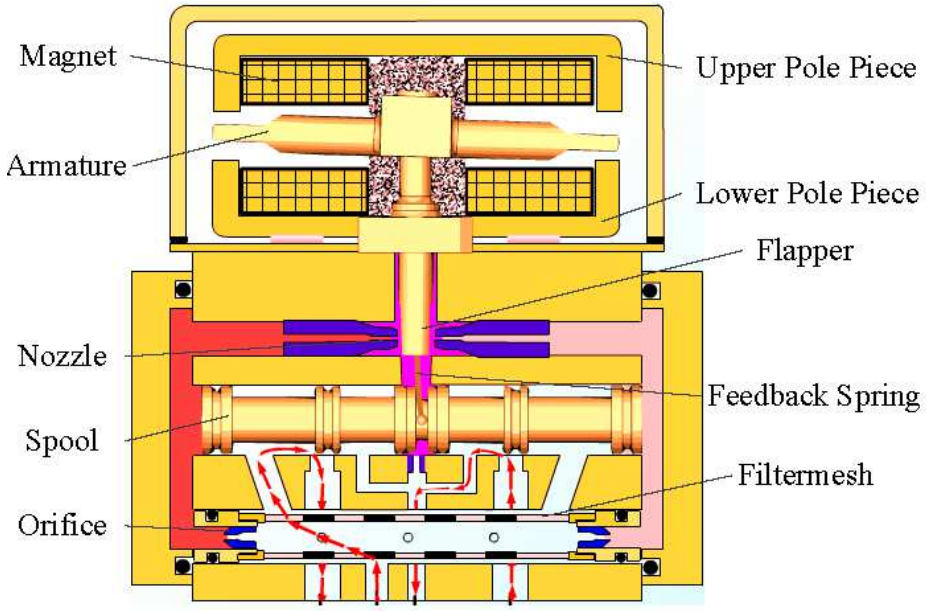

Figure 3.2: The internal diagram of the EHSV. [11].

movement of the actuator in the extended direction due to an aiding load.

3.2.2 Mathematical Modeling of the MFS

The mathematical model of the MFS system is provided in this subsection. Towards this, EHSV and PCU are modeled. The shut-off valve is considered to be always open, and thus, its dynamics are neglected. Sensor dynamics are also considered to be sufficiently fast and are ignored in the MFS model development [126].

EHSV Model

Figure 3.2 illustrates the internal diagram of the EHSV. A simple mathematical model of the EHSV can be formulated by a first-order dynamic system. The input of the system is the command current, I_{cmd}, and the position of the second spool is the output, X_v, as follows:

$$X_v = \frac{K_v}{s\tau_{ehsv} + 1}(I_{cmd} + I_0) \tag{3.1}$$

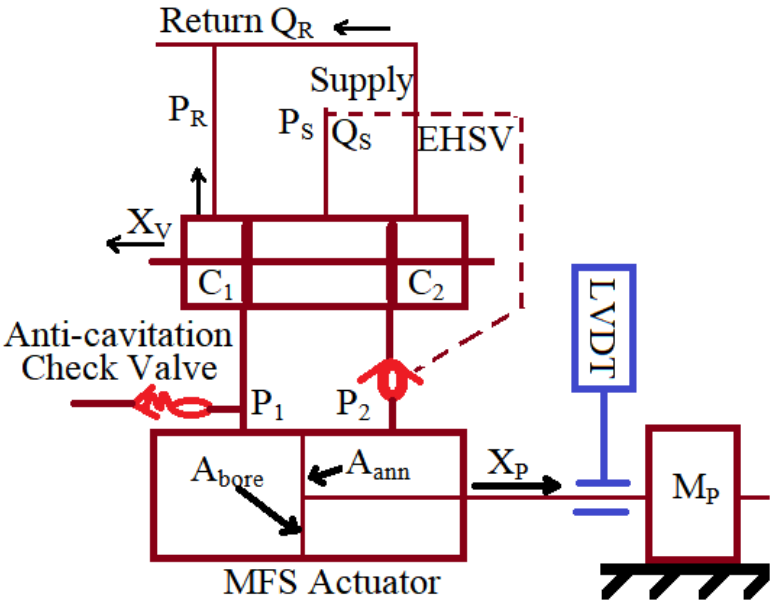

Figure 3.3: The PCU Block Diagram.

where K_v and I_0 are the EHSV gain and null bias current, respectively. Parameter τ_{ehsv} is the time constant. The second stage spool must have a bias to be able to retract. Thus, the flow is not null at zero current command. The value of the bias is about 0.25 of the maximum retraction flow. It is noted that SOV must be open to command the EHSV.

PCU Model

Figure 3.3 depicts the block diagram of the PCU. The EHSV is the element controlling piston actuation, by metering fluid to and from the actuator chamber in response to SECU electrical signals. The anti-extension check valve is pressure-operated and ensures that the surface remains in the retracted position in case of loss of hydraulic pressure, preventing surface upfloat. The valve is situated in the hydraulic cross-port to the actuator retraction chamber, between the EHSV and the cylinder chamber. The mathematical models of these parts are discussed in the following.

The flow in the oil gallery between EHSV and actuator bore side has a first order

dynamics as follows:

$$\frac{V_{01} + A_{bore}X_p}{\beta}\frac{dP_1}{dt} = Q_{C1} - A_{bore}\frac{dX_P}{dt} - C_L(P_1 - P_2) + Q_{ANTI} \tag{3.2}$$

where P_1 denotes the pressure between the extended gallery and bore chamber, and P_2 presents the pressure between the retract gallery and annulus chamber. Parameters A_{bore} and β denote the actuator bore area of the MFS and the oil bulk modulus, respectively. Parameter V_{01} is the oil volume of the extended (bore) chamber at the extended position. Therefore, $V_{01}+A_{bore}X_p$ is the extended chamber volume at piston position, X_p. Moreover, C_L is the leakage coefficient. Q_{C1} and Q_{ANTI} represent the EHSV flow in port C_1 and the flow in the anti-cavitation value, respectively. Their equations are written in the following:

$$Q_{C1} = -K_{boreretstdby}\sqrt{P_1 - P_{Rret}} \tag{3.3}$$

$$Q_{ANTI} = \begin{cases} 0, & P_R - P_1 \leq P_{CR} \\ K_{ANTI}\sqrt{P_R - P_1 - P_{CR}}, & P_R - P_1 > P_{CR} \end{cases} \tag{3.4}$$

Parameter $K_{boreretstdby}$ represents the nominal equivalent K factor at bore port in free retraction. Furthermore, K factor is related to the restriction property of the valve. The term P_{Rret} shows the return pressure whenever MFS retract. The value of P_{Rret} is nonlinear, and it requires to be calculated by interpolation equation. Parameter K_{ANTI} denotes the K factor of the anti-cavitation valve. The P_R and P_{CR} represent the return pressure and the cracking pressure of the anti-cavitation value, respectively.

In the same way, the flow of the oil gallery between EHSV and actuator annulus side can be determined by a first-order equation as follows:

$$\frac{V_{02} - A_{ann}X_p}{\beta}\frac{dP_2}{dt} = -Q_{C2} + A_{ann}\frac{dX_P}{dt} + C_L(P_1 - P_2) \tag{3.5}$$

where A_{ann} and V_{02} denote the actuator annulus area of the MFS and the oil volume of the retract (annulus) chamber at the retracted position, respectively. Therefore,

$V_{02} - A_{ann}X_p$ provides the retracted chamber volume at position X_p. It is noted that Q_{C2} is the EHSV flow in port C2 which can be computed as follows:

$$Q_{C1} = +K_{annretstdby}\sqrt{P_{Rret} - P_2} \tag{3.6}$$

The constant $K_{annretstdby}$ represents the nominal equivalent K factor at annulus port in free retraction. The piston dynamic is modeled as follows:

$$\begin{aligned} M_P\frac{d^2X_P}{dt^2} = &-B_V\frac{dX_P}{dt} - B_C sign(\frac{dX_P}{dt}) \\ &+ A_{bore}P_1 - A_{ann}P_2 - K_{ATT}(X_P - X_S) \end{aligned} \tag{3.7}$$

where variable X_P is piston position or system output. Constants B_V and B_C denote the viscous friction coefficient and the Coulomb friction coefficient, respectively. Parameter M_P presents the piston rod-end mass. Parameter K_{ATT} indicates the equivalent stiffness of the actuator which is in series with the rode-surface attachment. Furthermore, X_S is the linear surface displacement that can be provided as follows:

$$X_S = \theta_S r \tag{3.8}$$

where r can be given by a nonlinear function of θ_S which is computed as follows:

$$r = 8.888889 \times 10^{-9}\theta_S^2 + 1.091905 \times 10^{-2}\theta_S + 1.388057 \tag{3.9}$$

Finally, the MFS surface, θ_P, is a multi degree load system which is formulated by a second order spring mass damper system:

$$\frac{d^2\theta_P}{dt^2} = K_{ATT}(X_P - X_S)r = \frac{1}{J}(T_S - B_S\frac{d\theta_P}{dt} - T_L) \tag{3.10}$$

where J is the surface inertia of the actuator and B_S denotes the MFS structural damping coefficient. Furthermore, T_S is the input torque and T_L represents the aerodynamic moment.

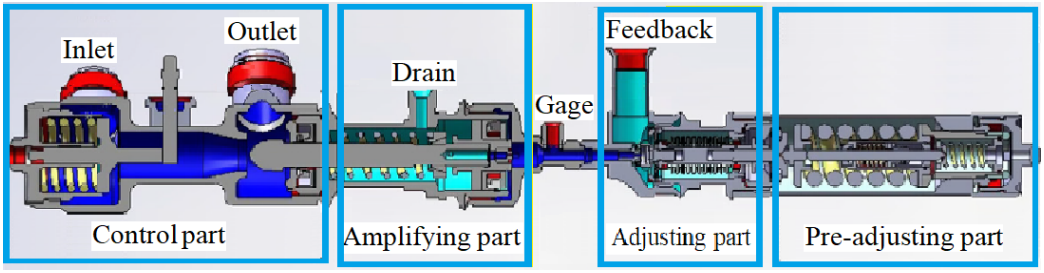

Figure 3.4: The HCV System.

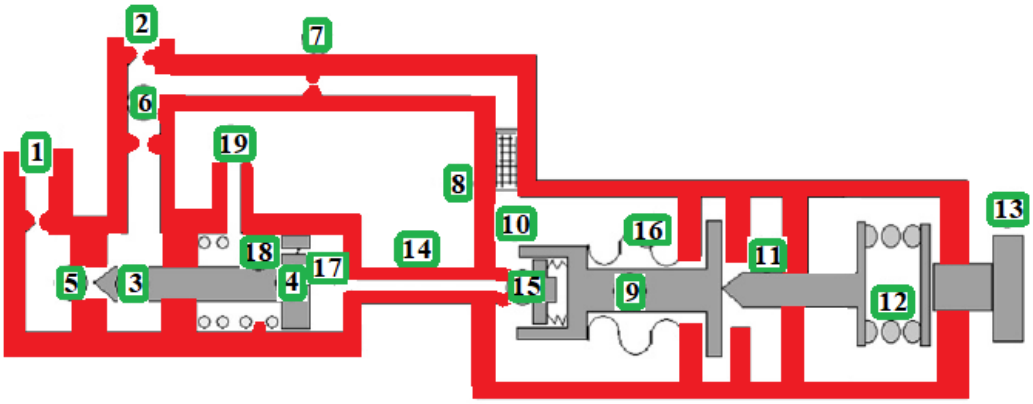

Figure 3.5: The HCV internal block diagram.

3.3 Hydro-Control Valve (HCV) System

This section illustrates the HCV system and its components. The HCV system considered in this research is used as a pressure regulator in the space launch vehicle propulsion system [128]. Figure 3.4 shows the HCV system.

It is noted from Figure 3.4 that the valve system has four main sections including control part, amplifying part, adjusting part, and pre-adjusting part. Figure 3.5 and Table 3.1 demonstrate the internal block diagram of the valve system and its components.

The control part consists of an inlet, control orifice, and outlet. This part regulates the pressure by altering the control orifice area. The amplifying part contains control piston, control subap, and drain pipe. The primary duty of the amplifying part is to strengthen the signal provided by the adjusting part. The adjusting part

Table 3.1: Components of the HCV system

numbers	components
1	Inlet
2	Outlet
3	Control subap
4	Control piston
5	Control orifice
6	Sense zone
7	Feedback pipe
8	Filter
9	Adjusting subap
10	Adjusting zone
11	Friction device
12	Adjusting spring
13	Adjusting screw
14	Connecting pipe
15	Adjusting orifice
16	Separation device
17	Piston front zone
18	Piston back zone
19	Drain pipe

includes feedback pipe, connecting pipe, filter, adjusting orifice, adjusting subap, and a separation device. The adjusting part is responsible for sensing the feedback signal and sending a command to amplifying part. The pre-adjusting part is composed of friction device, adjusting spring, and adjusting screw. This part is used to manually set the system via adjusting screw.

The valve system function is to maintain the outlet pressure at a desired value. To illustrate the mechanism of this process assume that the inlet pressure (1) is increasing (See Figure 3.5). This leads to an increase in the pressure of the sense zone (6), as continence of the pressure in the feedback pipe (7) and adjusting zone (10). Thus, the adjusting orifice (15) begins to open which forces piston in the amplifying part and leads to closing the control orifice (5). This process readjusts the sense zone (6) to go back to the previous value and regulates the outlet pressure.

Chapter 4

Data-driven FDP Method for an MFS System

4.1 Introduction

Development of FDP systems highly depends on the type of data, the data size, and accuracy. Therefore, different approaches can be considered with respect to system information and availability of the data. In this chapter, a novel data-driven FDP system is introduced for the MFS system.

The MFS systems consist of five main nonlinear components with uncertainty in their structures. Moreover, only two measurements including control feedback signal and LVDT sensor are available for monitoring purposes. Therefore, fault diagnosis and prognosis of these systems are very challenging due to these facts.

To overcome the above difficulties, this chapter introduces a novel modular design methodology for FDP of the MFS system. Assumptions for this research work are listed below:

1. The numbers of measurements are insufficient. Indeed, only LDVT sensor and

control feedback signal are accessible.

2. These measurements are very precise, and they are less affected by noise. Therefore, we add only 2% white noise to these measurements to mimic more realistic conditions.

3. Only one type of fault occurs in the system at a time period. The fault gradually grows in the system and finally leads to a complete failure.

The objective of this study is to isolate three significant faults consisting of null bias current, actuator leakage coefficient, and internal leakage in the MFS system. Then, the future statuses of faulty components are predicted. For this aim, first, three parallel blocks are developed to detect and isolate the mentioned faults. In each block, a new data fusion approach based on an integration of artificial neural network (ANN) and discrete wavelet transform methods are designed. Second, a parameter failure estimation unit is developed to estimate the failure parameter. Third, an RUL unit is constructed to predict the remaining useful life of the system using the estimated failure parameter via Bayesian theory. Finally, the relative accuracy is applied as a performance index to evaluate the efficiency of the proposed system.

In the next sections, the proposed FDP methods are illustrated. Then, design implementation and test results are explained. Finally, a summary of results is highlighted.

4.2 The proposed methods for the fault diagnosis and prognosis of the MFS

The proposed data-driven approach for fault diagnosis and prognosis (FDP) of the MFS is presented in this section. Figure 4.1 depicts the block diagram of the proposed FDP system.

It is noted from the Figure 4.1 that the proposed fault FDP system consists of three components including fault detection and diagnosis (FDD) unit, failure param-

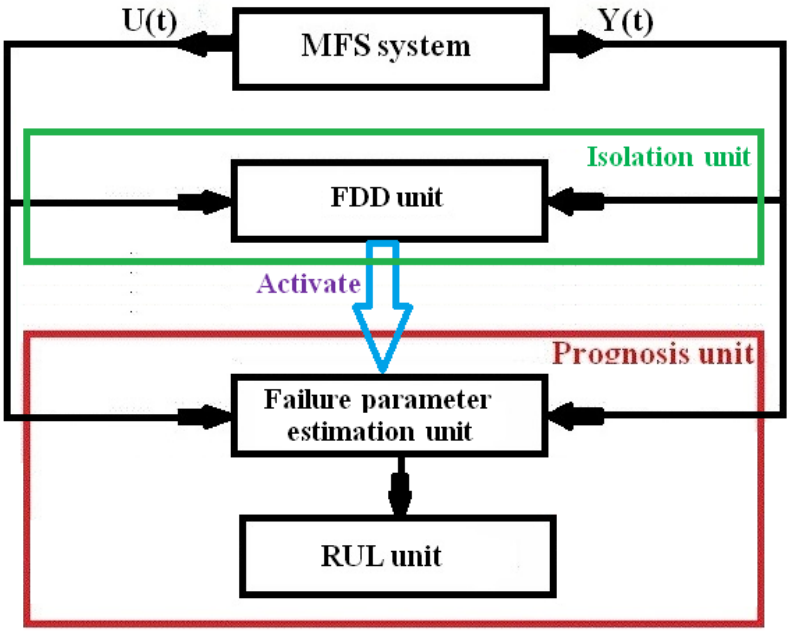

Figure 4.1: The structure of the proposed FDP system.

eter estimation unit, and remaining useful life (RUL) unit. The FDD unit identifies failure types, and then, activates the failure parameter estimation unit. The failure parameter is estimated in the failure parameter estimation unit based on FDD signal. Concurrently, the RUL unit forecasts the lifetime of the system with the estimated failure parameter. In the following, the MFS faults set of interest in this study is defined, and design procedures are introduced.

4.2.1 Faults set for the MFS system

Three types of faults can occur in the MFS which include mechanical faults, electrical faults, and sensor faults. However, electrical and sensor faults are instantaneous, and failure in them are fast and impossible to track [129]. Therefore, the mechanism of mechanical faults is only analyzed and studied in this thesis. A list of the MFS failures is collected in Table 4.1.

It is indicated that this list of failures consists of the posteriori effects which can be

Table 4.1: The MFS System Fault Types.

Failures parameter	Description
ΔI_0	Null current bias shift
ΔC_L	Actuator leakage coefficient degradation
ΔQ	Internal leakage

caused by one or more priori factors. For example, null bias current could represent either aging in the components or change in spring stiffness. It may cause smooth degradation of the PCU over time. Therefore, the null bias requires a new calibration. On the other hand, actuator leakage coefficient is created by the structure degradation of nozzle or flapper or even orifice [11]. Whenever actuator leakage coefficient failure occurs, it can lead to a fast deterioration in the PCU in a short period of time. Another failure is internal leakage which can occur due to effects such as wear on the spool corners.

Diagnosing of all a priori failures is prohibitively difficult to achieve since they can exhibit similar fault signatures where only a few measurements are available to observe the system. Furthermore, when a fault develops, it may lead to other faults which make it hard or impossible to recognize a priori main factors. In this study, three failures of EHSV null bias current (ΔI_0), actuator leakage coefficient (ΔC_L) and internal Leakage (ΔQ) in PCU which are the most common mechanical degradations in the MFS, have been considered.

4.2.2 The proposed data fusion method for the FDD unit

In this section, a parallel fusion structure is developed to identify the type of faults. Figure 4.2 shows the proposed fusion structure for the FDD unit.

It is indicated from Figure 4.2 that three parallel fusion blocks are constructed to isolate null bias current failure, actuator leakage coefficient and internal leakage, respectively. In each block, a fusion method based on a combination of the ANN and DWT methods is utilized to capture the failure dynamic type and identify the failure.

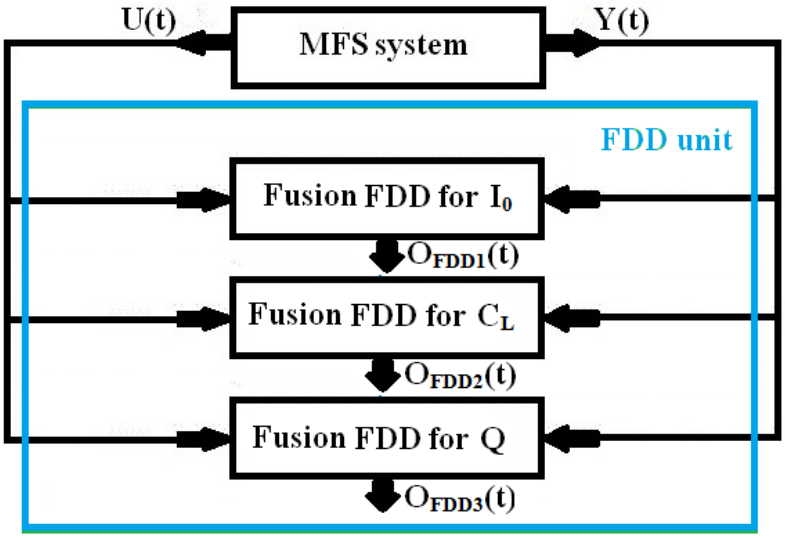

Figure 4.2: The structure of the proposed fusion FDD unit.

The methodologies are discussed in the following.

The discrete wavelet transform method

Wavelets are short-wave signals with localized properties in time and frequency [130]. Discrete wavelet transform (DWT) is a transformation which is constructed by discrete wavelets. The DWT has important advantages over Fourier transform which is its capability to capture both frequency and location information of the signal. Therefore, the DWT is a proper tool for fault diagnosis in industrial applications [131–133].

The DWT builds a signal with a combination of scaling functions and their wavelets at different locations (position) and scales (duration) [134]. Consider $f(t) \in L_2(R)$ as a signal which can be constructed by the linear combinations of orthogonal wavelets and their scaling functions as follows:

$$f(t) = \sum_{k=-\infty}^{+\infty} a_{0,k}\phi_{0,k}(t) + \sum_{m=-\infty}^{0}\sum_{k=-\infty}^{+\infty} d_{m,k}\psi_{m,k}(t) \tag{4.1}$$

$$\phi_{m,k}(t) = 2^{\frac{-m}{2}}\phi(2^{-m}t - k); m, k \in Z \tag{4.2}$$

$$\psi_{m,k}(t) = 2^{\frac{-m}{2}}\psi(2^{-m}t - k); m, k \in Z \tag{4.3}$$

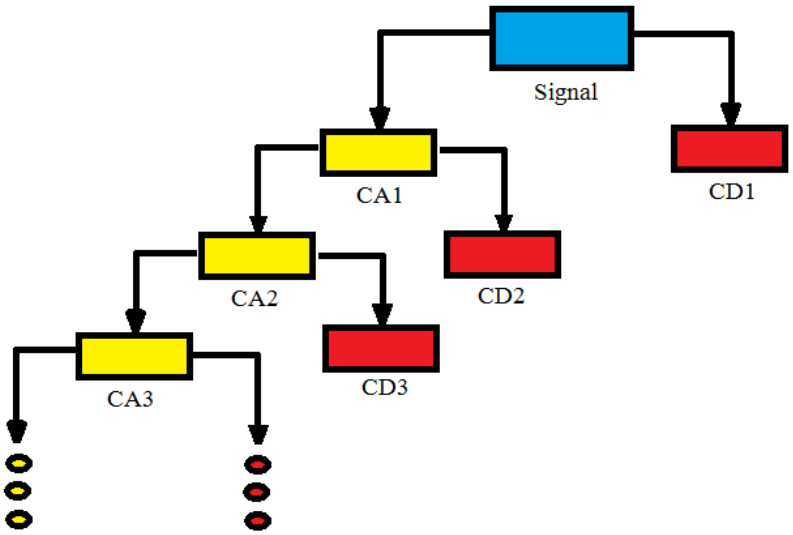

Figure 4.3: The block diagram of signal decomposition.

where $\phi(t)$ and $\psi(t)$ represent the scaling function and their orthogonal wavelets, respectively. In this project, Daubechies scaling functions and Daubechies wavelets are considered. Moreover, m and k indicate dilation and translation factors, respectively. The fraction $2^{\frac{-m}{2}}$ is utilized to provide a normalization. Sequence $a_{0,k}$ and $d_{m,k}$ can be calculated as follows:

$$a_{0,k} =< f, \phi_{0,k} > \tag{4.4}$$

$$d_{m,k} =< f, \psi_{m,k} > \tag{4.5}$$

The sequence $a_{0,k}$ and $d_{m,k}$ express the approximation and details coefficients of the signal at different levels and provide a decomposition of the signal. These coefficients are considered to identify a faulty signal. Figure 4.3 displays the block diagram of the decomposition of a signal.

$(CD_1, CD_2, \ldots, CD_m)$ in the Figure 4.3 are detail coefficients and (CA_m) is approximation coefficient at level m. If a fault occurs in the system, the magnitude of the detail coefficients will jump up at the time of faults. Thus, the type of the failure can be isolated by on-line analyzing of these coefficients.

The artificial neural network

Artificial neural network (ANN) is widely considered in fault diagnosis [135–138]. The ANN provides a significant computational power which is provided by the function of the nerve cells in the brain. Therefore, it is highly recommended for estimating complex non-linear functions. It constructs a mapping between input and output of a system through training of the system using available datasets [139]. The mathematical model of the ANN is provided in the following:

$$\begin{aligned} O_{NN_{I_0}}(t) &= NN_{I_0}(Y(t), U(t)) \\ O_{NN_{C_L}}(t) &= NN_{C_L}(Y(t), U(t)) \\ O_{NN_Q}(t) &= NN_Q(Y(t), U(t)) \end{aligned} \tag{4.6}$$

where NN_{I_0}, NN_{C_L} and NN_Q denote neural network FDD function for null bias current, actuator leakage and internal leakage failures, respectively. Variables $Y(t)$ and $U(t)$ symbolize LVDT sensor and control feedback signals, respectively. $O_{NN_{I_0}}(t)$, $O_{NN_{C_L}}(t)$ and $O_{NN_Q}(t)$ are outputs of the ANN for null bias current, actuator leakage and internal leakage, respectively.

The neural network FDD function uses a multilayer perceptron (MLP) in its structure which is usually a three-layer network including input, hidden and output layers. The inputs and outputs contain buffer and linear function. The hidden layer utilizes a nonlinear function like sigmoid. Various data sets at different operating points with healthy and faulty conditions are collected to train the system. The number of neurons in the hidden layer is set by trial and error. The output of the networks is set to 0 for healthy data and 1 for faulty data.

In the operating range conditions, any value of the output in a range of -0.5 to 0.9 is considered as a healthy condition where the range of $+0.9$ to $+1.5$ is assumed as a faulty situation, and any other value outside of -0.5 to $+1.5$ is supposed as an unknown failure. These values have been chosen by monitoring the system in various set points to minimize the false alarm rate. Moreover, to increase the reliability, the

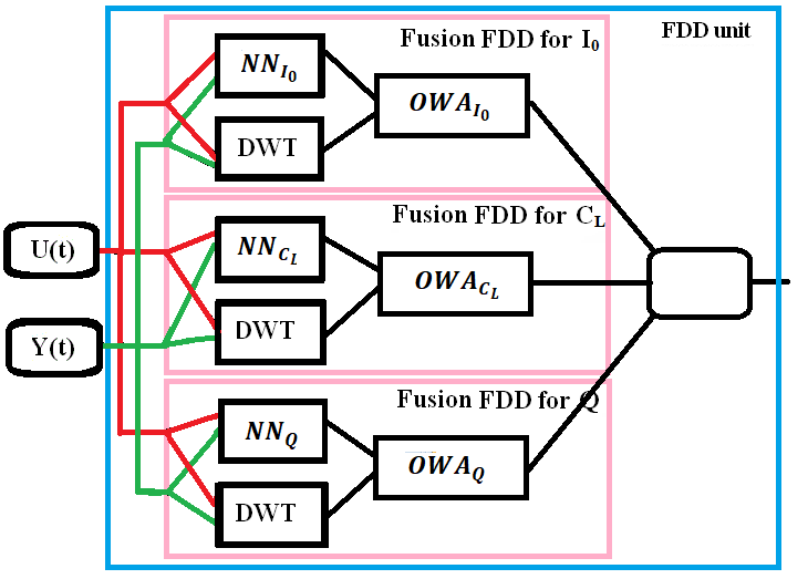

Figure 4.4: The internal diagram of the FDD unit based on fusion method.

same failure should occur ten times in a row to isolate that failure.

Fusion system based on ordered weighted averaging (OWA) operator

Data fusion method combines information from different sources to achieve a more precise decision with higher reliability due to complementariness existing in information resources. The fusion methodology are widely considered in fault diagnosis [140–143]. This chapter integrates the decision made by DWT and ANN methods with OWA operator. Figure 4.4 shows the internal diagram of the FDD unit based on fusion method.

It is indicated from the Figure 4.4 that three parallel blocks are built to identify failures in null bias, actuator leakage coefficient and internal leakage. In each block, a decision made by ANN and DWT methods are integrated into a unique framework using OWA approach. The OWA method provides a variety of operators like min, max, and average [144]. The OWA operator is considered as a tool in decision making, function approximation, and control [145, 146]. The fused outputs of the blocks are formulated as follows:

$$
\begin{aligned}
O_{OWA_{I_0}}(t) &= w_{NN,I_0} \times O_{NN_{I_0}}(t) + w_{DWT,I_0} \times O_{DWT}(t) \\
O_{OWA_{C_L}}(t) &= w_{NN,C_L} \times O_{NN_{C_L}}(t) + w_{DWT,C_L} \times O_{DWT}(t) \\
O_{OWA_Q}(t) &= w_{NN,Q} \times O_{NN_Q}(t) + w_{DWT,Q} \times O_{DWT}(t)
\end{aligned} \tag{4.7}
$$

subject to the following constraints:

$$
\begin{aligned}
w_{NN,I_0} + w_{DWT,I_0} &= 1 \\
w_{NN,C_L} + w_{DWT,C_L} &= 1 \\
w_{NN,Q} + w_{DWT,Q} &= 1
\end{aligned} \tag{4.8}
$$

where $O_{OWA_{I_0}}(t)$, $O_{OWA_{C_L}}(t)$ and $O_{OWA_Q}(t)$ are outputs of the OWA operator for null bias current, actuator leakage and internal leakage, respectively. $O_{DWT}(t)$ denotes the output of the DWT block. Moreover, w_{NN,I_0} and w_{DWT,I_0} are the weighting factors of the NN and DWA method for fusion FDD in null bias block. w_{NN,C_L} and w_{DWT,C_L} are the weighting factors of the NN and DWA methods for fusion FDD in the actuator leakage coefficient block. $w_{NN,Q}$ and $w_{DWT,Q}$ are the weighting factors of the NN and DWA methods for fusion FDD in internal leakage block. The main remaining task is how to obtain these weighting factors. They can be determined by optimizing the following cost function:

$$
Min \sum_{j=1}^{M} \left(W(o_1^j, \ldots, o_n^j) - T^j \right)^2 \tag{4.9}
$$

where W is a vector of weighting factors, o_j^i is the information of jth classifier at ith iteration and T^i is the ideal outcome for ith iteration.

4.2.3 Failure parameter estimation unit

This section develops a parameter estimation unit to observe the failure parameter. Figure 4.5 shows the proposed failure parameter estimation unit.

It should be noted from the Figure 4.5 that FDD unit identifies the failure type first, and then sends a signal to activate the corresponding failure parameter esti-

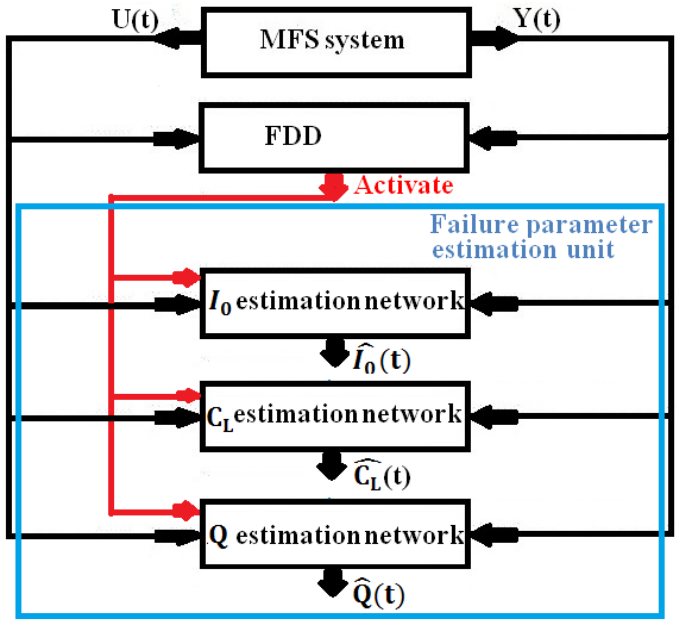

Figure 4.5: The proposed failure parameter estimation unit.

mation unit(s). If the FDD unit detects a failure but cannot isolate the failure to a specific type, the failure parameter estimation unit will not be activated. Therefore, in this condition, the FDD system can only identify an unknown failure and set up an warning alarm in the system.

The mathematical models of the failure parameters are formulated as follows:

$$\begin{aligned} \hat{I}_0(t) &= g_{I_0}(Y(t), U(t)) \\ \hat{C}_L(t) &= g_{C_L}(Y(t), U(t)) \\ \hat{Q}(t) &= g_Q(Y(t), U(t)) \end{aligned} \tag{4.10}$$

where $\hat{I}_0(t)$, $\hat{C}_L(t)$ and $\hat{Q}(t)$ are estimated null bias current, actuator leakage coefficient and internal leakage. g_{I_0}, g_{C_L} and g_Q are nonlinear function using MLP network for observing null bias current, actuator leakage coefficient and internal leakage. Like the NN FDD, the same datasets and procedures can be performed for the training and test of the failure parameter estimation unit. The only difference is that the output of the networks in this unit is set to failure parameter data.

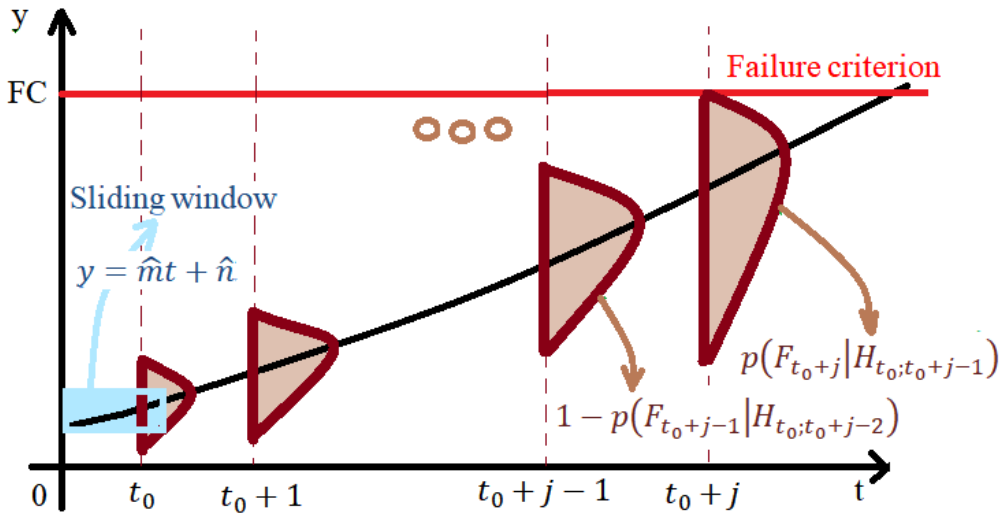

Figure 4.6: The proposed RUL method using Bayesian theory.

4.2.4 The remaining useful life (RUL) unit

The RUL is defined as the prediction of the remaining operational time of the faulty system before reaching a complete failure situation. The complete failure indicates the inability of the system to perform a given task [147]. The prognosis algorithm consists of two stages. The first stage includes the health monitoring of the system before a fault occurs. The second stage begins from the time when the fault has been isolated by the FDD to the time that system reaches the complete failure defined by an appropriately chosen criterion. The RUL is computed as the time difference between the predicted end of life, $t_{failure}$ and the time at which the prediction is made, $t_{prediction}$, as follows:

$$RUL = t_{failure} - t_{prediction} \tag{4.11}$$

To predict the RUL, a recursive Bayesian method is introduced in this research work. The proposed Bayesian algorithm is suitable to capture uncertainty in the system and predict the lifetime. Figure 4.6 illustrate the proposed RUL method using Bayesian theory.

It is indicted from Figure 4.6 that uncertainty propagates in the system and grows up with respect to prediction horizon, j. A sliding window is moved on the estimated parameter over time, and an optimal affine function of time is identified in the sliding window as follows:

$$y_t = \hat{m}t + \hat{n} + e_t \tag{4.12}$$

where $e_t \sim N(0, \sigma^2)$ denotes a Gaussian white noise error with zero mean and variance σ^2. Therefore, $y_{t_0} \sim N(\hat{m}t_0 + \hat{n}, \sigma^2)$. Furthermore, $\hat{y}_{t_0+j}$ is a j step ahead prediction with the following Gaussian distribution property:

$$\hat{y}_{t_0+j} \sim N(\hat{y_0} + mj, (j+1)\sigma^2) \tag{4.13}$$

Assume a failure model can be displayed by a non-stationary Bernoulli process [148]. Therefore, a sequence of process including healthy and faulty condition are assumed as follows:

$$\Omega_{failure} = \{H_{t_0}, H_{t_0+1}, \ldots, H_{t_0+j-1}, F_{t_0+j}\} \tag{4.14}$$

where $\Omega_{failure}$ is probability space which consists of a Bernoulli sequence. Variable H_t presents a healthy condition at time t and variable F_t denotes a complete failure at time t. Equation (4.14) implies that the sequence stays healthy until time $t_0 + j - 1$. A complete failure occurs at $t = t_0 + j$. The probability of failure at $t = t_0 + j$ can be formulated by a conditional probability as follows:

$$p(F_{t_0+j}) = \frac{p(F_{t_0+j}, H_{t_0:t_0+j-1})}{p(H_{t_0:t_0+j-1}|F_{t_0+j})} \tag{4.15}$$

where $p(F_{t_0+j})$ is probability of failure at $t = t_0 + j$. $p(F_{t_0+j}, H_{t_0:t_0+j-1})$ illustrates the probability of staying healthy until $t = t_0 + j - 1$ and failed at $t = t_0 + j$. $p(H_{t_0:t_0+j-1}|F_{t_0+j})$ denotes the probability of staying healthy conditional to a failure at $t = t_0+j$. It is noted that in real process, a failure occurs only one time. Therefore, $p(H_{t_0:t_0+j-1}|F_{t_0+j})$ is equal to *one*. Thus, Using joint probability formula, Equation 4.15 is rewritten as follows:

$$p(F_{t_0+j}) = p(F_{t_0+j}|H_{t_0:t_0+j-1})p(H_{t_0:t_0+j-1}) \tag{4.16}$$

where $p(H_{t_0:t_0+j-1})$ is probability of staying healthy until $t = t_0 + j - 1$. Probability $p(F_{t_0+j}|H_{t_0:t_0+j-1})$ is likelihood which is computed as follows:

$$\begin{aligned} p(F_{t_0+j}|H_{t_0:t_0+j-1}) &= p(y_{t_0+j} > FC) \\ &= Q(\frac{FC - [\hat{m}(t_0+j) + \hat{n}]}{\sigma\sqrt{j+1}}) \end{aligned} \tag{4.17}$$

where Q is the tail of the standard probability Gaussian distribution which is provided by probability Gaussian lookup table or can be coded in Matlab software. Moreover, FC is abbreviation of failure criterion.

Finally, function $p(H_{t_0:t_0+j-1})$ is determined by probability properties:

$$\begin{aligned} p(H_{t_0:t_0+j-1}) &= [1 - p(F_{t_0+1}|H_{t_0})] \times [1 - p(F_{t_0+2}|H_{t_0:t_0+2})] \\ &\cdots \times [1 - p(F_{t_0+j-1}|H_{t_0:t_0+j-2})] \end{aligned} \tag{4.18}$$

The failure probability, $p(F_{t_0+j}), j = 1 \ldots n$, is a monotonically increasing sequence until it reaches to a maximum. The maximum point is the RUL of the system.

4.3 Simulation Study & Results

In this section, simulation studies and results are demonstrated. For this aim, first, our proposed failure scenario is developed. Then, simulation studies and measured performances are illustrated, and test results are evaluated.

4.3.1 Fault scenarios

This thesis considers three failures of null bias, actuator leakage coefficient and internal leakage in the MFS system. Table 4.2 presents the healthy values and complete failure criteria for these failures.

It is noted that null bias current has a healthy value between $1.6mA$ to $2.4mA$. A failure is recognized if I_0 is out of this range, and the amount of $I_0 = 4.5mA$ is identified as the complete failure. This failure follows a slow degradation path from the start of the fault to complete failure. The actuator leakage coefficient and internal

Table 4.2: Healthy values and failure criteria

Failure parameter	Healthy value	Complete failure
I_0	$2 \pm 0.4(mA)$	$4.5(mA)$
C_L	$0(cis/psi)$	$2(cis/psi)$
Q	$0(cis/psi)$	$1(cis/psi)$

leakage take a value of $0(cis/psi)$ in healthy conditions, and they reach to complete failures in amounts of $1(cis/psi)$ and $2(cis/psi)$, respectively.

Moreover, to perform the failure studies, various ramp function with different slopes are injected into simulation models, and faulty data for the system are gathered.

4.3.2 Simulation studies and performance evaluation

The design criteria of the neural network FDD system and failure parameter NN system are considered. Second, discrete wavelet transform (DWT) design procedure will be discussed. Third, the fusion design criteria are investigated. Finally, an online performance index for the RUL prediction is introduced.

NN FDD system and failure parameter NN system

The system is operated in different operation conditions between $X_{p_{ref}} = 1$ and $X_{p_{ref}} = 1.45$ and different healthy datasets are gathered. Moreover, many failures with ramp functions are injected into the model, and faulty dataset is obtained. Then, the whole datasets are divided into two groups of training and test data. Levenberg Marquardt method [149] is considered for the training of the system and mean square error (MSE) is used for the evaluation of the networks. Table 4.3 presents the MSE measure for the training and test phases.

It is noted from the Table 4.3 that the NN FDD for the C_L provides the best performance with the lowest MSE while NN parameter estimation system for Q has the lowest MSE.

Table 4.3: The performance of the networks based on MSE evaluation.

Network	Training (MSE)	Test (MSE)
NN FDD for I_0	0.1375	0.2178
NN FDD for C_L	0.0335	0.0396
NN FDD for Q	0.0890	0.0949
I_0 estimation network	0.0274	0.0289
C_L estimation network	0.0473	0.0492
Q estimation network	0.0181	0.0184

Table 4.4: The performance evaluation for testing neural network FDD method.

Failure	isolated as I_0	isolated as C_L	isolated as Q	isolated as unknown
Failure in I_0	69%	18%	0	13%
Failure in C_L	6%	83%	0	11%
Failure in Q	0	0	86%	14%

Furthermore, several tests were carried out to evaluate the accuracy of the system for different failures. Table 4.4 illustrates the results of the isolation test.

It is indicated from the Table 4.4 that the NN FDD method isolates the null bias failure in 69% of occasions correctly. However, 18% of the null bias failure is misclassified as actuator leakage failure and 13% of the null bias failure is identified as an unknown failure. Similar rates for the actuator leakage and the internal leakage are higher indicating better classification of those faults. It is noted that the isolation rates obtained the proposed neural network are not sufficiently high. In the following subsections, the fusion method using OWA operator is applied to enhance the accuracy of the fault isolation.

The DWT design procedure

Detail coefficients in discrete wavelet transform are used to identify the failure. The detail coefficients show rapid changes upon occurrence of the faulty signal and thus can be exploited to detect the faults. To analyze the behavior of failure by the DWT

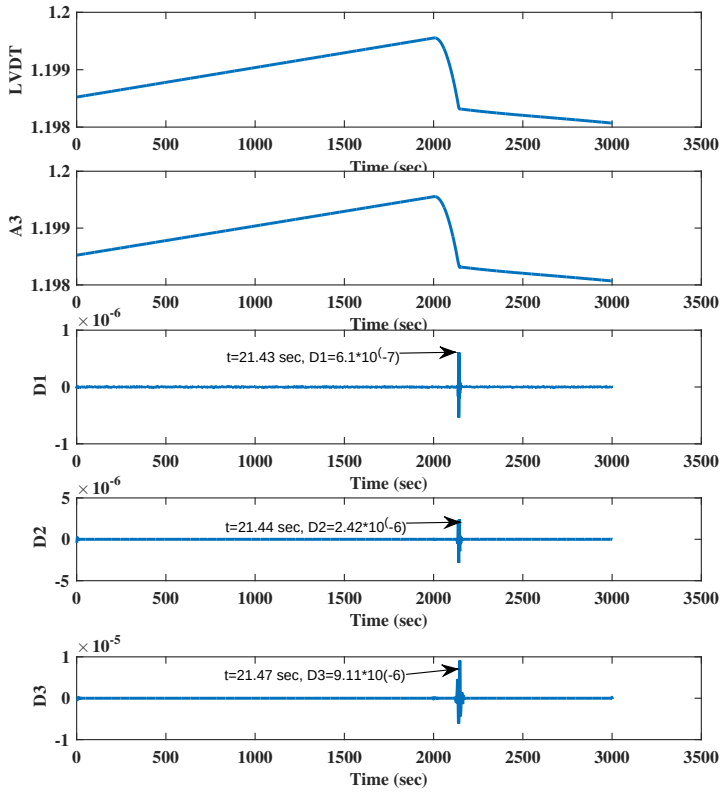

Figure 4.7: The approximation and detail coefficients of a failure for the LVDT sensor.

method, an actuator leakage coefficient with ramp function with a slope of 10^{-5} is considered in this section where the fault starts at $t = 20sec$. Figure 4.7 and Figure 4.8 show the behavior of the approximation and detail coefficients of the failure for the LVDT sensor and control signal.

It is noted from the figures that the details coefficients sharply jumps after the injection of failure. The detail coefficient 1 ($CD1$) contains sudden changes in the signal which indicates very high-frequency signals. Therefore, it may be affected by noise in the system. The detail coefficients 2 and 3 ($CD2$ and $CD3$) include high frequencies and fast changes in the signal and can be used for failure identification.

The DWT identification mechanism is straightforward. Null bias failure creates

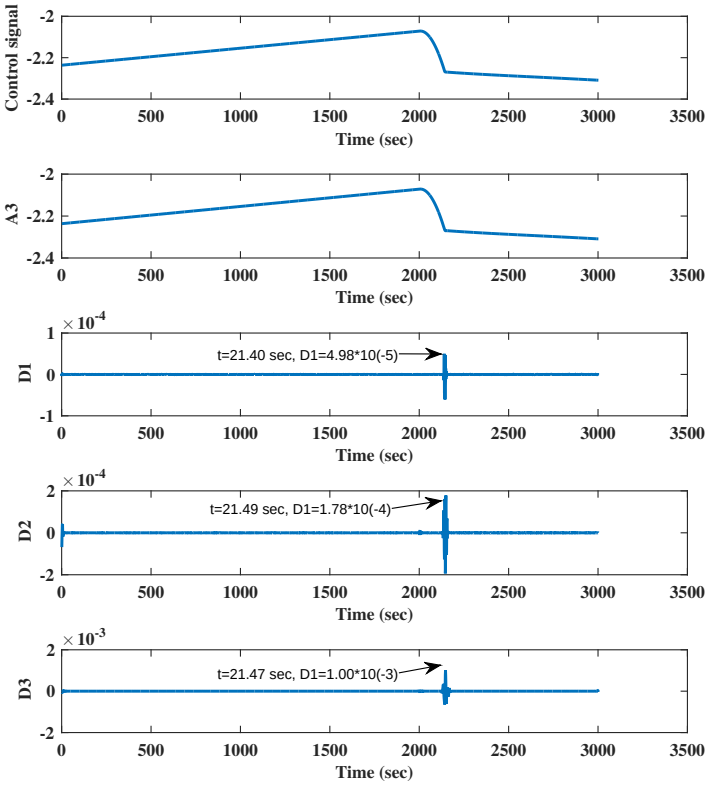

Figure 4.8: The approximation and detail coefficients of a failure for the control signal.

prolonged changes, and they are always unobservable at the start of the failure. The actuator leakage coefficient failure and internal leakage failures, on the other hand, cause sharp effects. Thus, these failures lead to much higher detail coefficients. This feature is considered to distinguish the null bias failure and actuator leakage, internal leakage failures from each other. Therefore, the following conditions are utilized for the fault isolation via the DWT method:

$$\begin{aligned} &\textbf{if } CD2 \textbf{ in control signal is higher then } 2\times10^{-5} \textbf{ and} \\ &CD3 \textbf{ in control signal is higher then } 10^{-4} \textbf{ and} \\ &CD3 \textbf{ in LVDT sensor is higher then } 4\times10^{-7} \textbf{ and} \\ &\textbf{isolate the failure as actuator leakage or internal leakage.} \end{aligned} \tag{4.19}$$

If the condition in Eq. (4.19) is satisfied, the system identifies an actuator leakage or internal leakage fault in the system. However, the DWT method cannot isolate the null bias failure.

Remark 4-1: The if-then rules in Eq. (4.19) are chosen by carefully monitoring various failures in the MFS system to maximize the accuracy of failure diagnosis method.

The DWT method can be combined with the ANN method to improve the accuracy of the FDD unit.

The OWA operator

Fusion block combines the decision of the DWT and ANN blocks. The fusion block diagram is shown in the Figure 4.4. The only task is to determine the weighting factor in the Eq. (4.7). The DWT cannot isolate the null bias failure. Therefore, the NN block is only used for isolating null bias failure. But, the DWT and ANN are considered to isolate the actuator leakage and internal leakage failures. The weighting factors of these block are determined by optimization method formulated in Eq. (4.9). Table 4.5 presents the weighting factors of the fusion method.

Table 4.5: Weighting factors of the OWA method for different failure.

weighting factors	value
w_{NN,I_0}	1
w_{DWT,I_0}	0
w_{NN,C_L}	0.43
w_{DWT,C_L}	0.57
$w_{NN,Q}$	0.38
$w_{DWT,Q}$	0.62

Table 4.6: The performance evaluation for testing OWA FDD method.

Failure	isolated as I_0	isolated as C_L	isolated as Q	isolated as unknown
Failure in I_0	84%	6%	0	10%
Failure in C_L	2%	91%	0	7%
Failure in Q	0	0	97%	3%

Moreover, several tests are performed to evaluate the accuracy of the fusion method for different failures. Table 4.6 illustrates the results of the isolation test.

It is noted from the Table 4.6 that the fusion method enhances the accuracy of the FDD unit in comparison with the proposed neural network. The OWA FDD method can isolate 84% of the null bias, 91% of the actuator leakage and 97% of the internal failure, correctly.

The online performance index

In the simulation test, relative accuracy (RA) is considered to measure the performance of the RUL method in online situations [58, 150]. This index is computed as follows :

$$RA = 1 - \frac{|RUL_{real}(t) - RUL_{predicted}(t)|}{RUL_{real}(t)} \tag{4.20}$$

where RUL_{real} denotes the real value of the RUL which can be calculated after the system has reached its end of the lifetime. $RUL_{predicted}$ indicates the predicted

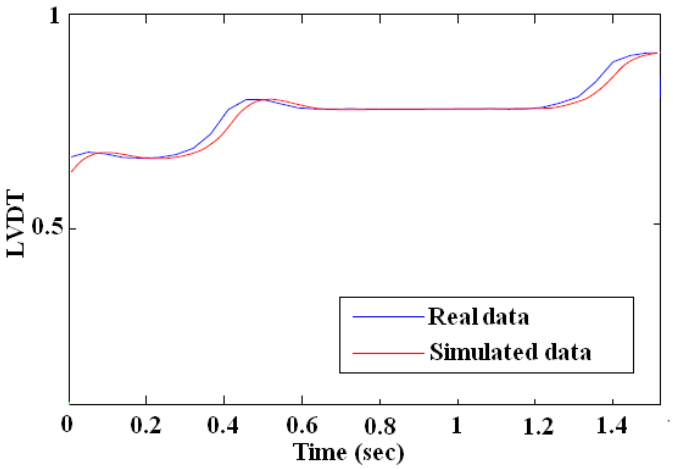

Figure 4.9: The experimental data and the estimated data of the LVDT sensor.

value of the RUL in real time. The RA is in the range of 0 and 1. The larger the RA signifies a better performance of the system.

4.3.3 The accuracy of the mathematical model

It is noted that the mathematical model of the MFS system was validated by our industrial partner in [126]. However, and for the sake of completeness, a comparison between the estimated data and the experimental data of the MFS system is made in this subsection. For this purpose, the experimental data of the MFS system is utilized. The data is gathered from the SECU system of LearJet 200 (LJ-200) aircraft during flight and consists of the control feedback signal and LVDT sensor data. To have a fair comparison, the experimental data of the control feedback signal is used in the mathematical model and the estimated LVDT sensor data is collected. Figure 4.9. presents the experimental data and the estimated data of the LVDT sensor.

It is seen from Figure 4.9 that there is a little difference between the experimental data of the LVDT sensor and the estimated data in transient response, but, the steady state behaviour of the estimated LVDT sensor and the experimental data of the system is very close. Moreover, different errors such as mean absolute error (MAE),

Table 4.7: The error values in various response condition in the MFS system.

Error	Max $\|e\|$	Min $\|e\|$	MAE
Response Error	0.0285	$1.0482e^{-5}$	0.0031

lower bound error (Min $|e|$) in steady state condition and upper bound error (Max $|e|$) in transient condition are obtained to evaluate matching between the experimental data and the estimated data of the MFS system. Table 4.7 illustrates the error values under various response condition in the MFS system.

The error of the MFS system in steady state condition at different set points is $1.0482e^{-5}$, which indicate a high fidelity of the model in steady state condition. Thus, the mathematical model can be considered at a certain set point when the system is at the steady state condition.

It is noted from the data validation test that the MFS system must not be considered for the failure diagnosis and prognosis during the transient condition. The transient data belongs to the time period that the aircraft change a direction such as a take-off or landing. However, the aircraft is cruising most of the time during its flight. Therefore, the MFS system is in steady state condition and hence, the mathematical model is highly accurate and valid, and the failure diagnosis and prognosis can be performed on the MFS system during this period.

4.3.4 Test results

In the following, the test results of the null bias, actuator leakage, and internal leakage failures are discussed.

1. **Null bias current**

   Consider a null bias failure with a slope of 0.001 at $t = 10$ *sec* as follows:

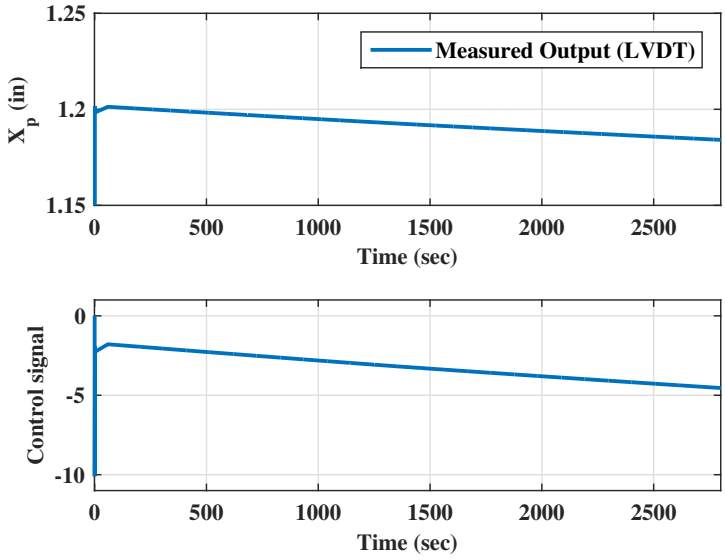

Figure 4.10: Failure caused by null current bias shift-measurements.

$$\Delta I_0 = \begin{cases} 0 & t \leq 10 \\ 0.001t & t > 10 \end{cases} \tag{4.21}$$

The setpoint of the system is $X_{p_{ref}} = 1.2$. Figure 4.10 indicates behaviors of the LVDT sensor and feedback control signal when a failure occurs.

Figure 4.11 shows the estimated null bias, the fusion FDD unit and RUL of the system under degradation of the null bias failure.

It is noted that the FDD unit identifies the failure at $t = 724.6sec$. This delay is due to the observability of this failure for the small value of fault. After the isolation of null bias failure, the FDD unit activates the failure parameter estimation unit. This unit can track the null bias. The value of the estimated null bias reaches $4.5mA$ at $t = 2510sec$. However, the real value of null bias is $4.5mA$ at $t = 2621sec$. The RUL predicts a value of $t = 1415sec$ at $t = 1025sec$. The RA performance index is 86.99% at $t = 1415sec$. Moreover, Figure 4.12 demonstrates the proposed Bayesian algorithm results at $t = 21940$ sec.

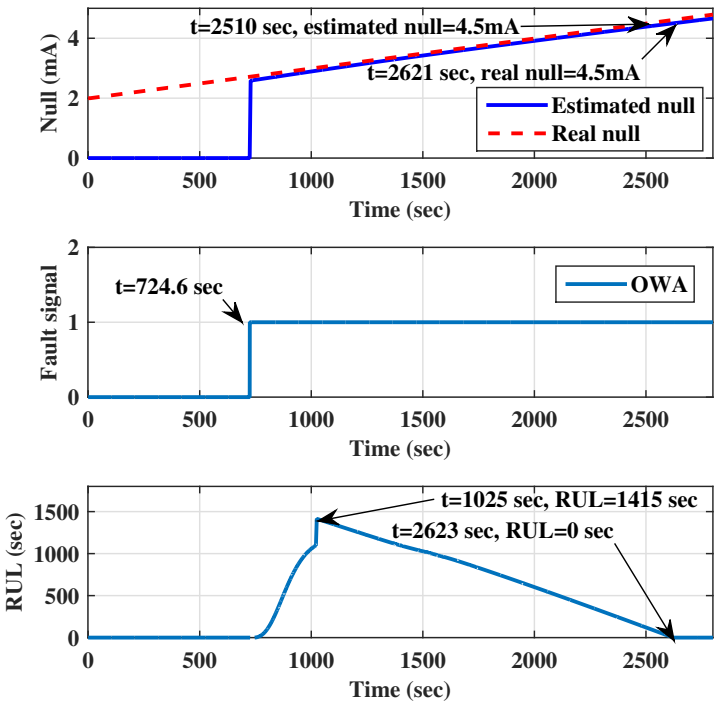

Figure 4.11: Failure caused by null current bias shift-monitoring units.

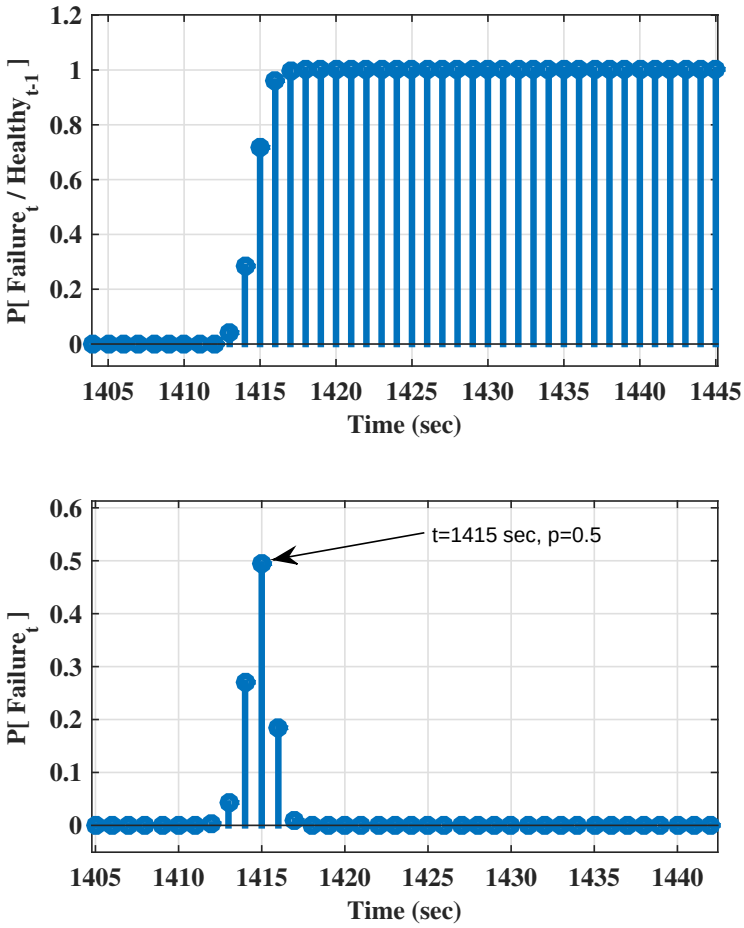

Figure 4.12: Bayesian algorithm-The null bias failure.

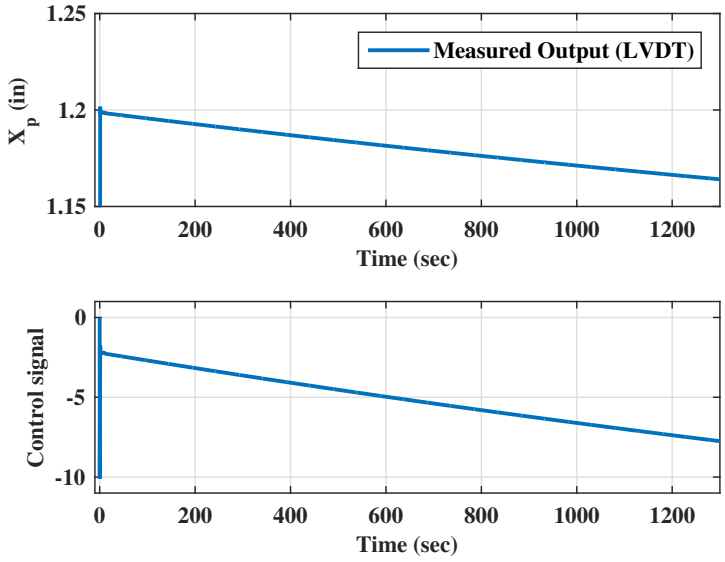

Figure 4.13: Failure caused by actuator leakage coefficient degradation with slope of 10^{-5}.

It is noted that likelihood reaches to 1, and the probability of failure is maximum at prediction horizon of 1415 *sec* which indicates a lifetime of the system at $t = 1025$ *sec*.

2. Actuator leakage coefficient degradation

   Assume an actuator leakage failure with a slope of 10^{-5} with the following equation:

$$\Delta C_L = \begin{cases} 0 & t \leq 10 \\ 10^{-5}t & t > 10 \end{cases} \tag{4.22}$$

   Figure 4.13 illustrates the LVDT sensor and control feedback signal under this failure.

   This failure has a severe effect, and even with a small value of the failure, the LVDT sensor and control feedback signal can be effected sharply. Figure 4.14

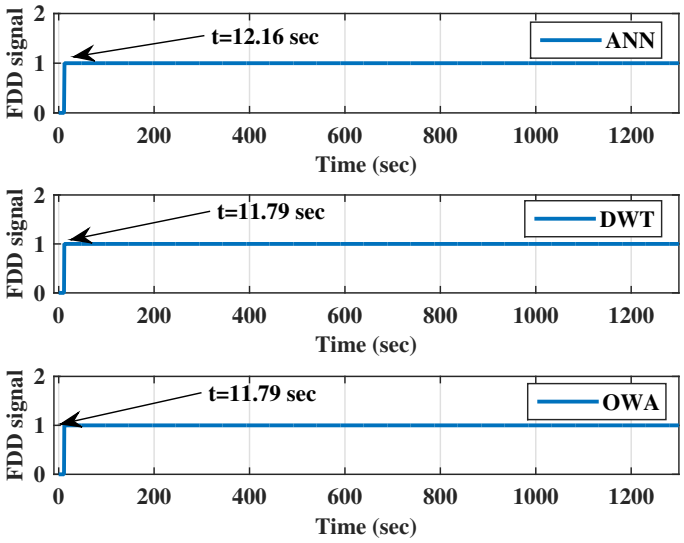

Figure 4.14: Failure caused by actuator leakage coefficient degradation with slope of 10^{-5}.

presents the FDD signal in the ANN, DWT and OWA block under the leakage coefficient degradation.

All the FDD unit isolate the failure fast due to the severity of the failure. The DWT and OWA block have a faster response in comparison with the ANN block. These blocks only need $1.79sec$ to identify the failure. Figure 4.15 shows the estimated actuator leakage coefficient and RUL of the system.

The failure parameter estimation unit successfully observes the actuator leakage. The estimated leakage reaches to $2psi$ at $t = 1286sec$ while the real value of leakage is $2psi$ at $t = 1297sec$. The RUL forecasts a value of $1148sec$ at $t = 46sec$. At this time, the RA index is 91.7%.

Now, the slope of the actuator coefficient failure is reduced to 10^{-6}. Figure 4.16 demonstrates the FDD signal of the ANN, DWT and OWA blocks under the actuator leakage coefficient with the slope of 10^{-6}.

DWT FDD provides the fastest isolation at $t = 13.85sec$. The OWA identifies the failure at $t = 30.94sec$ which is still faster then ANN block. It should be noted

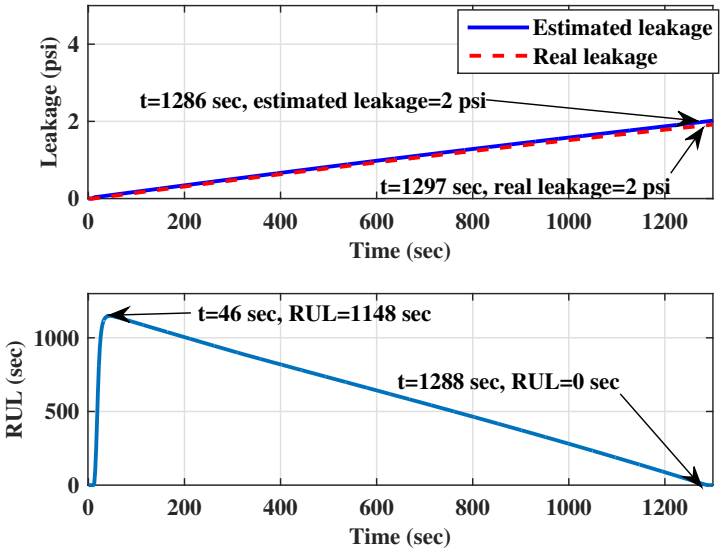

Figure 4.15: Failure caused by actuator leakage coefficient degradation with slope of 10^{-5}.

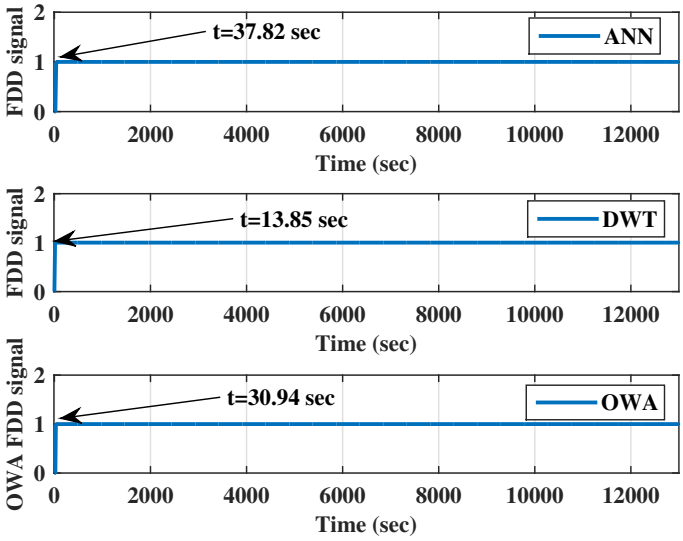

Figure 4.16: Failure caused by actuator leakage coefficient degradation with the slope of 10^{-6}.

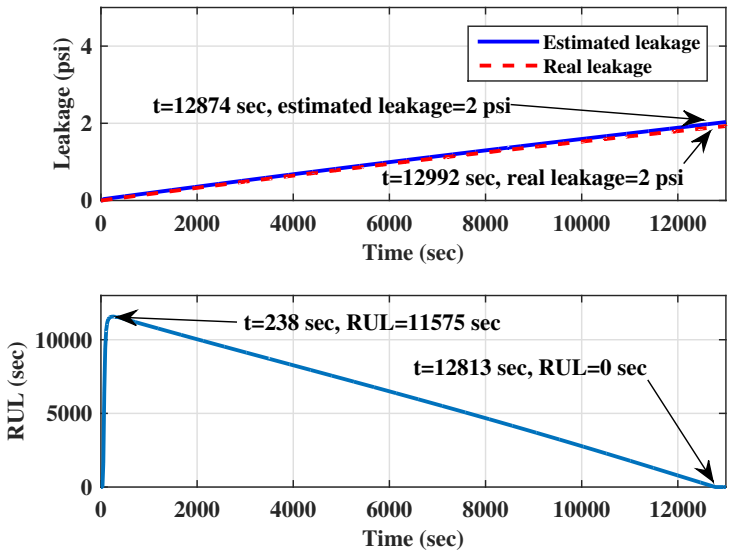

Figure 4.17: Failure caused by actuator leakage coefficient degradation with the slope of 10^{-6}.

that the OWA block provides more reliability in identification which is another advantage for the proposed system. Figure 4.17 shows the failure parameter and the RUL of the system under the mentioned failure.

The RUL unit predicts $11575sec$ which is acceptable behavior because the slope of the failure is decreased ten times. Therefore, the lifetime should be almost ten times larger. The RA index is 90.76% at $t = 238sec$.

3. Internal leakage

Consider an internal leakage failure with a slope of 0.001 in the system as follows:

$$\Delta Q = \begin{cases} 0 & t \leq 10 \\ 0.001t & t > 10 \end{cases} \tag{4.23}$$

Figure 4.18 illustrates the LVDT sensor output and control feedback signal.

The LVDT sensor and control feedback signal reveal a fast degradation in the system. Figure 4.19 illustrates the ANN, DWT and OWA blocks under the internal leakage failure.

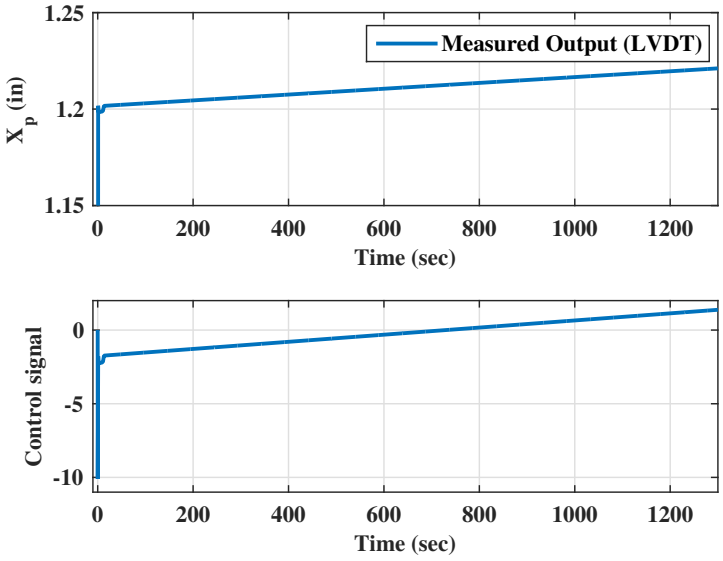

Figure 4.18: Failure caused by internal leakage.

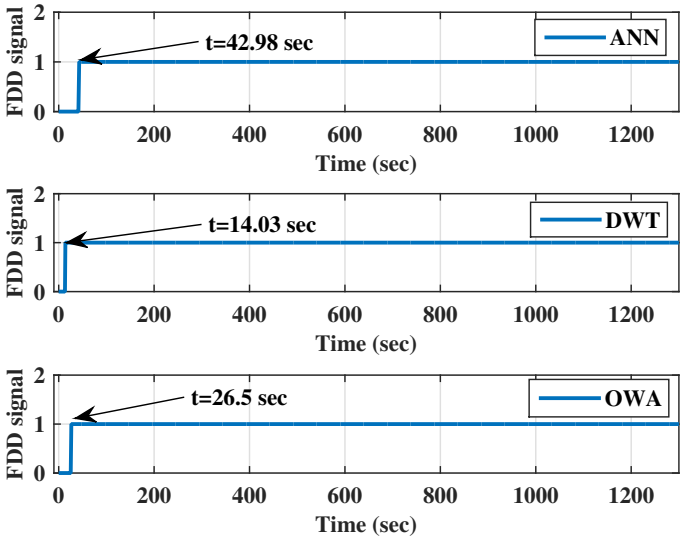

Figure 4.19: Failure caused by internal leakage.

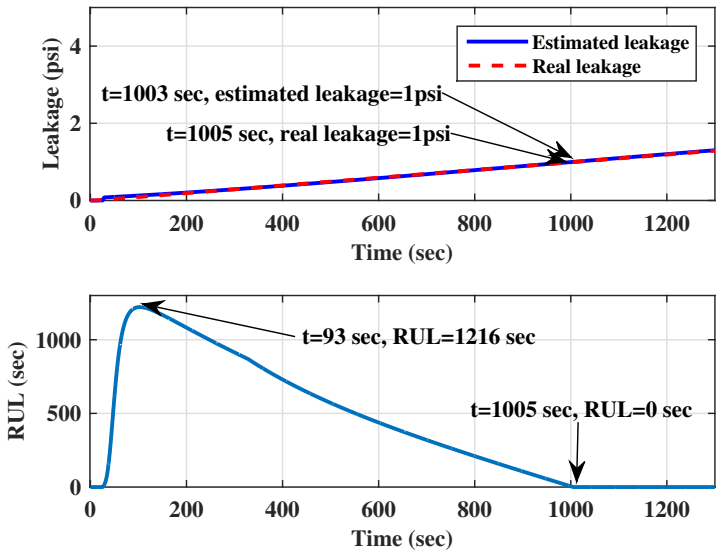

Figure 4.20: Failure caused by internal leakage.

Similarly, the OWA unit acts faster than ANN unit and isolates the failure at $26.5sec$. Figure 4.20 shows the estimated internal leakage and RUL of the system under the internal leakage failure.

The estimated value of leakage reaches to $1psi$ at $t = 1003sec$ which closely follows the real value, only two seconds delay between them. The RA is 66.67% at $t = 93sec$.

4.4 Conclusion

A modular structure is proposed to perform the task of fault diagnosis and prognosis in the MFS system. For this purpose, a novel data fusion method is designed by a combination of ANN and DWT blocks using OWA operator. The proposed fusion methodology improves the reliability and decreases the fault isolation time in the system. Then, the failure parameter estimation unit observes the failure parameters via a parallel neural network framework. The suggested structure helps to increase the

accuracy of the estimations. Finally, an optimization method via Bayesian algorithm is developed to forecast the lifetime of the system.

The main advantage of the FDP system was its proposed structure based on divide and conquer which improved the accuracy of the system. Moreover, the parallel networks reduced the complexity of the networks, lowered errors and consequently enhanced the speed and precision of the system. The proposed RUL unit captured an optimal model of the failure parameter and provided a remaining lifetime of the system based on a Bayesian algorithm which was suitable for real-time implementation. Moreover, several simulation tests were performed, and RA index was utilized for the evaluation which showed a high accuracy of the system.

Chapter 5

Data-driven FDP Approach Using a Multi-sensor Data Information

5.1 Introduction

Data-driven FDP methods rely on historical data. Therefore, redundancy in measurements helps to improve the accuracy of failure estimation and prediction. In this chapter, an FDP method is developed based on multi-sensor data information for the hydro-control valve (HCV) system, where several sensors are available to monitor the system.

The HCV system considered in this study is an important system in space launch vehicle propulsion systems and is responsible for regulating the pressure in spacecraft. Healthy operation of this unit is vital for the safe and reliable operation of the spacecraft. The HCV system consists of several subsystems with nonlinearity and uncertainty in their model, which make the condition monitoring of this system a challenging task.

To overcome the above complexities, this chapter introduces an innovative modular

structure to utilize the redundancy in sensors and reach a higher precision in the prediction of the RUL.

Assumptions for this research work are listed below:

1. Multiple sensors exist in the system that can be employed in health monitoring system.

2. These measurements are precise, and they are less affected by noise. Therefore, we add only 2% white noise to these measurements to mimic more realistic conditions.

3. Only one type of fault occurs in the system at a time period. The fault gradually grows in the system and finally leads to a complete failure.

The objective of this research work is to develop an FDP system for the HCV system. For this purpose, the analytical redundancy afforded through sensor measurements from the HCV system is employed using a feature selection technique to develop the FDP system. The proposed FDP system includes three parts, namely an FDD unit, a PE unit, and an RUL unit. The FDD unit is designed based on a feature selection technique and SVM method to isolate the type of a fault. Whenever the FDD unit identifies the type of failure, it sends a signal to activate the PE unit. In the PE unit, the failure parameter (resistance coefficient) is estimated using a distributed ANFIS network. Meanwhile, The RUL unit forecasts the remaining lifetime of the system using estimated failure parameter via an adaptive Bayesian algorithm.

In the next sections, a preliminary theory of the proposed FDP is introduced. Then, design implementation and test results are provided. Finally, a summary of results is given.

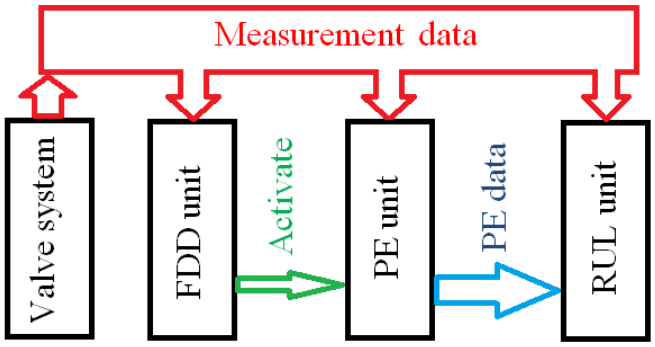

Figure 5.1: The proposed fault diagnosis and prognosis System.

5.2 A preliminary theory of the proposed fault diagnosis and prognosis method

This section introduces the preliminary theory of the proposed modular FDP method. Figure 5.1 shows the proposed FDP System.

The proposed FDP system includes FDD unit, PE unit, and RUL unit. In the following, various HCV failures are discussed, and brief underlying theories of the proposed techniques are presented.

5.2.1 The HCV failures

Three most common failures in the HCV system are considered as follows: piston leakage, drain blockage, and filter malfunction [11]. It must be noted that two areas in the front (zone 17 in Figure 3.5) and back (zone 18 in Figure 3.5) of the piston are sealed from each other. If there is a leakage in the sealed area around the piston, it leads to performance degradation of the system, and eventually, instability in the operation of the system. The drain blockage is a result of any congestion in the drain pipe (zone 19 in Figure 3.5). The drain pipe can get congested by impurities in the fluid, even though, the filter (zone 8 in Figure 3.5) is responsible for extracting the suspended impurities in the liquid. However, if the contamination gradually passes

through the filter over a long period, it may lead to congestion in the drain pipe. Filter malfunction can occur due to filter degradation. This happens due to the impurities in the fluid.

5.2.2 The fault detection and diagnosis (FDD) method

This section introduces the design methodology for the FDD unit. The main aim is to detect and identify the types of the failures. The proposed FDD method includes feature selection technique and SVM method. The feature selection technique is utilized to choose proper measurements for the input of SVM method. The SVM method is considered as a classifier to isolate the type of a failure in the system.

Feature selection

Pre-processing of data and proper feature selection are often necessary steps in machine learning applications where a significant amount of data or measurements are available. It is often the case that data pre-processing, and judicious feature selection can lead to more accuracy and less computational complexity in the classification scheme, see, e.g., [151]. In this work, correlation analysis is used to select relevant measurements of the sensors to be used in monitoring. For this aim, the Pearson product-moment rank correlation coefficient is formulated as follows [152]:

$$r = \frac{\sum_{i=1}^{n}(x_i - \bar{x})(y_i - \bar{y})}{\sqrt{\sum_{i=1}^{n}(x_i - \bar{x})^2}\sqrt{\sum_{i=1}^{n}(y_i - \bar{y})^2}} \tag{5.1}$$

where x_i is a variable which is desired to determine its dependency on output variable, y_i. Variables $\bar{x}$ and $\bar{y}$ are the mean values of x_i and y_i, respectively. Parameter n is the number of each variable. Variable r is correlation coefficient which get a value in range of $[-1, 1]$. An absolute value near one signifies a high dependency between variables, and the value near zero reveals a weak dependency or independence.

Support vector machine (SVM) classifer

Support vector machine (SVM) is a powerful classification technique based on statistical learning theory [141]. In SVM classifier, a line or a hyperplane is found based on optimization to maximize separability between classes. The SVM classification has been originally introduced for two class problems (binary SVM). Consider $\{(x_1, y_1), (x_2, y_2), \cdots, (x_m, y_m)\}$ that $x_i \in R^n$ are inputs, selected measurements, and $y_i \in \{-1, 1\}$ are class labels. The optimization problem can be formulated as follows:

$$\begin{aligned} & min_w \frac{1}{2} w^T w + c \sum_{i=1}^{m} \xi_i \\ & y_i(w\phi(x_i) + b) \geq 1 - \xi_i; \forall i = 1, \cdots, m; \xi_i \geq 0 \end{aligned} \tag{5.2}$$

where w is a normal vector to the hyperplane, and $c \geq 0$ is a penalty parameter. Variables ξ_i are positive slack. Function $\phi(0)$ is a feature mapping rule. Eq. (5.2) can be solved by Lagrange method, and a hyperplane is obtained as follows:

$$f(x) = sgn(\sum_{i=1}^{m} y_i \alpha_i K(x_i, x_j) + b) \tag{5.3}$$

where $K(x_i, x_j) = \phi(x_i)\phi(x_j)$ is known as a kernel of SVM classifier. The hyperplane, $f(x)$, is a surface which separates classes from each other. Different kernels can be used for the SVM methods such as linear, Gaussian, RBF. If more than two classes exist, binary SVM cannot directly solve the classification problem. In this case, There are two popular approaches which attempt to combine binary SVM to solve the problem. These are commonly known as "one against one" and "one against all" [153].

5.2.3 The parameter estimation (PE) method based on ANFIS networks

The ANFIS was introduced by Takagi and Hayashi [154] and benefits from a combination of fuzzy logic and neural network structure. ANFIS is chosen for the parameter estimation since it can provide accurate results for this task.

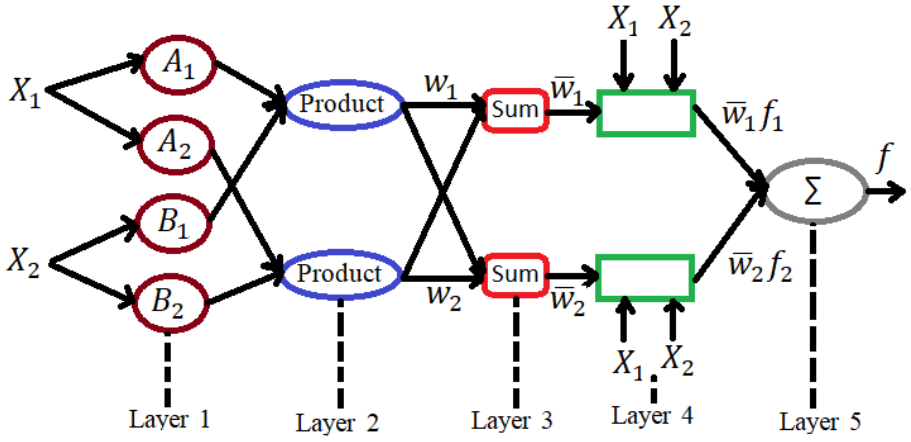

Figure 5.2: A Typical ANFIS Network with two inputs.

ANFIS network is an adaptive network that applies a supervised learning algorithm with an inference system similar to Takagi-Sugeno and is computationally efficient [151]. A set of rules are derived with respect to Sugeno fuzzy model as follows:

Rule 1: If x_1 is A_1 and x_2 is B_1, then $f_1 = p_1 x_1 + q_1 x_2 + r_1$

Rule 2: If x_1 is A_2 and x_2 is B_2, then $f_2 = p_2 x_1 + q_2 x_2 + r_2$

where A_i and B_i are the membership functions of input x_1 and x_2, respectively, and p_i, q_i and r_i denote adaptive parameters. Figure 5.2 shows a typical ANFIS network with two inputs and one output. As indicated in Figure 5.2, the ANFIS network contains five layers with a feed-forward structure. The mathematical representation of each layer is given as follows [141]:

Layer 1: Each adaptive node has a linguistic label, and the output of the node is the membership function of that label:

$$\begin{aligned} O_{1,i} &= \mu_{A_i}(x_1), \quad i = 1, 2. \\ O_{1,i} &= \mu_{B_{i-2}}(x_2), \quad i = 3, 4. \end{aligned} \tag{5.4}$$

Layer 2: Each node in this layer is fixed. Each node of this layer depicts a firing strength (w_i) for each rule. A T-norm operator like "AND operator" is considered to

compute the output:

$$O_{2,i} = w_i = \mu_{A_i}(x_1) \times \mu_{B_i}(x_2) \quad i = 1, 2. \tag{5.5}$$

Layer 3: Similar to layer 2, every node in this layer is fixed. A normalization is made in this layer to obtain relative firing strengths ($\bar{w_i}$) as follows:

$$O_{3,i} = \bar{w_i} = \frac{w_i}{\sum_{j=1}^{2} w_i} \quad i = 1, 2. \tag{5.6}$$

Layer 4: Each node is adaptive in this layer. A Multiplication of the relative firing strengths and the adaptive parameters are considered to formulate the outputs as follows:

$$O_{4,i} = \bar{w_i} f_i = \bar{w_i}(p_i x_1 + q_i x_2 + r_i) \quad i = 1, 2. \tag{5.7}$$

Layer 5: This layer has only one node whose output is the summation of all signals obtained by the previous layer:

$$O_{5,1} = \sum_{i=1}^{2} \bar{w_i} f_i = \frac{\sum_i^2 w_i f_i}{\sum_i^2 w_i} \tag{5.8}$$

Backpropagation algorithm or hybrid learning which combines gradient descent and the least-squares schemes can be used to train the ANFIS network. These algorithms optimize the adaptive parameters in layers 1 and 4 to achieve a minimum error in the output of the network.

5.2.4 The remaining useful life (RUL)

The RUL task is to predict the remaining lifetime of the system before complete failure occurs. In here, a similar Bayesian algorithm like the one introduced in the previous chapter is applied to compute the RUL of the system.

5.3 Simulation studies and test results

This section introduces the structure of the proposed FDP system and considers several test studies to investigate the performance of the system. In the following,

Table 5.1: Failure parameters with the healthy values and complete failure criteria.

Failure	Failure parameter	Healthy value	failure
Piston leakage	Piston resistance($\frac{kg}{m^4 s}$)	$7.7e^{+11}$	$4.5\ e^{+11}$
Drain blockage	Drain resistance($\frac{kg}{m^4 s}$)	$2.4e^{+11}$	$3.5e^{+11}$
Filter damage	Filter resistance($\frac{kg}{m^4 s}$)	$5.2e^{+10}$	$7.5\ e^{+11}$

failure scenarios are considered. Then, the structure of the FDP system is developed. Afterwards, the accuracy of the Simulation model is demonstrated using experimental data of the HCV system. Finally, few test studies are discussed.

5.3.1 Failure scenarios

Three prominent HCV failures, i.e., piston leakage, drain blockage, and filter malfunction are examined in the sequel. It is noted that piston leakage, drain blockage and filter malfunction lead to gradual changes in the piston leakage resistant coefficient, drain resistance coefficient and filter resistance coefficient, respectively. Therefore, degradations can be simulated through a change in these parameters. Six hundred ramp functions with different slopes are injected into the Simulink model to create failures in the system. Table 5.1 displays the healthy value of these parameters as well as complete failure criteria.

Remark 5-1: Complete failure criteria are chosen by carefully monitoring the system to ensure safety in the HCV system. However, different complete failure criteria may be selected in different types of spacecraft.

5.3.2 The proposed FDD unit

The proposed approach for FDD is accomplished in two-stage consisting of feature selection and SVM classification. Fourteen measurements from sensors, e.g., pressure gauges, flow Meters, and position sensor are available. However, using all of them

Table 5.2: Correlation coefficients for the feature selection in FDD unit

Measurement	Correlation
Pressure in inlet (1)	0
Pressure in outlet (2)	0
Pressure in drain (19)	0
Pressure in control orifice zone (5)	-0.59
Pressure in piston front zone (17)	-0.60
Flows in inlet (1)	0.25
Flows in outlet (2)	-0.10
Flows in drain (19)	-0.59
Flows in control orifice zone (5)	-0.44
Flows in connecting pipe (14)	-0.24
Flows in feedback pipe (7)	-0.57
Piston position in x direction (x_p)	0.56
Piston position in y direction (y_p)	0.17
Piston position in z direction (z_p)	0.19

may not necessarily result in a more accurate classification ability and will result in added computational burden. Hence, feature selection using the correlation coefficient formula introduced in Eq. (5.1) is considered to select the measurements with the highest impact on the failures. Table 5.2 presents measurements and their correlation coefficient with the failures for the task of fault diagnosis.

It is noted from Table 5.2 that the pressure in piston front zone, the pressure in control orifice zone, the flows in feedback pipe and piston position in x-direction have highest correlation coefficients, and hence, they are selected as the input of SVM classifier.

To design SVM classifier, RBF kernel is utilized. Furthermore, three types of faults must be investigated. These three types of failures along with the healthy operating condition result in four different classes. To design the SVM classifier, six binary SVMs are developed using one against one approach to construct four classes.

Table 5.3: The performance of the proposed FDD system in isolating type of failure.

Failure	classified 1	classified 2	classified 3
Piston leakage (1)	96%	4%	0%
Drain blockage (2)	14%	82%	4%
Filter damage (3)	0%	12%	88%

Moreover, 100 new tests are performed to evaluate the accuracy of the FDD method. Table 5.3 illustrates the performance of the proposed FDD unit in isolating the type of failure.

As indicated in Table 5.3, the proposed FDD system correctly isolates 96% of the Piston leakage (fault #1), whereas accuracy of drain blockage (fault #2) and filter malfunction (fault #3) are 82% and 88%, respectively.

5.3.3 The proposed PE unit

After a fault is isolated by the FDD unit. A signal is sent from the FDD unit to activate the PE unit (See Figure 5.1). The PE unit estimates the degradation path of the failure parameter. To observes the degradation paths of failures, it is common to monitor changes in the parameters that are proportional to the degradation paths. In this study, piston leakage resistant coefficient, drain resistance coefficient, and filter resistance coefficient are considered as parameters to monitor piston leakage, drain blockage and filter malfunction, respectively. Then, a network of three ANFIS is developed to observe these parameters using available online measurements. Figure 5.3 shows the proposed parameter estimation unit.

It is noted that once a fault is detected and isolated, only one of these ANFIS blocks corresponding to the fault is activated. The number and types of measurements used as inputs of the ANFIS blocks are chosen via correlation analysis presented by Eq. (5.1). The outputs are set to failure parameters. For training, a hybrid method which is a combination of the gradient descent method and the least-squares scheme is considered. The proposed parallel PE structure increases the accuracy of

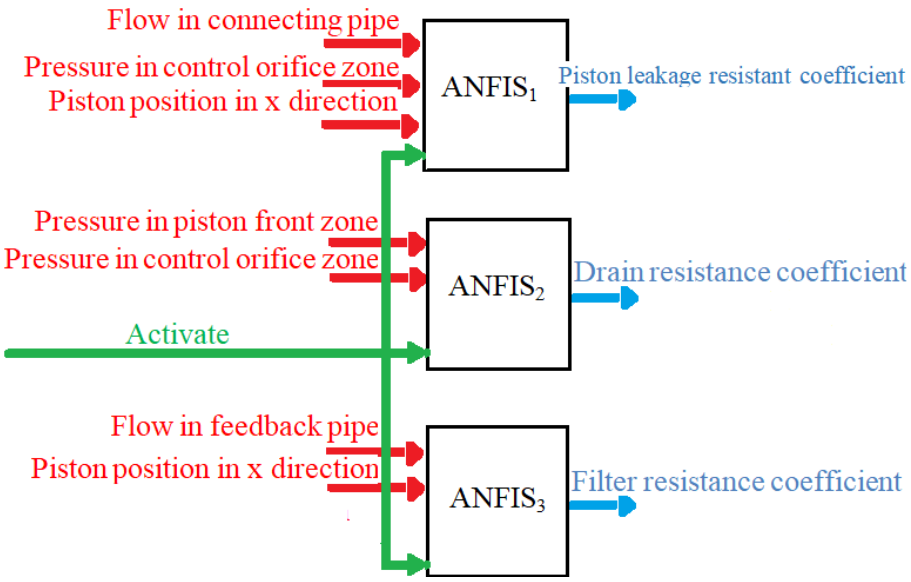

Figure 5.3: The proposed parameter estimation (PE) unit.

Table 5.4: Parameter estimation error of the distributed ANFIS method.

Parameter	Training error	Test error
Piston resistant	0.0327	0.0387
Drain resistant	0.0066	0.0069
Filter resistant	0.0527	0.0594

the estimation as each network has its own training phase. Furthermore, parallel processing reduces computational time at each step and makes it suitable for online implementation. Table 5.4 demonstrates parameter estimation error of the distributed ANFIS networks in training and test phases based on mean absolute percentage error (MAPE) criterion.

It is noted from Table 5.4 that the drain resistant has the best result with least error.

Remark 5-2: To evaluate the performance of the proposed distributed ANFIS method in PE unit, a comparison with a centralized ANFIS network is made in Table

Table 5.5: Parameter estimation error of the centralized ANFIS method.

Parameter	Training error	Test error
Piston resistant	0.1073	0.1227
Drain resistant	0.0902	0.1027
Filter resistant	0.0826	0.0938

5.5. The centralized ANFIS method is developed using one ANFIS network. All the five measurements used in the decentralized method are considered as the inputs of the estimation unit. Moreover, only one output is considered in the output layer. The healthy and faulty values of the failure parameters are used in the output layer for training and test of the network. It is noted from Table 5.5 that the failure parameters have higher errors in comparison with the distributed ANFIS method.

5.3.4 The proposed RUL unit

The RUL unit takes the estimated data of the failure parameter from the PE unit and forecasts the remaining lifetime of the system (See Figure 5.1). For this purpose, an optimal affine model of failure parameter is identified by using Eq. (4.12). Then, The likelihood and probability of failure $t = t_0 + j$ are calculated by Eqs. (4.17) and (4.16), respectively. The prediction horizon that maximizes the probability of the failure is the RUL of the system.

Furthermore, to evaluate the accuracy of the RUL unit, a relative accuracy measure is considered as follows [58, 155]:

$$RA = 1 - \frac{|RUL_{real}(t) - RUL_{predicted}(t)|}{RUL_{real}(t)} \tag{5.9}$$

where $RUL_{real}(t)$ is the real amount of RUL which can be obtained after the complete failure of the system. $RUL_{predicted}(t)$ is a predicted value for the RUL which is provided by the RUL unit. RA is in a range of $[0, 1]$. The larger value of RA indicates a higher accuracy of the system.

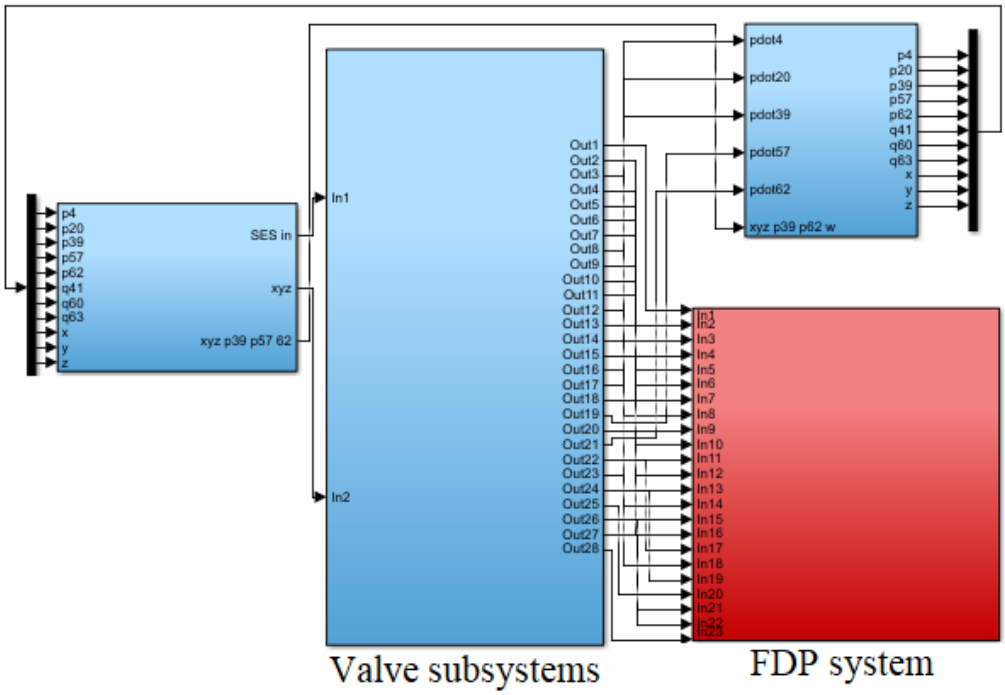

Figure 5.4: The simulink model of HCV system and its FDP system.

5.3.5 The accuracy of the Simulation model

In this research work, the Simulink model of the HCV system is utilized to apply for health monitoring purposes. Figure 5.4 shows the Simulink model of HCV system and its FDP system.

This Simulink model is constructed by considering a nonlinear model of the HCV system using Bond Graph method. The Simulink model takes different non-linear effects into accounts such as hydraulic resistances, flow forces, Coulomb friction and fluid chamber compressibility. For this aim, sets of non-linear state equations are extracted by the Bond Graph method. Then, various operating conditions are simulated (See [128] for more details about the high fidelity of the Simulink model).

To validate the accuracy of Simulink model, the response of the real HCV system is compared to the response of the Simulink model in this section. Figure 5.5 presents the real response of the HCV system in comparison with the simulated model.

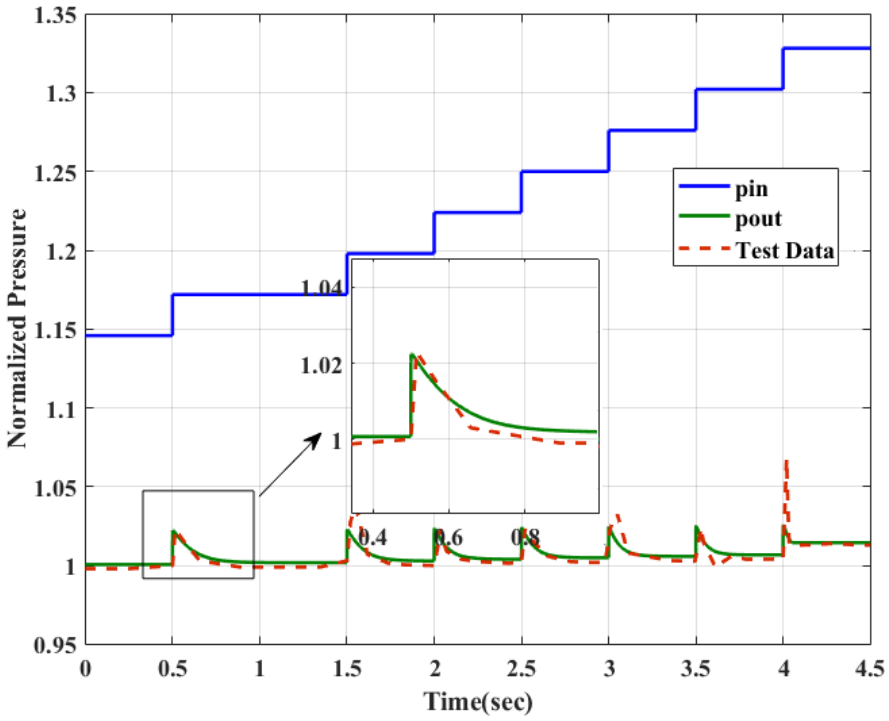

Figure 5.5: The real response of the HCV system in comparison with the simulated model.

To verify the high fidelity of the Simulink model, we consider several positive stepwise rises in the inlet pressure (Upper blue line) until the HCV reaches to the upper saturation state. The green line indicates the simulated outlet pressure of the system. This pressure is recorded from where the pressure sensor can be mounted. The experimental data from the pressure sensor is depicted as a red cross-point line. As it is seen, the simulated outlet pressure is desirably verified with the experimental results showing high accuracy of the Simulink model. In all operating conditions, the error of Simulink model is less than 0.1% which indicates a high accuracy of the Simulink model.

5.3.6 Test results

In this subsection, several tests are developed to evaluate the performance of the proposed method.

1. **Piston leakage failure**

   A piston leakage failure is injected into the system through a ramp function with a slope of -5×10^{-6} in piston resistant coefficient at $t = 2000$ *sec*. Figure 5.6 shows the measurements applied to the input of the PE unit (ANFIS 1) in the piston leakage failure.

   It is noted from Figure 5.6 that all the measurement data start changing after the onset of piston leakage fault. Reducing the piston leakage resistant coefficient will cause a leakage in the piston, which can be seen from the increase in the flow of the connecting pipe. The piston pressure balance thus is altered resulting in the opening of the control orifice, and consequently, increased outlet pressure. This behavior is clearly illustrated in Figure 5.6. The change in the piston leakage resistant coefficient of the system, in fact, can change the design parameter of the system so that it directly affects the operational condition of the system. Figure 5.7 displays the FDD unit, PE unit and RUL unit under the piston leakage

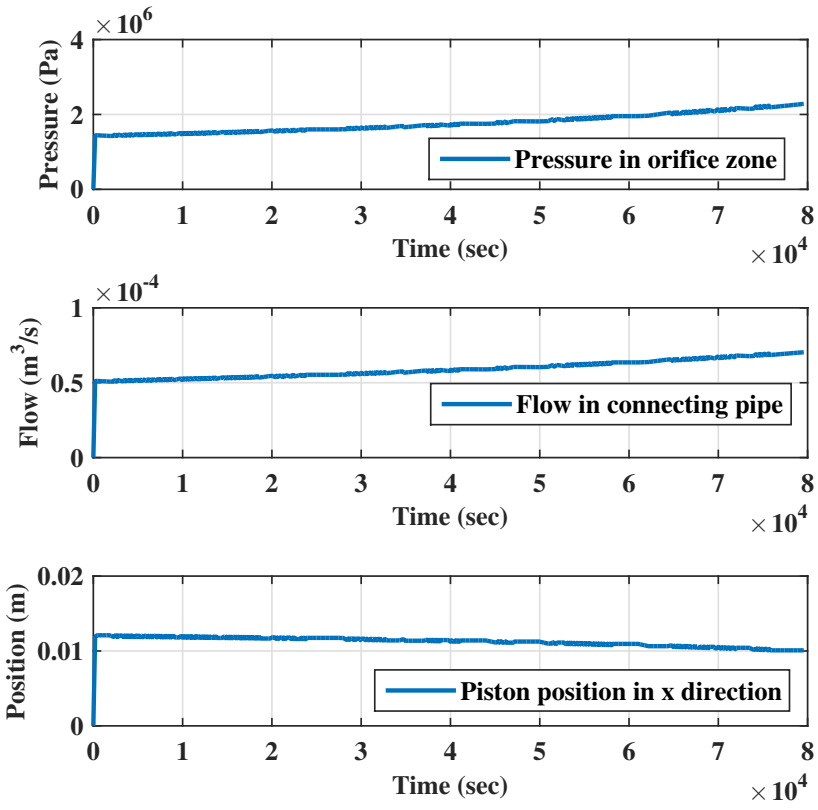

Figure 5.6: The measurements applied in the input of the PE unit (ANFIS 1)-The piston leakage failure.

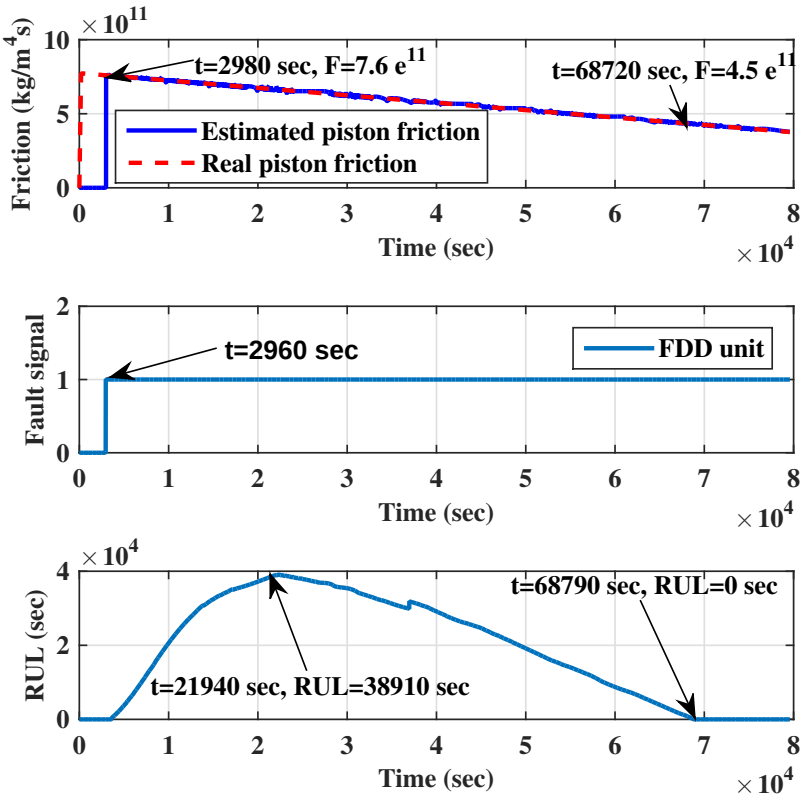

Figure 5.7: The FDD unit, PE unit and RUL unit under the piston leakage failure.

failure.

The FDD unit isolates the piston leakage failure at $t = 2960$ *sec*. Then, the FDD unit activates the PE unit. The PE unit observes the failure parameter. However, there is a little fluctuation in the estimated failure parameter which is due to disturbance in the measurement of the HCV system. The length of the sliding window in the RUL unit is adjusted to 4000 samples. The RUL is 38910 *sec* at $t = 21940$ *sec* which indicates an RA of %54. Furthermore, at $t = 68720$ *sec*, the estimated piston friction parameter reaches to $4.5e^{11}$ which implies the end of the lifetime of the HCV system. Furthermore, the RUL unit shows a value of zero for the system at $t = 68790$ *sec* which only has a delay of

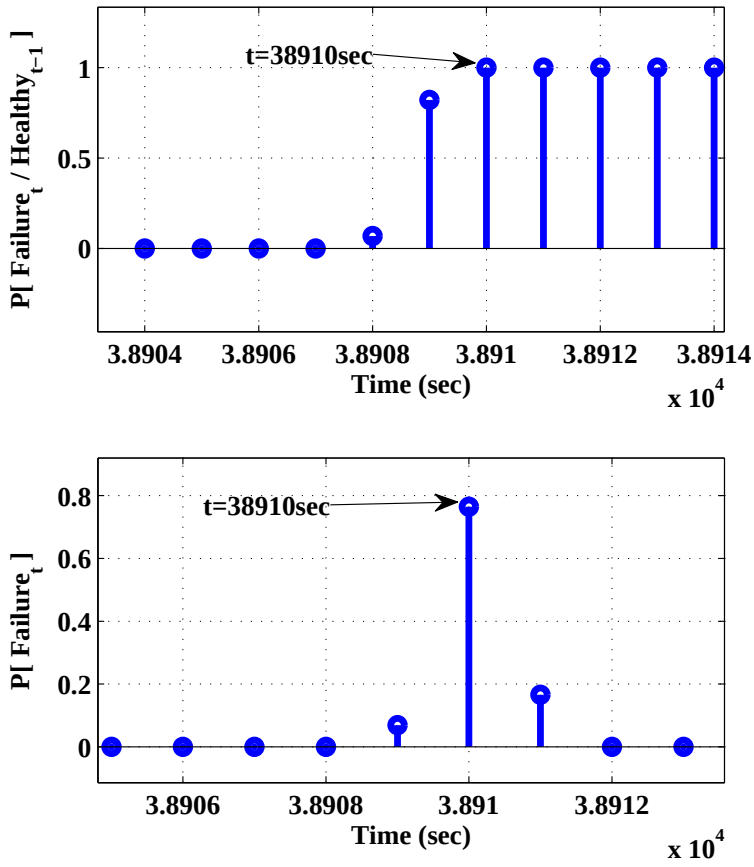

Figure 5.8: The proposed Bayesian algorithm-The piston leakage failure.

$70sec$ in announcing the correct value for the end of life of the system. Figure 5.8 demonstrates the proposed Bayesian algorithm results at $t = 21940$ *sec*.

It is noted that likelihood reaches to 1, and the probability of failure is maximum at prediction horizon of 38910 *sec* which indicates a lifetime of the system at $t = 21940$ *sec*.

2. **Drain blockage failure**

A drain blockage failure is injected into the system via a ramp function with a slope of 10^{-6} in drain resistance parameter at $t = 2000$ *sec*. Figure 5.9 shows

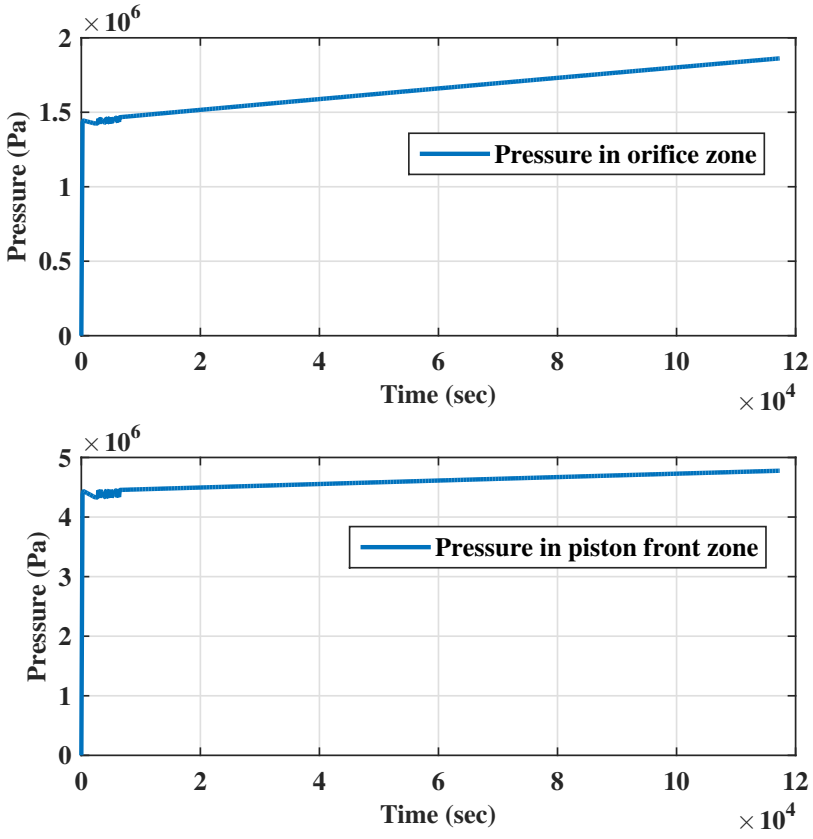

Figure 5.9: The measurements applied in the input of the PE unit (ANFIS 2)-The drain blockage failure

the measurements applied at the input of the PE unit (ANFIS 2) in the drain blockage failure.

Similarly, the proposed measurements start deviation from healthy conditions after the drain blockage failure. This failure directly affects the piston pressure balance in amplifying part. The gradual blockage of the drain pipe leads to an increase in the hydraulic pressure in the piston back zone, thus pushing the piston toward opening the control orifice. As a result, the pressure loss in the control zone decreases and the outlet pressure rises. Figure 5.10 illustrates the FDD unit, PE unit and RUL unit under the drain blockage failure.

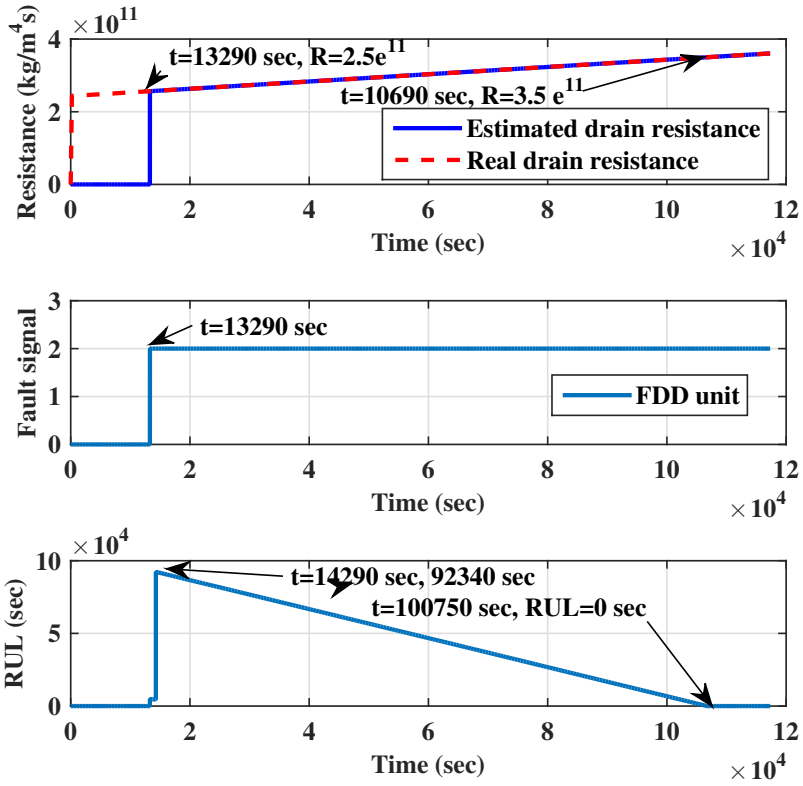

Figure 5.10: The FDD unit, PE unit and RUL unit under the drain blockage failure.

The FDD method identifies the drain blockage failure at $t = 13290$ *sec*. A particular explanation for this delay can be provided by considering the impact of the failure on the design parameters of the FDD method and the performance of the chosen HCV system. Unlike the previous failure, drain blockage does not cause design parameter alteration in the system. Thus, the system would be able to compensate the effect of this failure. Given the chosen HCV system is indeed a regulator, it will perform toward compensation of the failure. Therefore, depending on the severity of the failure, the consequent might remain hidden. Therefore, this failure is hard to capture.

It is noted that the estimated drain resistance can successfully track its real value in the PE unit. The length of the sliding window in RUL unit is set to 100 samples. The RUL unit shows a value of 92340 *sec* at $t = 14290$ *sec* which indicates an accuracy of $RA = \%93$. Moreover, the estimated drain resistance arrives at $3.5 \times e^{11}$ at $t = 100690$ *sec* that it indicates the end of the lifetime of the HCV system. The RUL also shows a value of zero at $t = 100750$ *sec*, again, a small delay in announcing the end of the lifetime for the RUL system. Figure 5.11 illustrates the proposed Bayesian algorithm results at $t = 14290$ *sec*.

The probability of the failure is maximum at prediction horizon of 92340 *sec* which implies the RUL for time 14290 *sec*.

3. **Filter failure**

A filter failure is injected into the system by changing filter resistance using a ramp function with a slope of 2×10^{-5} at $t = 2000$ *sec*. Figure 5.12 demonstrates the measurements applied at the input of the PE unit (ANFIS 3) in the filter failure.

It is seen from Figure 5.12 that the measured data begins changing with the growing failure. Filter resistance failure, in fact, changes the operational conditions in the adjusting part of the HCV system, which is the commander for the

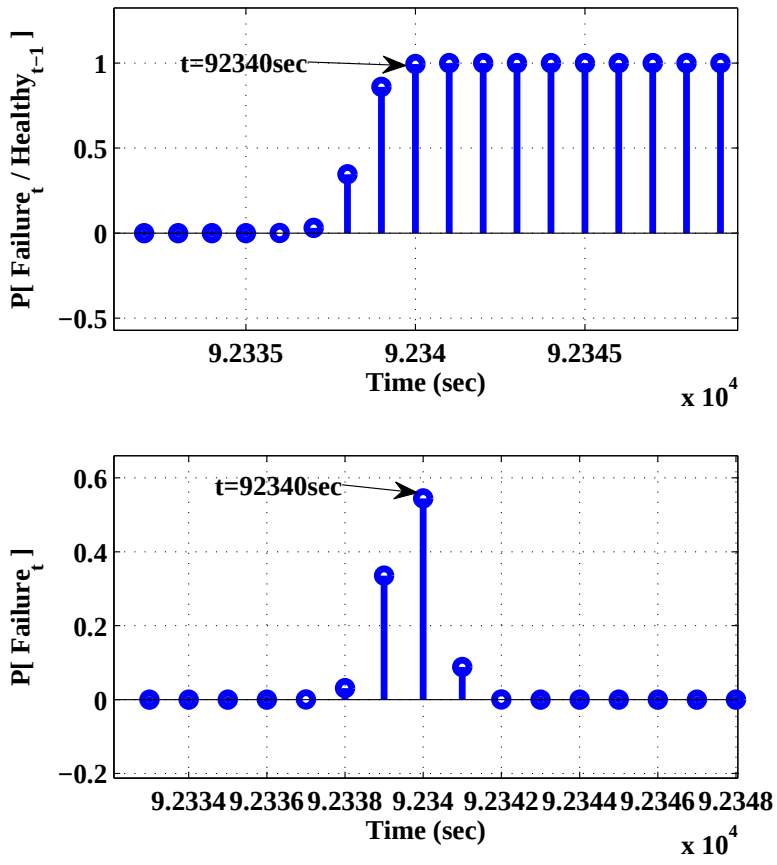

Figure 5.11: The proposed Bayesian algorithm-The drain blockage failure.

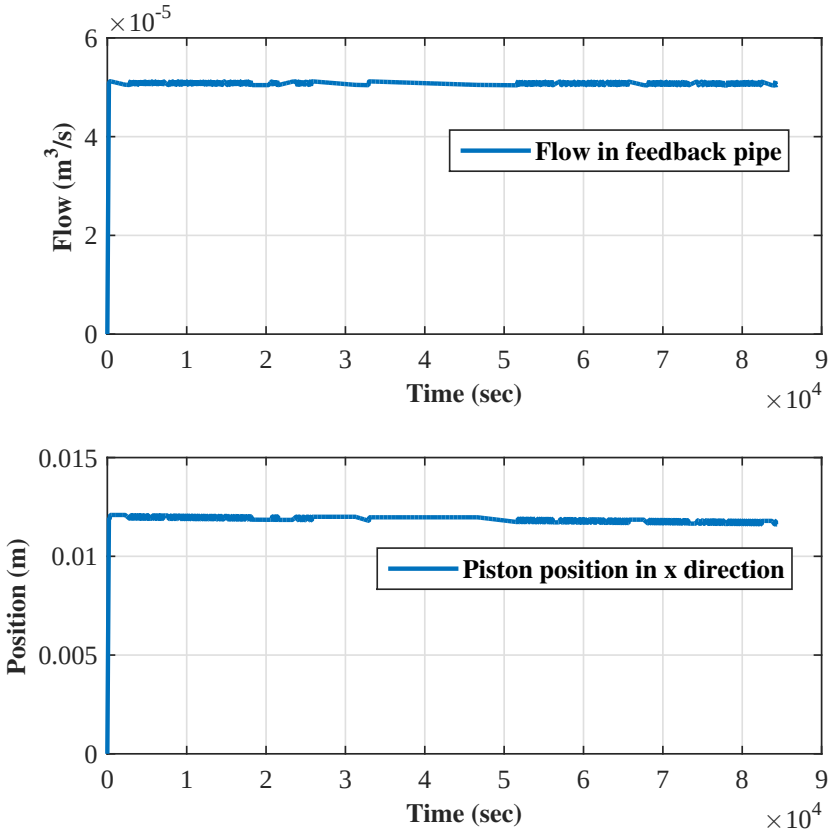

Figure 5.12: The measurements applied in the input of the PE unit (ANFIS 3) in the filter failure.

amplifying part. Therefore any changes in this part will dictate corresponding changes in the amplifying part. The anticipated consequence for the considered failure is an increased outlet pressure; however, the outlet pressure rise would compensate the increased pressure loss induced by the acknowledged failure. Although one may expect a reduction, this can explain why there is no change in feedback flow. However, the creepy backward motion of the piston can be as a indicator for outlet pressure increase. Overall, one can see the affected behavior of the HCV system is mainly due to the interactive dynamics of the HCV's internal moving components (control and adjusting subap). It should be mentioned that in the development of this interactive dynamic the Coulomb friction plays a significant role. Considering the slope of the implemented failure, these forces will cause fluctuations in the results which may affect further analysis. Figure 5.13 indicates the FDD unit, PE unit and RUL unit under the filter failure.

The FDD unit isolates the failure at $t = 10770$ *sec*. The estimated filter resistance tracks its real value. However, there is a fluctuation in the parameter estimation which is due to disturbances and oscillation in the measurements. The RUL forecasts a value of 33610 *sec* at $t = 34180$ *sec*. The RA measure at this time is %96. Furthermore, the estimated parameter reaches $7.5 \times e^{11}$ at $t = 67480$ *sec* which is near the value of the RUL unit for the end of the lifetime ($t = 67640$ *sec*). It must be noted that the RUL takes more time to initialize and reach a maximum at $t = 34180$ *sec*. The particular reason for this is that the measurements have disturbance and oscillation. Therefore, we adjust the length of sliding window to 5000, which leads to slow initialization of the RUL unit. Figure 5.14 illustrates the proposed Bayesian algorithm results at $t = 34180$ *sec*. Similarly, the failure sequence has a maximum of 33610 *sec* which can be treated as the RUL of the system.

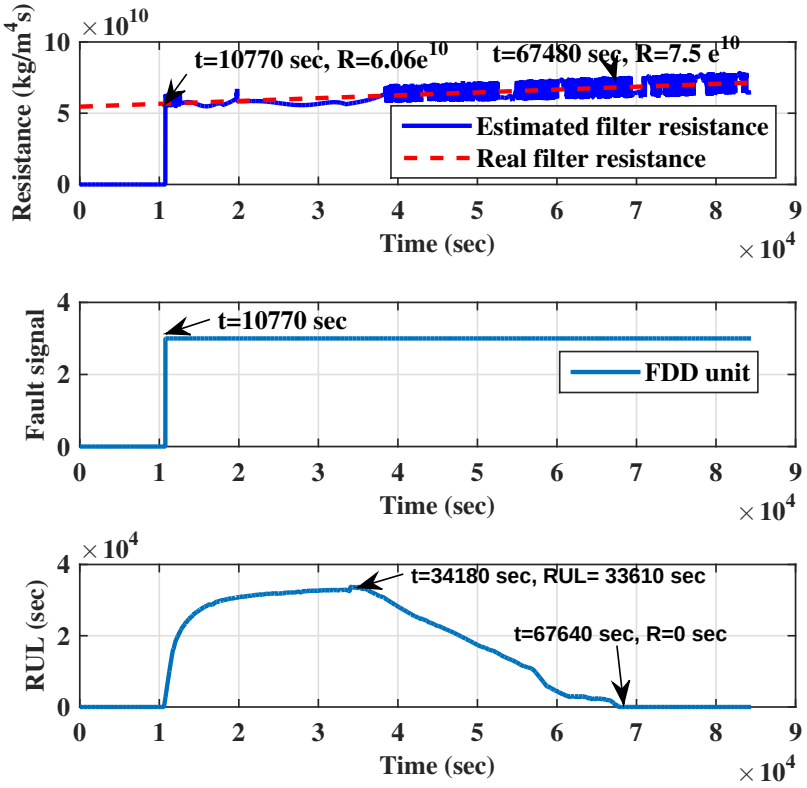

Figure 5.13: The FDD unit, PE unit and RUL unit under the filter failure.

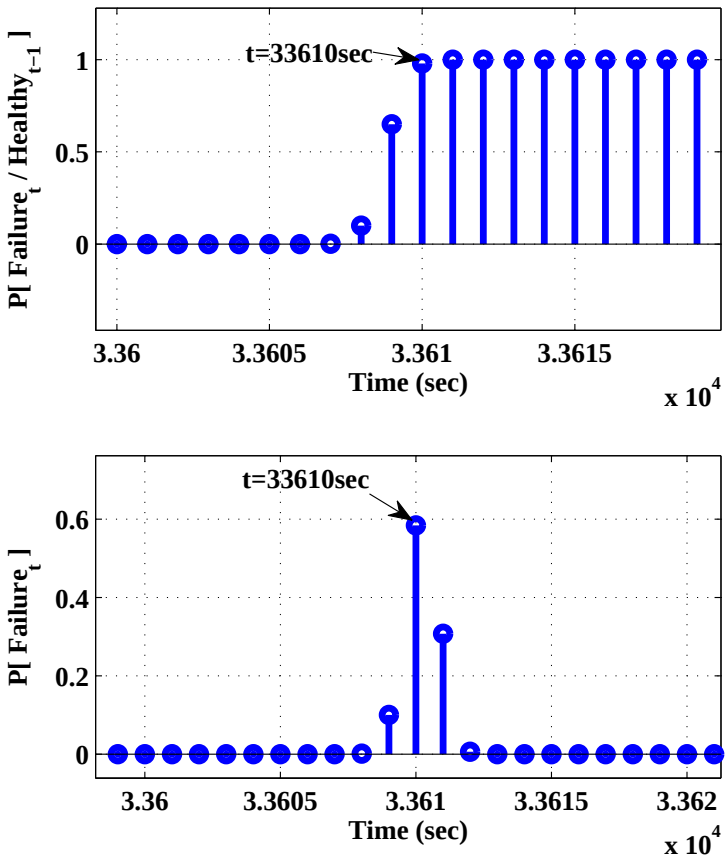

Figure 5.14: The proposed Bayesian algorithm-The filter failure.

5.4 Conclusions

In this chapter, we presented a new health monitoring system for an HCV system. Three main failures consisting of piston leakage, drain blockage, and filter malfunction were considered in the HCV system. Then, a new FDP method based on redundancy in multi-sensor data information was designed to monitor the system. The proposed FDP system had a modular structure and included an FDD unit, a PE unit, and an RUL unit. The FDD unit isolated the fault type using a combination of feature selection and SVM methods. The PE unit observed the failure parameter via a distributed network of three ANFIS. The RUL unit computed the remaining useful life of the system via a recursive Bayesian method. Several simulation studies were performed, and RA index was employed to evaluate the performance of the proposed method. The RA measure showed a high accuracy of the proposed methods.

The main advantage of the proposed FDP method was in its modular structure which improved the accuracy of the prognosis system. Moreover, proper feature selection allowed the FDD unit and PE unit reach a higher performance in the tasks of fault isolation and parameter estimation, respectively. Furthermore, the distributed structure of the PE unit decreased the computational complexity and consequently improved the accuracy of the parameter failure estimation in comparison with centralized design methodology.

Chapter 6

Model-based FDP Approach Using an Integrated EKF Method and Bayesian Algorithm

6.1 Introduction

If a suitable model of the failure is available or can be estimated, this model can be considered to predict the RUL of the system. In this chapter, a model-based fault prognosis of MFS system is developed.

The MFS system consists of five main components with highly non-linear dynamics in their structure. Furthermore, only two measurements including control feedback signal and LVDT sensor are available for monitoring the system. Therefore, the condition monitoring of this system is very challenging due to these facts.

To tackle the above complexities, this chapter introduces a novel model-based prognosis method for predicting the RUL of the MFS system. Assumptions for this research work are listed below:

1. A very accurate model of the system is available. In fact, we have shown the MFS system is accurate in chapter 3.
2. These measurements are precise, and they are less affected by noise. Therefore, we add only 2% white noise to these measurements to mimic more realistic conditions.
3. One type of fault or multiple faults can concurrently occur. The fault gradually grows in the system and finally leads to a complete failure.

The objective of this research work is to develop a prognosis system for the MFS system. For this purpose, This chapter introduces a novel fault prognosis of MFS systems based a combination of extended Kalman filter (EKF) and Bayesian approach. For this purpose, the EKF is employed to identify the progress of fault using residual generation. Then, a transformation is utilized to obtain nonlinear degradation path (DP) for the system. Afterwards, an adaptive predictor based on Bayesian approach is applied to the estimated degradation path to forecast the RUL of the system.

In the following sections, a preliminary theory of proposed model-based fault prognosis is introduced. Then, design implementation and test results are discussed. Finally, a conclusion is illustrated.

6.2 Preliminary Theory of Model-based Fault Prognosis of MFS System

Fault prognosis design methodology for the MFS system is discussed in this section. The objective is to introduce a prognosis system strategy to detect some common faults and predict the remaining useful life of the system. For this purpose, the progress of the failure is identified by an EKF and is fed to the next stage to estimate the degradation path (DP) of the system. Finally, the prediction of the RUL is obtained using an adaptive Bayesian algorithm. The block diagram in Figure 6.1 illustrates the various subsystems/tasks in the proposed prognostic system.

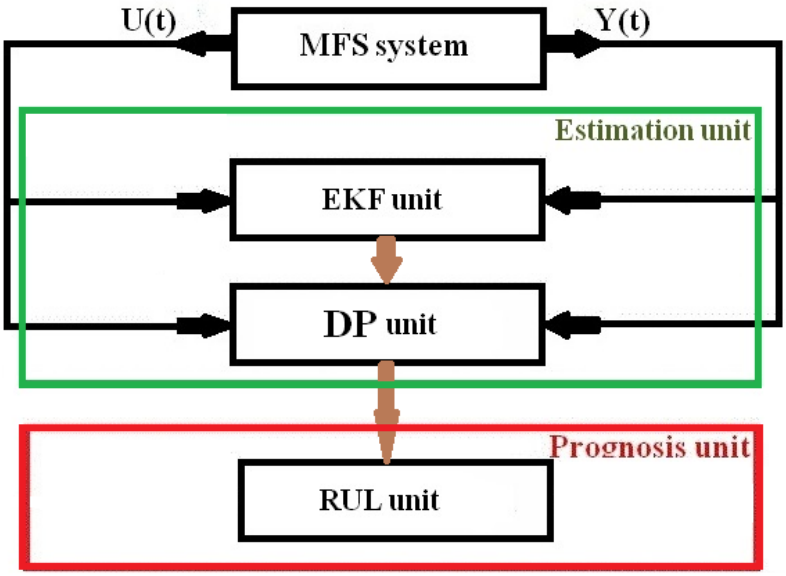

Figure 6.1: The structure of the proposed prognosis system.

6.2.1 MFS System Faults

In general, three types of faults, i.e., mechanical, electrical, and sensor faults can occur in the MFS System. Due to the instantaneous occurrence of the electrical and sensor faults and their abrupt effect on the behavior of the system, they cannot be evaluated for failure degradation analysis [129]. Therefore, only mechanical faults have been considered in here.

Table 6.1 illustrates a list of potential failures in the MFS system. However, a posteriori effects of the faults are addressed here as failures. These effects could be initiated by one or more priori factors. For instance, the null current bias shift fault is usually caused by altering the stiffness of the spring or by component's aging. This fault always causes a slow degradation path in the MFS. However, the MFS system needs to be re-calibrated after this failure to operate healthy again. Another critical failure is actuator leakage coefficient which could be caused by different primary factors such as nozzle deformation, restructuring in flapper or even orifice [11]. The actuator leakage induces a fast nonlinear degradation dynamic in the PCU. Internal

Table 6.1: The MFS System Fault Types.

Failure parameter	Description
ΔI_0	Null current bias shift
ΔC_L	Actuator leakage coefficient degradation
ΔQ	Internal leakage

leakage is another failure which can usually be the result of spool corners wearing.

Identifying a priori factors causing failures is not an easy task since a number of failures may have the same fault signatures on the measurements. Moreover, when a failure occurs, it may, in turn, lead to other failures. Therefore, isolating the main factor or root cause of the problem is prohibitively difficult. This thesis considers three broad failures: a) the EHSV null bias current (ΔI_0), b) actuator leakage coefficient (ΔC_L), and c) internal leakage (ΔQ) which are the most prominent mechanical degradations in the MFS. In the appendix, the mathematical model of the faulty component is provided.

6.2.2 The EKF method

Kalman Filter [156, 157] is an optimal filter with respect to a linear quadratic cost function. Given a linear system described in state space form in the presence of uncorrelated plant and measurement Gaussian noise, the KF algorithm only requires present measurements and the previously estimated state of the system to provide optimal state estimation. The algorithm is well suited for real-time applications and can be applied to nonlinear systems using the Extended Kalman Filtering (EKF) approach.

The discrete KF algorithm involves a two-step process including prediction and updating. The KF algorithm estimates the current state variables with their uncertainties in the prediction step. Then, the state estimate is corrected when the next set of measurements becomes available. However, the continuous Kalman filter known as the Kalman-Bucy filter must be applied to the continuous systems. The

main difference between the continuous KF and the discrete KF is that the two-step process in the discrete algorithm are combined together and cannot be distinguished from one another in the continuous case [158].

The continuous EKF algorithm considers the system model as a differential non-linear equation in state space form as follows:

$$\dot{x}(t) = f(x(t), u(t)) + w(t) \tag{6.1}$$

$$z(t) = h(x(t)) + v(t) \tag{6.2}$$

where $x(t)$ is a vector of the state variables, $u(t)$ is the control signal or system input, $z(t)$ is the measurement/outputs. Functions $f(x(t), u(t))$ and $h(x(t))$ are non-linear functions representing the system and output dynamics, respectively. Moreover, $w(t)$ is a zero-mean, Gaussian distributed process noise and $v(t)$ is also a zero-mean, Gaussian distributed measurement noise which is uncorrelated with $w(t)$. The state estimation using the continuous EKF algorithm can be obtained as follows:

$$\dot{\hat{x}}(t) = f(\hat{x}(t), u(t)) + K(t)[z(t) - h(\hat{x}(t))] \tag{6.3}$$

where $\hat{x}$ denotes the estimated state and $K(t)$ is Kalman Gain at each sampling time. The Kalman Gain is computed as follows:

$$\dot{P}(t) = F(t)P(t) + P(t)F(t)^T - K(t)H(t)P(t) + Q(t) \tag{6.4}$$

$$K(t) = P(t)H(t)^T R(t)^{-1} \tag{6.5}$$

where $F(t)$ and $H(t)$ are linearised system and output matrices, respectively, and can be obtained as follows:

$$\begin{aligned} F(t) &= \frac{df}{dx}|_{\hat{x}(t),u(t)} \\ H(t) &= \frac{dh}{dx}|_{\hat{x}(t)} \end{aligned} \tag{6.6}$$

Furthermore, $Q(t)$ and $R(t)$ are the covariance matrices of the process noise and measurement noise at each sampling time, respectively. Matrix $P(t)$ denotes the state covariance at each sampling time.

In this study, the healthy model is employed in the EKF algorithm. Therefore, the observation made by the EKF are not affected by faults or degradation of the system parameters. Hence, assuming that the system's mathematical model is an accurate representation of the actual system, any difference between the system's actual output and that estimated by the EKF can be attributed to the presence of a fault. This difference, known as residual or innovation process of the filter, is defined as follows:

$$res = z(t) - h(\hat{x}(t)) \tag{6.7}$$

where $z(t)$ is system output and $h(\hat{x}(t))$ is estimated system output.

6.2.3 Transformation for estimating the degradation path (DP)

The residual obtained in Eq. 6.7 shows the progress of the failure in the system. It is noted that the severity of the failure is a nonlinear function of residual and system's set point. Moreover, the slope of the residual profile generated is dependent on the set point value and the fault scenario in the system.

In the literature, different transformations are performed in prognosis task [159–161]. In this chapter, we introduce a new transformation to facilitate the prediction of RUL. The transformation, DP (degradation path), is defined as follows:

$$DP = (1 - \left|\frac{res}{setpoint}\right|) \times 100 \tag{6.8}$$

where res is the residual of the system output. The DP, as defined above, is a performance assessment measure for the system and quantifies how close the system is functioning with respect to the healthy system.

6.2.4 The remaining useful life (RUL) unit

The RUL task is to predict the remaining lifetime of the system before a complete failure. The complete failure is considered as an inability of the system to satisfactorily perform its duty [147]. The prognosis algorithm is divided into two stages. The first stage is the health monitoring of the system before the onset of a fault in the system. The second stage starts from the first detection time until the system reaches complete failure state defined by an appropriately chosen criterion. The RUL is formulated as the time difference between the predicted end of life, $t_{failure}$ and the time at which the prediction is made, $t_{prediction}$, as follows:

$$RUL = t_{failure} - t_{prediction} \tag{6.9}$$

An adaptive algorithm is developed by Bayesian theorem to predict the RUL using available data of the degradation path. The proposed method is suitable for online prediction of the future status of the faulty system with uncertainty exists in the prediction horizon. Figure 6.2 presents the proposed RUL method based on Bayesian theory.

It is noted that a recursive optimal affine function of time is identified in a sliding window as follows:

$$y_t = \hat{m}t + \hat{n} + e_t \tag{6.10}$$

where $e_t \sim N(0, \sigma^2)$ represents a Gaussian white noise error with zero mean and variance σ^2. Thus, y_{t_0} is a Gaussian random variable with the distribution $N(\hat{m}t_0 + \hat{n}, \sigma^2)$, and j step ahead output prediction is also a Gaussian random variable with the following distribution characteristics:

$$\hat{y}_{t_0+j} \sim N(\hat{y_0} + mj, (j+1)\sigma^2) \tag{6.11}$$

Assume a fault is diagnosed in the system at time t_0 and the system is still functioning and healthy until it reaches a complete failure. Thus, a probability space can

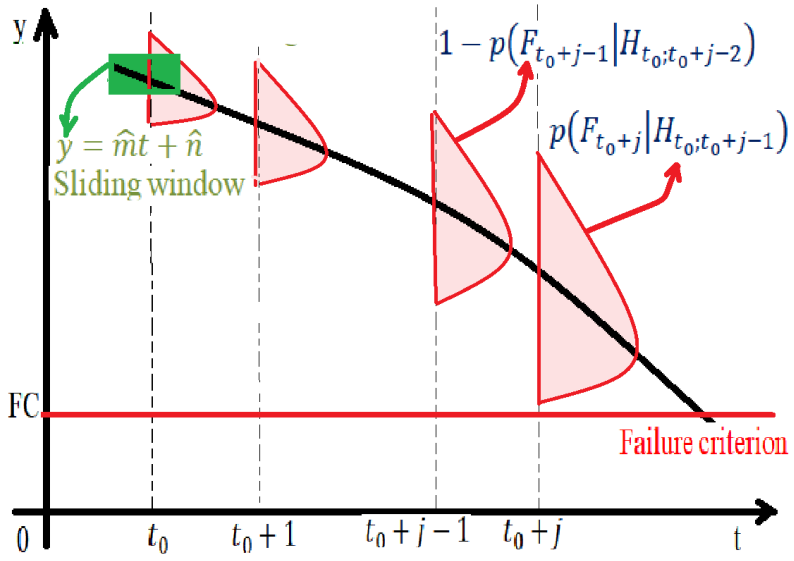

Figure 6.2: The proposed RUL method based on the Bayesian theory.

be considered as follows:

$$\Omega_{failure} = \{H_{t_0}, H_{t_0+1}, \ldots, H_{t_0+j-1}, F_{t_0+j}\} \tag{6.12}$$

where $\Omega_{failure}$ presents the probability space with all healthy and failure samples. Variable H_{t_k} is a healthy condition at time t_k, and variable F_{t_k} is faulty condition at time t_k. These variable conditions can be modelled as Bernoulli sequence which is remained healthy until a complete failure at time $t_0 + j$. Then, the probability of failure at $t = t_0 + j$ is formulated using conditional probability as follows [148]:

$$p(F_{t_0+j}) = \frac{p(F_{t_0+j}, H_{t_0:t_0+j-1})}{p(H_{t_0:t_0+j-1}|F_{t_0+j})} \tag{6.13}$$

where $p(F_{t_0+j})$ indicates probability of failure at $t = t_0+j$. Function $p(F_{t_0+j}, H_{t_0:t_0+j-1})$ is the probability of staying healthy until $t = t_0 + j - 1$ and occurring a failure at $t = t_0+j$. Function $p(H_{t_0:t_0+j-1}|F_{t_0+j})$ is the probability of staying healthy subject to a failure at $t = t_0+j$. If a failure occurs at $t = t_0+j$, the times before the occurrence of the failure, the system is healthy. Because, a complete failure can happen only one

time. Therefore, $p(H_{t_0:t_0+j-1}|F_{t_0+j})$ is equal to one. Due to these fact and using joint probability definition Equation 6.13 can be simplified as follows:

$$p(F_{t_0+j}) = p(F_{t_0+j}|H_{t_0:t_0+j-1})p(H_{t_0:t_0+j-1}) \tag{6.14}$$

where $p(H_{t_0:t_0+j-1})$ represents probability of being healthy until $t = t_0 + j - 1$. Probability $p(F_{t_0+j}|H_{t_0:t_0+j-1})$ is known as the likelihood function is computed as follows:

$$\begin{aligned} p(F_{t_0+j}|H_{t_0:t_0+j-1}) &= p(y_{t_0+j} > FC) \\ &= Q(\frac{FC - [\hat{m}(t_0+j) + \hat{n}]}{\sigma\sqrt{j+1}}) \end{aligned} \tag{6.15}$$

Function Q represents the tail of the standard probability Gaussian distribution which is provided by normal distribution probability look-up table or can be computed with a Matlab software code. Parameter FC is the complete failure criterion.

Remark 6-1: Parameter FC is selected with respect to the type of the failure. It is noted that the type of failure can be identified by fault diagnosis method. In this research, we consider that the type of failure is known and only prognosis task is required to be performed due to space limitation.

After computing the likelihood function, Function $p(H_{t_0:t_0+j-1})$ can be obtained using the properties of probability theory as follows:

$$\begin{aligned} p(H_{t_0:t_0+j-1}) &= [1 - p(F_{t_0+1}|H_{t_0})] \times [1 - p(F_{t_0+2}|H_{t_0:t_0+2})] \\ &\cdots \times [1 - p(F_{t_0+j-1}|H_{t_0:t_0+j-2})] \end{aligned} \tag{6.16}$$

The failure probability sequences, $p(F_{t_0+j})$, is a monotonically increasing sequence until reaching a maximum at a prediction horizon j. That maximum is the RUL of the system.

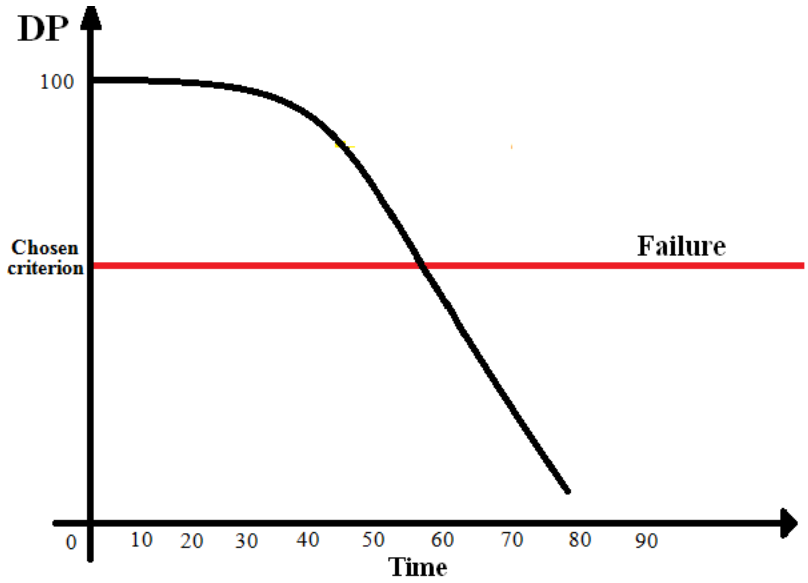

Figure 6.3: The DP curve and the chosen criterion for fault prognosis.

6.3 Design implementation and test results

In this section, different test studies have been developed to verify the performance of the proposed fault prognosis system. First, we shall outline the suggested faulty scenarios. Then, the design implementation is illustrated. Finally, different simulation tests are performed, and the results are discussed.

6.3.1 Faulty scenarios

Various failure paths including null current bias shift, actuator leakage or internal leakage are injected into the simulation model of the MFS system to generate different faulty scenarios. The estimated DP curve is utilized to define different criteria for condition monitoring (CM) maintenance. Figure 6.3 depicts the DP curve and the chosen criterion for fault prognosis.

Different failures can be initiated by various root causes. Therefore, they are distinct in nature and manifest themselves differently with different dynamic behaviors. For instance, null current bias shift has a slow effect on the output. The health system

Table 6.2: Healthy values and failure criterions

Failure parameter	Healthy value	Criterion at set point 1.4	Complete failure criterion (FC)
I_0	$2 \pm 0.4(mA)$	$6(mA)$	98%
C_L	$0(cis/psi)$	$3(cis/psi)$	97%
Q	$0(cis/psi)$	$1.4(cis/psi)$	97%

has a null bias of $2 \pm 0.4(mA)$, and changes in the null bias in the range of 1.6 to 2.4, do not affect the output of the MFS in a considerable way, and thus, such effects are not normally observable. The output, however, starts to degrade with a mild slope, if the null bias is out of the range $[1.6, 2.4]$ reaching to 98% of the set-point when null bias is $6.0(mA)$ at set point 1.4. It is noted that the system is nonlinear, and the null bias has a different value within the range of $[5.0, 6.0](mA)$ when the output of the system is 98% with respect to different set points. In this study, the threshold of 2% of degradation with respect to set-point is chosen as the criterion to recognize a complete failure in the null bias. Table 6.2 illustrates the healthy values and criteria for the various failures.

The healthy value for actuator leakage coefficient is $0(cis/psi)$. The actuator leakage failure leads to a sharp degradation of the output and when output degrades to 96.6, the failure dynamic drops abruptly. Therefore, the failure criterion of 97% is selected for the actuator leakage coefficient failure which occurs at $3psi$ for the set point of 1.4. Finally, the same criterion is selected for internal leakage.

To avoid and eliminate the effect of the disturbance and noise on RUL estimation, degradation is considered to have occurred once DP estimated curve declines to 99.8%. For any value of $DP \geq 99.8$, the system is considered to be healthy and no RUL estimation is launched.

6.3.2 The design implementation of the proposed prognosis method

In this subsection, design implementation is demonstrated. The proposed method takes the input signal (the command current, I_{cmd}) and the system output (LVDT

sensor data, $X_P(t)$) and estimates the state variables using EKF method formulated in Eq. (6.3) and Eq. (6.6). Then, residual is calculated by the system output (LVDT sensor data, X_P) and estimated state variable $\hat{X}_P(t)$ using Eq. (6.7). Meanwhile, the DP curve is constructed using transformation by Eq.(6.8). Afterward, an optimal affine function of time is identified by Eq. (6.10). Then, the likelihood and probability of failure $t = t_0 + j$ are computed by Eqs. (6.15) and (6.14), respectively. Finally, the prediction horizon j at which the failure probability is maximum is the RUL of the system.

To evaluate the proposed prognosis method, the relative accuracy (RA) measure is employed as follows [58, 150]:

$$RA = 1 - \frac{|RUL_{real}(t) - RUL_{predicted}(t)|}{RUL_{real}(t)} \tag{6.17}$$

where RUL_{real} is the real amount of the RUL calculated when the system has reached its end of life and $RUL_{predicted}$ is the predicted RUL at real time. The RA is a positive value between 0 and 1, and larger value of the RA signifies a better accuracy of the RUL method.

6.3.3 Simulation Results

In the following, five different fault scenarios are considered in the MFS system and the performance of the system is discussed.

1. **Null current bias**

   (a) Fast Fault

   A null current bias shift with a slope of 0.01 is injected in the MFS at $t = 5$ *sec* (see Eq. 6.18). The setpoint is adjusted on $X_{p_{ref}} = 1.4$. Figure 6.4 depicts the output of the LVDT sensor, the EKF estimator, and progress of the failure based on residual estimation.

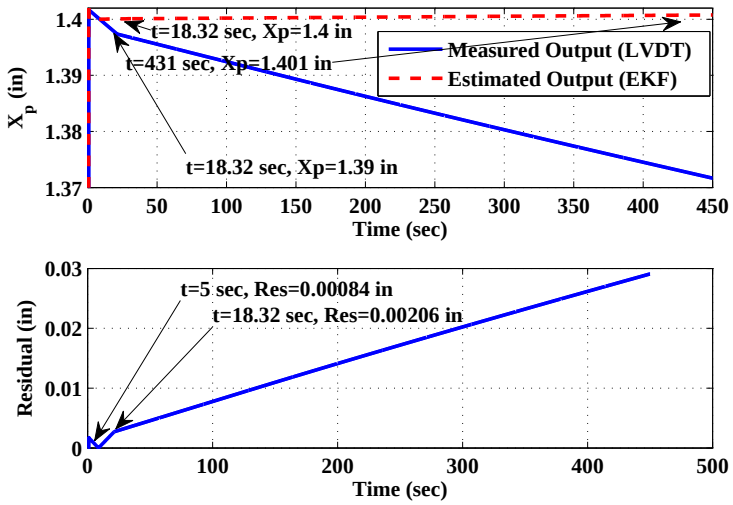

Figure 6.4: Failure caused by null current bias shift (fast fault).

$$\Delta I_0 = \begin{cases} 0 & t \leq 5 \\ 0.01t & t > 5 \end{cases} \tag{6.18}$$

It can be seen from the Figure 6.4 that the measured output of the system begins to degrade after $t = 18.32$ *sec*. However, the estimated output by the EKF method tracks the setpoint value with a very small influence caused by fault due to the fact the system model employed in EKF algorithm is healthy, and the controller compensates for the fault. Therefore, the difference between the measured output and the estimated output known as the residual starts to increase as the fault progresses. The estimated residual is considered as the progress of the failure. Figure 6.5 shows the estimated DP and RUL of the system under the injected null bias failure.

The DP curve reaches the value of 99.8% at $t = 22.12$ *sec*. The RUL initiates the estimation of the useful remaining life at $t = 24$ *sec*. However, the RUL method takes 1.88 *sec* to estimate a meaningful value for the remaining useful life. This gap depends on the nature of the degradation

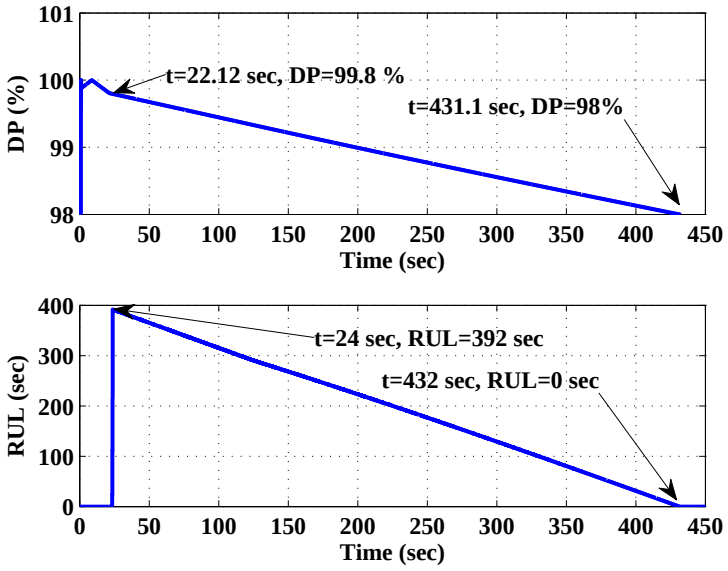

Figure 6.5: Failure caused by null current bias shift (fast fault).

dynamics, the set point and also the size of the sliding window for the regression method. The RUL of the system is estimated to be 392 *sec* at $t = 24$ *sec* which decreases as the time progresses. The RUL estimates the end of system lifetime at $t = 432$ *sec* which is almost near the DP value at 98%. Furthermore, the RA performance index of the system calculated by Eq. 6.17 is 96% at $t = 24$ *sec*.

Figure 6.6 shows the proposed RUL method based on the Bayesian algorithm at $t = 24$ *sec*.

It is indicated from Figure 6.6 that likelihood reaches to 1 at 392 *sec*. Moreover, the failure probability sequence has a maximum probability at $t = 392$ *sec* which denotes the RUL of the system at $t = 24$ *sec*.

(b) Moderate Fault

Another failure dynamic like Eq. (6.18) with a slope of 0.001 is considered in null bias. Figure 6.7 shows the MFS LVDT sensor, the EKF estimation and the progress of the failure.

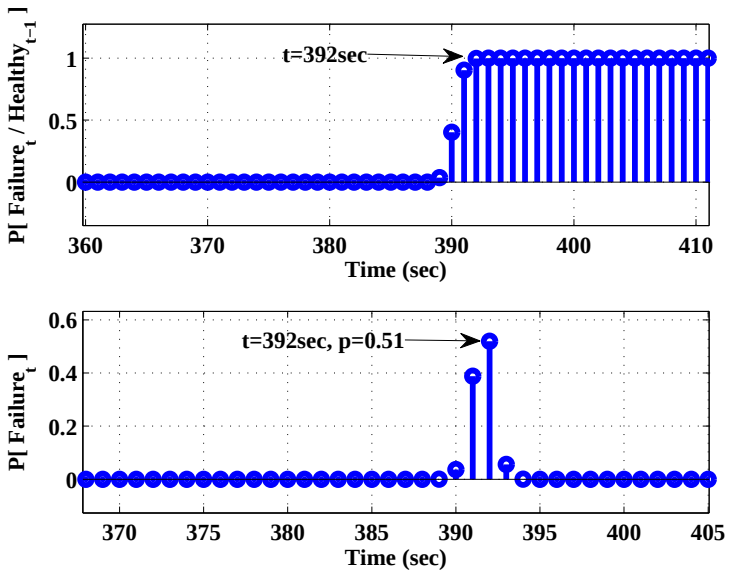

Figure 6.6: Failure caused by fast null current bias shift (Bayesian algorithm).

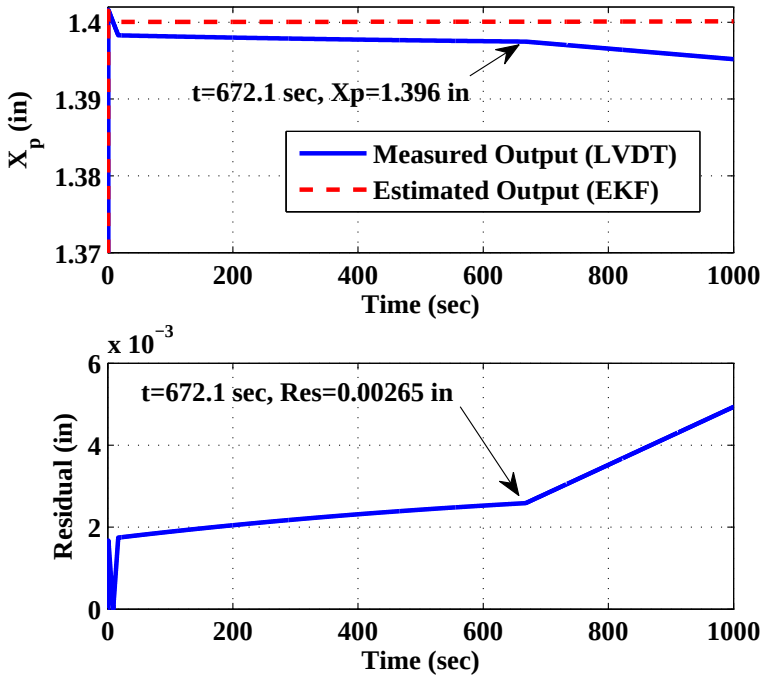

Figure 6.7: Failure caused by null current bias shift (Moderate fault).

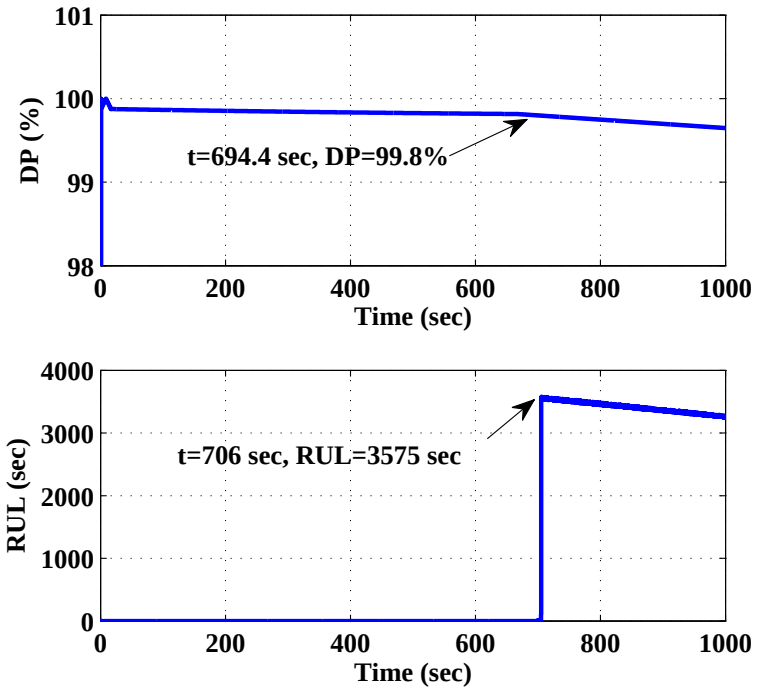

Figure 6.8: Failure caused by null current bias shift (Moderate fault).

It is noted that although the failure starts at $t = 5$ *sec*, residual dynamics reacts at $t = 672.1$ *sec* due to lack of the observability while the null bias lies in the range of $2 \pm 0.4(mA)$. Figure 6.8 presents the DP and RUL of the system.

Accordingly, the DP reaches to 99.8% at $t = 694.4$ *sec*, and the RUL predicts $t = 3575$ *sec* at $t = 706$ *sec* for the lifetime of the MFS. It is interesting to note that this value is in compliance with the results achieved for fast null-bias fault. The failure dynamics reduces with a slope ten times slower than the fast failure, and therefore we expect to reach the end of life of the system ten times slower compared to the fast failure which is actually what has been attained here.

Similarly, Figure 6.9 presents the prognosis method based on the Bayesian algorithm at $t = 706$ *sec*. It is seen from Figure 6.9 that likelihood increases

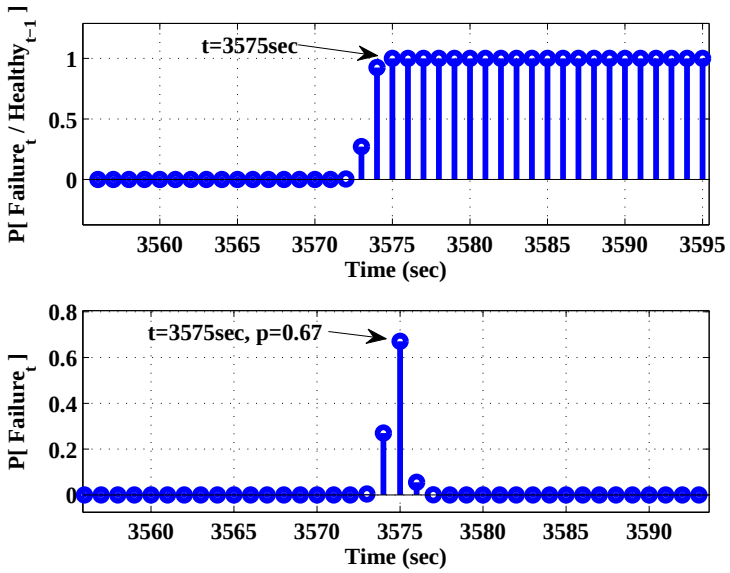

Figure 6.9: Failure caused by moderate null current bias shift (Bayesian algorithm).

to 1 at 3575 *sec*. Furthermore, the probability of failure reaches a maximum at $t = 3575$ *sec* which indicates the RUL at $t = 706$ *sec*.

2. **Actuator leakage coefficient degradation**

(a) Moderate Fault

An actuator leakage fault with a slope of 10^{-5} is considered by the following equation:

$$\Delta C_L = \begin{cases} 0 & t \leq 5 \\ 10^{-5}t & t > 5 \end{cases} \tag{6.19}$$

The actuator leakage coefficient failure causes rapid degradation. Therefore, the failure with the slope of 10^{-5} may cause a moderate effect. Figure 6.10 displays the output of the LVDT sensor, the EKF estimator and the progress of the failure.

It is noted from the Figure 6.10 that the actuator leakage coefficient failure

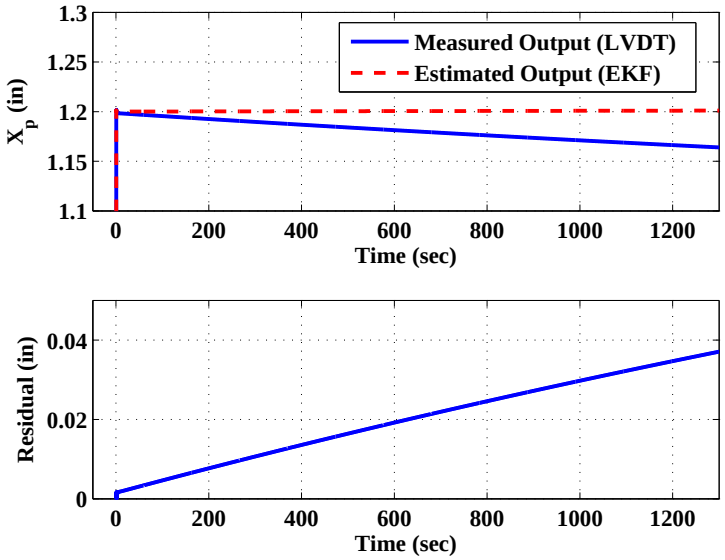

Figure 6.10: Failure caused by actuator leakage coefficient degradation (Moderate fault).

has a sharp residual growing. Figure 6.11 presents the DP and RUL of the system.

The DP has the value of 99.80% at $t = 27.72$ *sec* and the prognosis system detects the fault at $t = 29$ *sec* with the RUL of $t = 1075$ *sec*. The DP becomes 97% at $t = 1255$ *sec* at which time the lifetime of the system is ended. The RA index at $t = 29$ *sec* is 97%.

(b) Slow Fault

A slow failure with a slope of 10^{-7} is considered in the actuator leakage coefficient. Figure 6.12 displays the output of the LVDT sensor, the EKF estimator and the progress of the failure.

The residual shows a very smooth degradation path. This is due to the slow slope of the failure dynamics. Figure 6.13 presents the DP and RUL of the system.

It is clear from the Figure 6.13 that the DP has a prolonged rate with a value of 99.8 at $t = 2177$ *sec* which initiates the RUL unit. The RUL

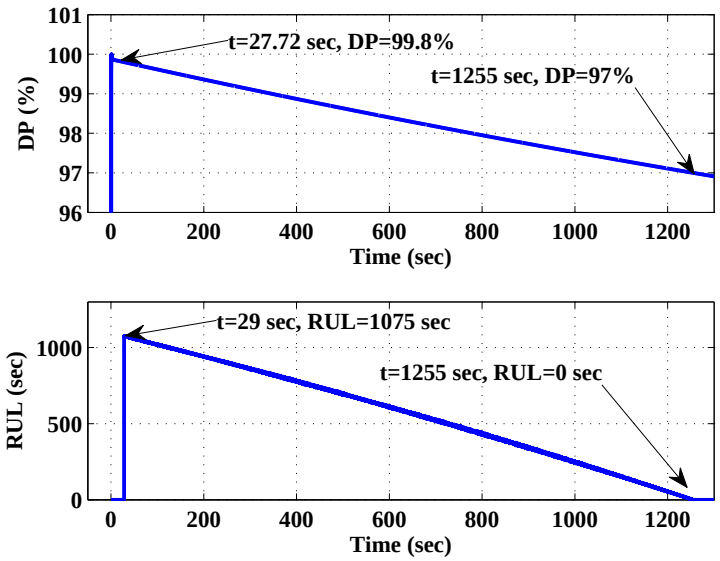

Figure 6.11: Failure caused by actuator leakage coefficient degradation (Moderate fault).

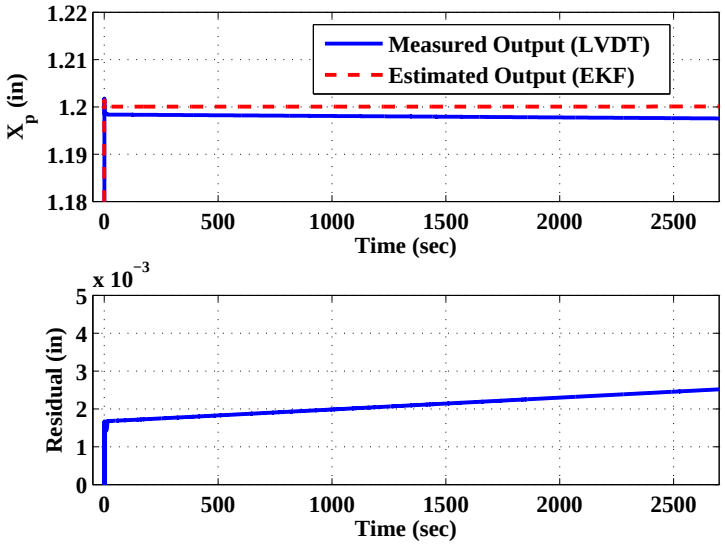

Figure 6.12: Failure caused by actuator leakage coefficient degradation (Slow fault).

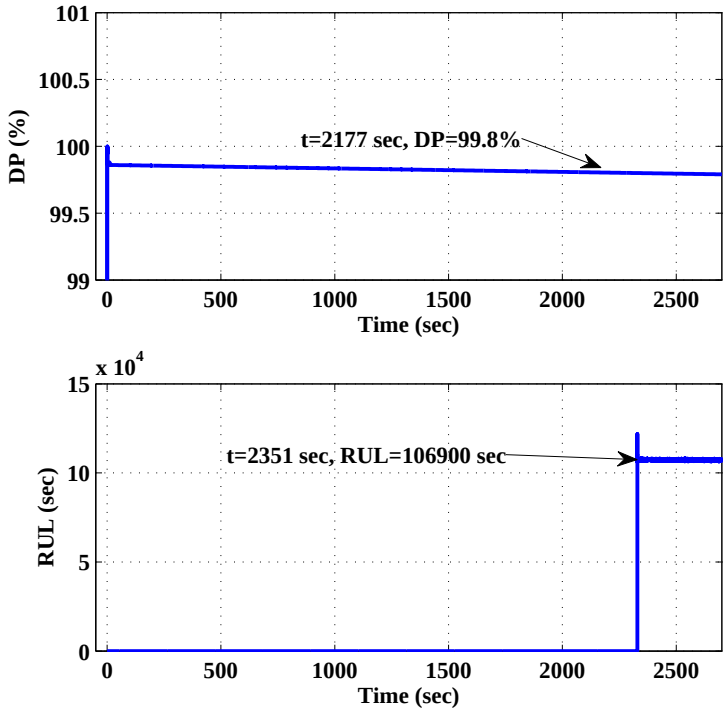

Figure 6.13: Failure caused by actuator leakage coefficient degradation (Slow fault).

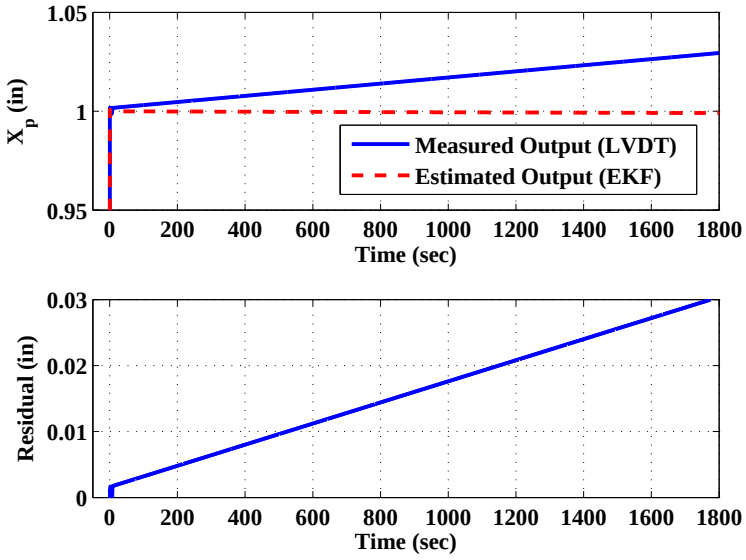

Figure 6.14: Failure caused by internal leakage.

predicts a time of 106900 for the lifetime at $t = 2351$ *sec*. It is noted that the predicted lifetime in this slow degradation is almost 100 times longer than the moderate one which is the result of lowering down the slope of the failure by 100 times.

3. **Internal leakage**

An internal leakage fault path with a slope of 0.001 is injected into the system by the following equation:

$$\Delta Q = \begin{cases} 0 & t \leq 5 \\ 0.001t & t > 5 \end{cases} \tag{6.20}$$

Figure 6.14 illustrates the output of the LVDT sensor, the EKF estimator and the estimated residual of the output.

Similarly, the residual has a sharp slope as internal leakage progresses fast in the system. Figure 6.15 depicts the DP and RUL of the system.

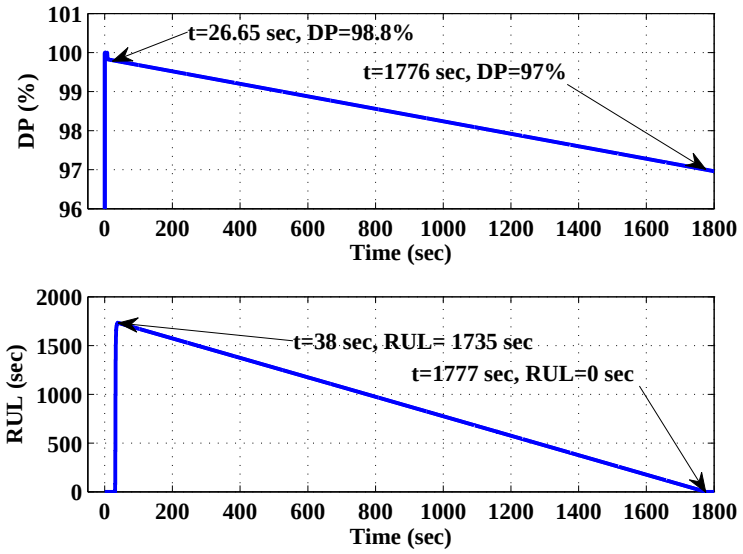

Figure 6.15: Failure caused by internal leakage.

The DP reaches 99.8% at $t = 26.65$ *sec* and the proposed fault prognosis detects the starting time of the failure. However, the RUL predicts a value of 1735 *sec* for the lifetime of the system at $t = 38$ *sec*. The RA index at $t = 38$ *sec* is 99% which indicates an accurate prognosis system.

4. **Null current bias + actuator leakage coefficient**

The proposed prognosis system can handle simultaneous failures. To examine this property, two dynamic faults formulated by Eqs.(6.18) and (6.19) are considered in the system. Figure 6.16 displays the output of the LVDT sensor, the EKF estimator, and the residual estimation.

It is indicated from the figure that rate of changes in residual is more than the changes in individual suggested failures. Figure 6.17 displays the DP and RUL of the system.

It is noted the criterion for the RUL is chosen 97.5 which is the average of the two individual proposed failures. The value of DP is 99.8% at 14.31s *sec*, a faster detecting in comparison with the individual fault. The RUL method forecasts a

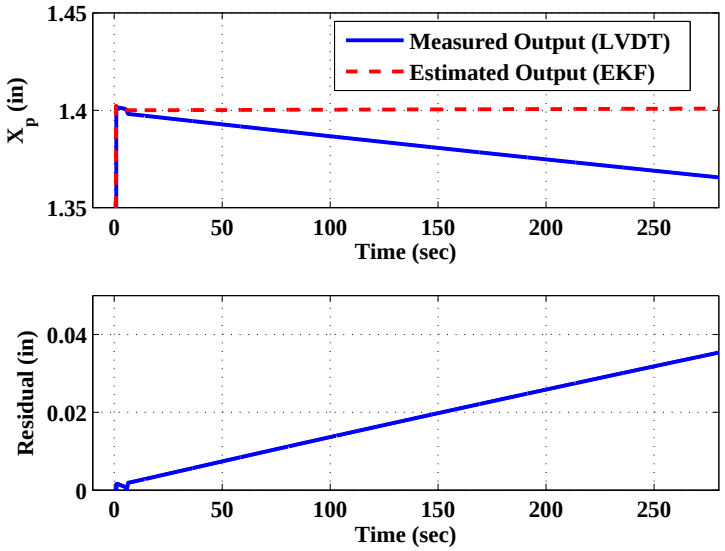

Figure 6.16: Failure caused by an actuator leakage coefficient and a null current bias.

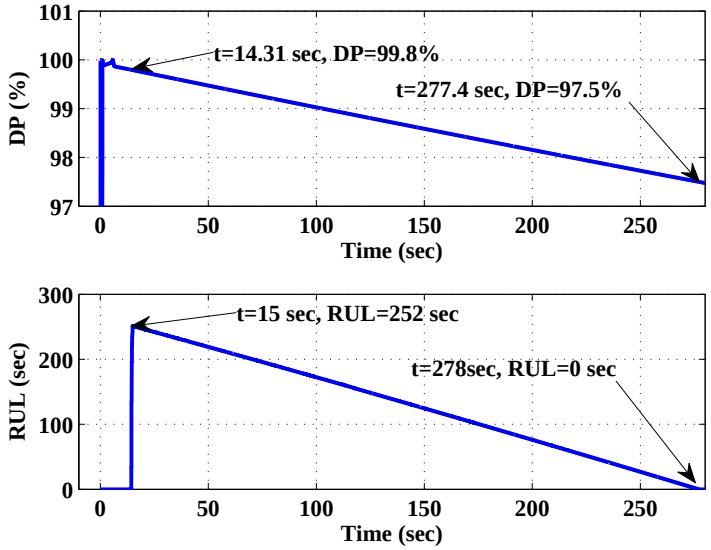

Figure 6.17: Failure caused by an actuator leakage coefficient and a null current bias.

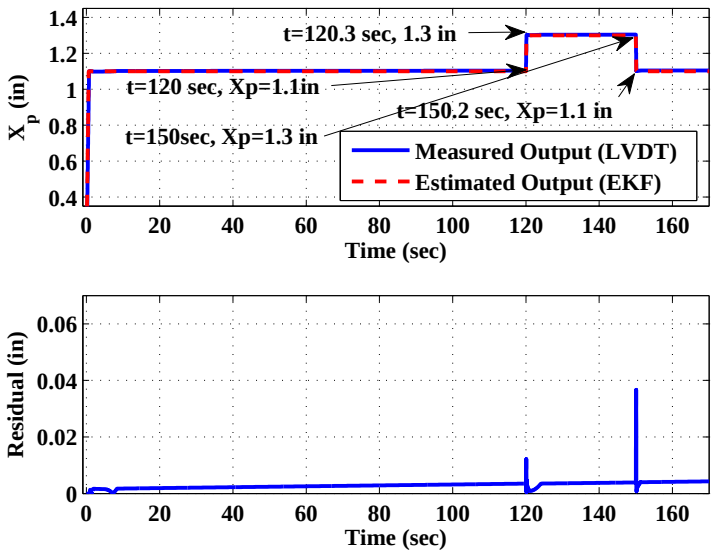

Figure 6.18: The performance of the system under set point tracking.

value of 252sec for the system at 15 sec. The RA index for the MFS at 15 sec is 95%.

5. **Performance of the prognosis system under setpoint tracking**

   An internal leakage is injected in the system by Eq. (6.20), and a square-wave set point is considered where the setpoint is changed from 1.1in to 1.3in at $t = 120sec$ and goes back to 1.1in after 30sec. Figure 6.18 displays the output of the LVDT sensor, the EKF estimator, and the residual estimation.

   It is clear from the Figure 6.18 that the output of the system and the EKF observer can track the signal. However, there is a jump in the residual whenever the setpoint is changed. Figure 6.19 displays the DP and RUL of the system.

   It can be seen from the Figure 6.19 that the RUL has a value of 1865 sec just before changing the set point at $t = 120sec$. Then, it goes to zero due to a sharp increase in the DP curve. The RUL recovers itself with a value of 2303sec after 7sec at $t = 127sec$. However, it should be noticed that this value is different from the previous value which is due to the nonlinear behavior of the system at

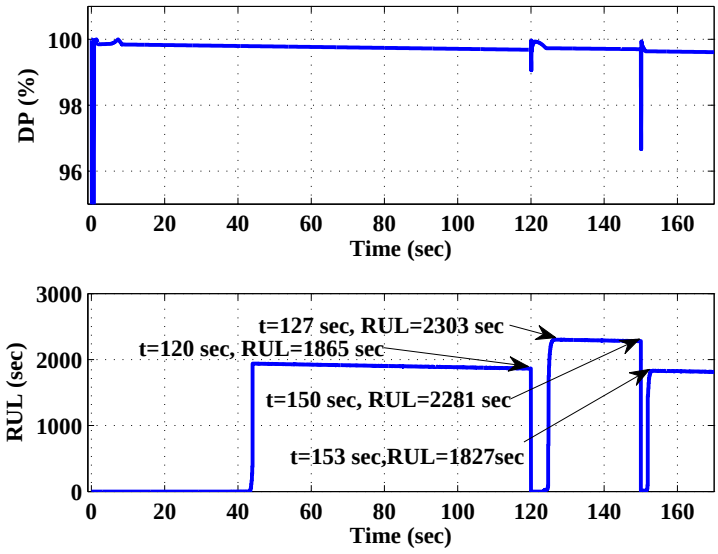

Figure 6.19: The performance of the system under setpoint tracking.

different set points. Finally, RUL goes back to 1827 *sec* at 153 *sec* as a result of returning to the previous setpoint. It is worthwhile to note that the RUL unit can maintain its performance under changes in the setpoint which is likely to occur in practice.

6.4 Conclusions

A model-based prognosis method was introduced to discover the degradation model of the failures in the MFS system. An EKF was used to generate residuals and to capture the progress of the failure. Then, a transformation was made to estimate the degradation path (DP) in the system. Then, the RUL of the system was predicted by using a recursive Bayesian method.

The main advantage of the fault prognosis system was its model-based method which improved the accuracy of the system using residual generation and then transformation. Furthermore, the RUL algorithm identified an optimal affine function of time using available data of the degradation path (DP) and provided a remaining

lifetime of the system based on Gaussian probability theory which was suitable with uncertainty inherited in the prediction horizon and it was also proper for real-time implementation of the system.

Moreover, RA measure was utilized to evaluate the performance of the proposed prognosis method. The simulation results showed the capability of the proposed prognosis system not only for the different individual failures but potentially for simultaneous failures.

Chapter 7

Conclusions and Future Work Suggestions

We believe that fault diagnosis and failure prognosis are essential fields of study for future of safety-critical systems. They present an opportunity to move from the current methodology of maintenance which is based on constant time interval to advanced condition-based maintenance. The new maintenance method may have a better cost-benefit and even provide more reliable framework due to effective monitoring of the system. To reach this goal, however, the existing challenges regarding the monitoring, and safety should be adequately addressed. Thus, this area provides an exciting field of research with enticing challenges and numerous opportunity. Our hope is that this thesis may shed some light on the monitoring, fault diagnosis and failure prognosis challenges for safety-critical systems, and planted some ideas that might grow to become mainstream in the future. In this chapter, we summarize and point out the main results that have been achieved in this thesis. Besides, several directions and ideas for future research are presented.

7.1 Conclusions and Contributions

In this thesis, the problem of fault diagnosis and failure prognosis for safety-critical systems was investigated from multiple angles. In this regard, three novel approaches were examined on two safety-critical systems. The concluding remarks of each developed methodology would be briefly outlined in the following sections.

7.1.1 Data-driven FDP Approach Using a Few Numbers of Measurements

A new data-driven method based on divide and conquer strategy was employed for the fault diagnosis and prognosis in MFS system. The MFS system included several highly nonlinear components with uncertainty in their structures. It also had two measurements available for monitoring purposes. Therefore, health monitoring of this system was extremely difficult and challenging work. The proposed methodology could split the FDP task into three subtasks named fault detection and diagnosis (FDD) task, failure parameter estimation task, and remaining useful life (RUL) task. The proposed structure reduced the computational complexity and increased preciousness of both fault diagnosis and failure prognosis systems.

The proposed FDD method was developed by a combination of NN and DWT methods. The DWT applied wavelet transform and obtained the decomposition sequences of the measurement signal and analyzed them using fuzzy rules to isolate a fault in the system. We showed that the DWT could only detect actuator leakage and internal leakage in the system, but failed to identify null bias failure. However, when the DWT combined with the NN method, the accuracy of the system increased in comparison with implementing the NN method alone. Moreover, we had more reliability in isolating types of failures.

After isolating the type of the failure, failure parameter estimation unit observed the failure parameter using a distributed system of three parallel neural networks. It was shown that the distributed system enhanced the accuracy of the failure parameter

in comparison with a centralized neural network. Finally, the lifetime of the system was predicted using an optimal Bayesian method. The accuracy of the RUL was investigated by relatively (RA) index.

7.1.2 Data-driven FDP Approach Using a Multi-sensor Data Information

Multi-sensor data integration is the best choice whenever several sensors are available for health monitoring systems. A novel FDP approach was designed for hydro control valve system. The primary goal was to utilize real-time information of system through measurements of multiple sensors and improved the accuracy of the FDP system.

For this purpose, first, type of a fault was identified based on feature selection and SVM methods. An incremental feature selection method using correlation formula was used to choose highly correlated sensors as the inputs of the SVM classifier. For classification task, RBF nonlinear function was considered along with one against one strategy to perform the problem of the multi-classes. The proposed FDD system could raise the accuracy of isolation unit and provided a highly reliable system. Then, a distributed ANFIS network was used to estimate the failure parameter. Similarly, a recursive Bayesian algorithm was developed to forecast the lifetime of the system. It was also shown that the proper sensor selection could significantly increase the performance of the prognosis task.

7.1.3 Model-based FDP Approach Using an Integrated EKF Method and Bayesian Algorithm

Model-based methods could provide an accurate prognosis results if a high fidelity model of the system is available. A novel prognosis method was proposed in this thesis for MFS system. For this aim, a residual estimation method using extended Kalman filter was implemented to capture the nonlinearity of the failure dynamic. Then, a new measure, DP, was defined using a transformation to model the degradation path. After this stage, the DP is considered to forecast the RUL of the system via

the Bayesian algorithm. The Bayesian algorithm is cooperatively in touch with the real-time data of the DP to provide an optimal prediction of the RUL.

7.1.4 Contributions

The most important contributions of this thesis are summarized as follows:

1. To the best of our knowledge, the proposed data-driven method based on divide and conquer strategy was the first attempt to split the FDP tasks and increase the performance of the FDP system. The nature of the algorithm made it possible to employ subtasks to ease the problem and achieved more accurate results.

2. Using a distributed system for failure parameter estimation unit reduced computational complexity and also decreased the error of the system in training and testing phases in comparison with a centralized system. It is worth to mention that the estimated parameter was used to identify an optimal model for the prediction of the RUL. Therefore, a higher accuracy of the estimation task would result in an increase in the performance of the prognosis task.

3. Applying real-time optimal Bayesian algorithm led to an effective approach for prediction of the RUL. Furthermore, this unit was recursively in touch with the real-time data of degradation path that helped to enrich the quality of the prediction.

4. Utilizing multi-sensor data information for the FDP system led to more accurate and reliable isolation in FDD unit and also improved the accuracy of parameter estimation and finally helped to have a accurate measure of RUL.

5. Another main novelty was to apply the concept of residual estimation for capturing the nonlinearity of the degradation dynamic using EKF method. It helped us to cope with complicated dynamics of the MFS system and had an accurate prediction.

6. Considering transformation was another contribution of the thesis. The proposed transformation assisted in modeling the degradation path.

7.2 Future Work

We believe that health monitoring of safety-critical systems would be an important field of research in the years to come and have the potential to provide a safe and appropriate framework for condition-based maintenance. In the following, we review some directions that seem promising for future research efforts in this field.

1. Concurrent failures

   Considering concurrent failures occurs in the system and developing methods to isolate them and predict the RUL of the system.

2. Considering complex dynamics for failures

   Dynamics of the failure can have more complex structure and lead to more difficulties for the prognosis task. We modeled a failure with ramp function and identified it with an optimal linear affine function of time using the Bayesian algorithm. However, nonlinear failures can occur and also, a failure may lead to another failure which makes the prognosis task more difficult to solve.

3. Apply particle filter for the task of prognosis

   Particle filter is a proper method for the task of fault diagnosis and failure prognosis. This method is perfect to capture the nonlinear dynamics and achieve an accurate result. However, it should be noted that it also increases the computation which may be a negative aspect for the real-time implementation of the method.

4. Utilizing fuzzy logic method for prognosis task

   Fuzzy logic membership functions can be applied to obtain multiple models to capture the nonlinear dynamics of the degradation path and improve the

performance of the prediction.

5. Using an online performance monitoring with the task of the prognosis

   The prognosis task is always unreliable due to uncertainties exist in the prediction horizon of the failure. Therefore, it is often desirable to perform an online performance assessment to evaluate the accuracy of the prognosis.

References

[1] D. Gucik-Derigny, R. Outbib, and M. Ouladsine, "A comparative study of unknown-input observers for prognosis applied to an electromechanical system," *IEEE Transactions on Reliability*, vol. 65, no. 2, pp. 704–717, 2016.

[2] M. E. Orchard, "A particle filtering-based framework for on-line fault diagnosis and failure prognosis," *PhD thesis*, 2006.

[3] P. Wang and G. Vachtsevanos, "Fault prognostics using dynamic wavelet neural networks," *AI EDAM*, vol. 15, no. 4, pp. 349–365, 2001.

[4] Q. Liu, M. Dong, W. Lv, X. Geng, and Y. Li, "A novel method using adaptive hidden semi-markov model for multi-sensor monitoring equipment health prognosis," *Mechanical Systems and Signal Processing*, 2015.

[5] L. Datong, P. Yu, and P. Xiyuan, "Online adaptive status prediction strategy for data-driven fault prognostics of complex systems," in *Prognostics and System Health Management Conference (PHM-Shenzhen), 2011.* IEEE, 2011, pp. 1–6.

[6] F. Zhao, J. Chen, L. Guo, and X. Li, "Neuro-fuzzy based condition prediction of bearing health," *Journal of Vibration and Control*, vol. 15, no. 7, pp. 1079–1091, 2009.

[7] G. Li, S. J. Qin, Y. Ji, and D. Zhou, "Reconstruction based fault prognosis for continuous processes," *Control Engineering Practice*, vol. 18, no. 10, pp. 1211–1219, 2010.

[8] L. Liao and F. Köttig, "Review of hybrid prognostics approaches for remaining useful life prediction of engineered systems, and an application to battery life prediction," *IEEE Transactions on Reliability*, vol. 63, no. 1, pp. 191–207, 2014.

[9] K. Medjaher, D. A. Tobon-Mejia, and N. Zerhouni, "Remaining useful life estimation of critical components with application to bearings," *IEEE Transactions on Reliability*, vol. 61, no. 2, pp. 292–302, 2012.

[10] M. Daigle and K. Goebel, "Model-based prognostics under limited sensing," in *Aerospace Conference, 2010 IEEE.* IEEE, 2010, pp. 1–12.

[11] K. Zhang, J. Yao, T. Jiang, X. Yin, and X. Yu, "Degradation behavior analysis of electro-hydraulic servo valve under erosion wear," in *Prognostics and Health Management (PHM), 2013 IEEE Conference on*. IEEE, 2013, pp. 1–7.

[12] N. M. Vichare and M. G. Pecht, "Prognostics and health management of electronics," *Components and Packaging Technologies, IEEE Transactions on*, vol. 29, no. 1, pp. 222–229, 2006.

[13] R. Sekhon, H. Bassily, and J. Wagner, "A comparison of two trending strategies for gas turbine performance prediction," *Journal of Engineering for Gas Turbines and Power*, vol. 130, no. 4, p. 041601, 2008.

[14] W. Ahmad, S. A. Khan, and J.-M. Kim, "A hybrid prognostics technique for rolling element bearings using adaptive predictive models," *IEEE Transactions on Industrial Electronics*, 2017.

[15] Z. Wang, J. Zarader, and S. Argentieri, "A novel aircraft fault diagnosis and prognosis system based on gaussian mixture models," in *Control Automation Robotics & Vision (ICARCV), 2012 12th International Conference on*. IEEE, 2012, pp. 1794–1799.

[16] C. Sankavaram, B. Pattipati, A. Kodali, K. Pattipati, M. Azam, S. Kumar, and M. Pecht, "Model-based and data-driven prognosis of automotive and electronic systems," in *Automation Science and Engineering, 2009. CASE 2009. IEEE International Conference on*. IEEE, 2009, pp. 96–101.

[17] M. Corbetta, C. Sbarufatti, A. Manes, and M. Giglio, "Real-time prognosis of crack growth evolution using sequential monte carlo methods and statistical model parameters," *IEEE Transactions on Reliability*, vol. 64, no. 2, pp. 736–753, 2015.

[18] P. S. Kiran, S. VijayaramKumar, P. Vijayakumar, V. Varakhedi, and V. Upendranath, "Application of kalman filter to prognostic method for estimating the rul of a bridge rectifier," in *Emerging Trends in Communication, Control, Signal Processing & Computing Applications (C2SPCA), 2013 International Conference on*. IEEE, 2013, pp. 1–9.

[19] L. Feng, H. Wang, X. Si, and H. Zou, "A state-space-based prognostic model for hidden and age-dependent nonlinear degradation process," *IEEE Transactions on Automation Science and Engineering*, vol. 10, no. 4, pp. 1072–1086, 2013.

[20] A. Heng, S. Zhang, A. C. Tan, and J. Mathew, "Rotating machinery prognostics: State of the art, challenges and opportunities," *Mechanical systems and signal processing*, vol. 23, no. 3, pp. 724–739, 2009.

[21] C. Song, K. Liu, and X. Zhang, "Integration of data-level fusion model and kernel methods for degradation modeling and prognostic analysis," *IEEE Transactions on Reliability*, 2017.

[22] X.-S. Si, W. Wang, C.-H. Hu, and D.-H. Zhou, "Remaining useful life estimation–a review on the statistical data driven approaches," *European Journal of Operational Research*, vol. 213, no. 1, pp. 1–14, 2011.

[23] W. Wang, "A two-stage prognosis model in condition based maintenance," *European Journal of Operational Research*, vol. 182, no. 3, pp. 1177–1187, 2007.

[24] G. J. Vachtsevanos, F. Lewis, A. Hess, and B. Wu, *Intelligent fault diagnosis and prognosis for engineering systems*. Wiley Online Library, 2006.

[25] D. Banjevic, "Remaining useful life in theory and practice," *Metrika*, vol. 69, no. 2-3, pp. 337–349, 2009.

[26] C. Chen, G. Vachtsevanos, and M. E. Orchard, "Machine remaining useful life prediction: An integrated adaptive neuro-fuzzy and high-order particle filtering approach," *Mechanical Systems and Signal Processing*, vol. 28, pp. 597–607, 2012.

[27] J. Son, Q. Zhou, S. Zhou, X. Mao, and M. Salman, "Evaluation and comparison of mixed effects model based prognosis for hard failure," *Reliability, IEEE Transactions on*, vol. 62, no. 2, pp. 379–394, 2013.

[28] J. Lee, F. Wu, W. Zhao, M. Ghaffari, L. Liao, and D. Siegel, "Prognostics and health management design for rotary machinery systemsreviews, methodology and applications," *Mechanical systems and signal processing*, vol. 42, no. 1-2, pp. 314–334, 2014.

[29] D. An, J. H. Choi, and N. H. Kim, "Options for prognostics methods: A review of data-driven and physics-based prognostics," in *54th AIAA/ASME/ASCE/AHS/ASC Structures, Structural Dynamics, and Materials Conference*, 2013, p. 1940.

[30] M. S. Kan, A. C. Tan, and J. Mathew, "A review on prognostic techniques for non-stationary and non-linear rotating systems," *Mechanical Systems and Signal Processing*, vol. 62, pp. 1–20, 2015.

[31] A. K. Jardine, D. Lin, and D. Banjevic, "A review on machinery diagnostics and prognostics implementing condition-based maintenance," *Mechanical systems and signal processing*, vol. 20, no. 7, pp. 1483–1510, 2006.

[32] W. Bartelmus and R. Zimroz, "Vibration condition monitoring of planetary gearbox under varying external load," *Mechanical Systems and Signal Processing*, vol. 23, no. 1, pp. 246–257, 2009.

[33] G. Kacprzynski, A. Sarlashkar, M. Roemer, A. Hess, and B. Hardman, "Predicting remaining life by fusing the physics of failure modeling with diagnostics," *JOm*, vol. 56, no. 3, pp. 29–35, 2004.

[34] C. H. Oppenheimer and K. A. Loparo, "Physically based diagnosis and prognosis of cracked rotor shafts," in *Component and Systems Diagnostics, Prognostics, and Health Management II*, vol. 4733. International Society for Optics and Photonics, 2002, pp. 122–133.

[35] J. Luo, A. Bixby, K. Pattipati, L. Qiao, M. Kawamoto, and S. Chigusa, "An interacting multiple model approach to model-based prognostics," in *Systems, Man and Cybernetics, 2003. IEEE International Conference on*, vol. 1. IEEE, 2003, pp. 189–194.

[36] O. Ondel, E. Boutleux, E. Blanco, and G. Clerc, "Coupling pattern recognition with state estimation using kalman filter for fault diagnosis," *Industrial Electronics, IEEE Transactions on*, vol. 59, no. 11, pp. 4293–4300, 2012.

[37] R. K. Singleton, E. G. Strangas, and S. Aviyente, "Extended kalman filtering for remaining-useful-life estimation of bearings," *IEEE Transactions on Industrial Electronics*, vol. 62, no. 3, pp. 1781–1790, 2015.

[38] M. Gašperin, D. Juriçić, and P. Boškoski, "Condition prognosis of mechanical drives based on nonlinear dynamical models," in *Control and Fault-Tolerant Systems (SysTol), 2010 Conference on*. IEEE, 2010, pp. 430–435.

[39] D. A. Pola, H. F. Navarrete, M. E. Orchard, R. S. Rabié, M. A. Cerda, B. E. Olivares, J. F. Silva, P. A. Espinoza, and A. Pérez, "Particle-filtering-based discharge time prognosis for lithium-ion batteries with a statistical characterization of use profiles," *IEEE Transactions on Reliability*, vol. 64, no. 2, pp. 710–720, 2015.

[40] M. Yu, D. Wang, and M. Luo, "An integrated approach to prognosis of hybrid systems with unknown mode changes," *IEEE Transactions on Industrial Electronics*, vol. 62, no. 1, pp. 503–515, 2015.

[41] B. E. Olivares, M. A. C. Munoz, M. E. Orchard, and J. F. Silva, "Particle-filtering-based prognosis framework for energy storage devices with a statistical characterization of state-of-health regeneration phenomena," *IEEE Transactions on Instrumentation and Measurement*, vol. 62, no. 2, pp. 364–376, 2013.

[42] L. Tang, J. DeCastro, G. Kacprzynski, K. Goebel, and G. Vachtsevanos, "Filtering and prediction techniques for model-based prognosis and uncertainty management," in *Prognostics and Health Management Conference, 2010. PHM'10.* IEEE, 2010, pp. 1–10.

[43] H. Ferdowsi, D. L. Raja, and S. Jagannathan, "A decentralized fault prognosis scheme for nonlinear interconnected discrete-time systems," in *American Control Conference (ACC), 2012*. IEEE, 2012, pp. 5900–5905.

[44] F. Heidtmann and D. Söffker, "Virtual sensors for diagnosis and prognosis purposes in the context of elastic mechanical structures," *Sensors Journal, IEEE*, vol. 9, no. 11, pp. 1577–1588, 2009.

[45] R. K. Singleton, E. G. Strangas, and S. Aviyente, "The use of bearing currents and vibrations in lifetime estimation of bearings," *IEEE Transactions on Industrial Informatics*, vol. 13, no. 3, pp. 1301–1309, 2017.

[46] J. Son, S. Zhou, C. Sankavaram, X. Du, and Y. Zhang, "Remaining useful life prediction based on noisy condition monitoring signals using constrained kalman filter," *Reliability Engineering & System Safety*, vol. 152, pp. 38–50, 2016.

[47] M. J. Daigle and K. F. Goebel, "Improving computational efficiency of prediction in model-based prognostics using the unscented transform," 2010.

[48] M. E. Orchard and G. J. Vachtsevanos, "A particle filtering-based framework for real-time fault diagnosis and failure prognosis in a turbine engine," in *Control & Automation, 2007. MED'07. Mediterranean Conference on*. IEEE, 2007, pp. 1–6.

[49] M. E. Orchard, P. Hevia-Koch, B. Zhang, and L. Tang, "Risk measures for particle-filtering-based state-of-charge prognosis in lithium-ion batteries," *Industrial Electronics, IEEE Transactions on*, vol. 60, no. 11, pp. 5260–5269, 2013.

[50] D. Pola, H. F. Navarrete, M. E. Orchard, R. S. Rabie, M. Cerda, B. E. Olivares, J. F. Silva, P. Espinoza, A. Pérez *et al.*, "Particle-filtering-based discharge time prognosis for lithium-ion batteries with a statistical characterization of use profiles," *Reliability, IEEE Transactions on*, 2014.

[51] Y. Wen, J. Wu, and Y. Yuan, "Multiple-phase modeling of degradation signal for condition monitoring and remaining useful life prediction," *IEEE Transactions on Reliability*, vol. 66, no. 3, pp. 924–938, 2017.

[52] C. Hu, B. D. Youn, T. Kim, and J. Chung, "Online estimation of lithium-ion battery state-of-charge and capacity with a multiscale filtering technique," *Transition*, vol. 1, no. 1, 2011.

[53] J. Sikorska, M. Hodkiewicz, and L. Ma, "Prognostic modelling options for remaining useful life estimation by industry," *Mechanical Systems and Signal Processing*, vol. 25, no. 5, pp. 1803–1836, 2011.

[54] J. Luo, M. Namburu, K. Pattipati, L. Qiao, M. Kawamoto, and S. Chigusa, "Model-based prognostic techniques [maintenance applications]," in *AUTOTESTCON 2003. IEEE Systems Readiness Technology Conference. Proceedings.* IEEE, 2003, pp. 330–340.

[55] D. C. Swanson, J. M. Spencer, and S. H. Arzoumanian, "Prognostic modelling of crack growth in a tensioned steel band," *Mechanical systems and signal processing*, vol. 14, no. 5, pp. 789–803, 2000.

[56] A. Ray and S. Tangirala, "Stochastic modeling of fatigue crack dynamics for on-line failure prognostics," *IEEE Transactions on Control Systems Technology*, vol. 4, no. 4, pp. 443–451, 1996.

[57] X. Jin, Y. Sun, Z. Que, Y. Wang, and T. W. Chow, "Anomaly detection and fault prognosis for bearings," *IEEE Transactions on Instrumentation and Measurement*, vol. 65, no. 9, pp. 2046–2054, 2016.

[58] X. Zheng and H. Fang, "An integrated unscented kalman filter and relevance vector regression approach for lithium-ion battery remaining useful life and short-term capacity prediction," *Reliability Engineering & System Safety*, vol. 144, pp. 74–82, 2015.

[59] M. Djeziri, B. Ananou, and M. Ouladsine, "Data driven and model based fault prognosis applied to a mechatronic system," in *Power Engineering, Energy and Electrical Drives (POWERENG), 2013 Fourth International Conference on.* IEEE, 2013, pp. 534–539.

[60] A. Malhi, R. Yan, and R. X. Gao, "Prognosis of defect propagation based on recurrent neural networks," *IEEE Transactions on Instrumentation and Measurement*, vol. 60, no. 3, pp. 703–711, 2011.

[61] D. Li, W. Wang, and F. Ismail, "Fuzzy neural network technique for system state forecasting," *IEEE transactions on cybernetics*, vol. 43, no. 5, pp. 1484–1494, 2013.

[62] M. Elforjani and S. Shanbr, "Prognosis of bearing acoustic emission signals using supervised machine learning," *IEEE Transactions on Industrial Electronics*, 2017.

[63] B.-S. Yang, A. C. C. Tan *et al.*, "Multi-step ahead direct prediction for the machine condition prognosis using regression trees and neuro-fuzzy systems," *Expert Systems with Applications*, vol. 36, no. 5, pp. 9378–9387, 2009.

[64] A. Soualhi, M. Makdessi, R. German, F. RIVAS, H. Razik, S. Ali, P. Venet, and G. CLERC, "Heath monitoring of capacitors and supercapacitors using neo fuzzy neural approach," *IEEE Transactions on Industrial Informatics*, 2017.

[65] A. Soualhi, H. Razik, G. Clerc, and D. D. Doan, "Prognosis of bearing failures using hidden markov models and the adaptive neuro-fuzzy inference system," *IEEE Transactions on Industrial Electronics*, vol. 61, no. 6, pp. 2864–2874, 2014.

[66] M. Dong and D. He, "Hidden semi-markov model-based methodology for multi-sensor equipment health diagnosis and prognosis," *European Journal of Operational Research*, vol. 178, no. 3, pp. 858–878, 2007.

[67] C. Chen, D. Brown, C. Sconyers, B. Zhang, G. Vachtsevanos, and M. E. Orchard, "An integrated architecture for fault diagnosis and failure prognosis of complex engineering systems," *Expert Systems with Applications*, vol. 39, no. 10, pp. 9031–9040, 2012.

[68] J. W. Sheppard, M. Kaufman *et al.*, "A bayesian approach to diagnosis and prognosis using built-in test," *Instrumentation and Measurement, IEEE Transactions on*, vol. 54, no. 3, pp. 1003–1018, 2005.

[69] J. Hu, L. Zhang, L. Ma, and W. Liang, "An integrated safety prognosis model for complex system based on dynamic bayesian network and ant colony algorithm," *Expert Systems with Applications*, vol. 38, no. 3, pp. 1431–1446, 2011.

[70] H.-E. Kim, A. C. Tan, J. Mathew, and B.-K. Choi, "Bearing fault prognosis based on health state probability estimation," *Expert Systems with Applications*, vol. 39, no. 5, pp. 5200–5213, 2012.

[71] J. Qiu, H. Wang, D. Lin, B. He, W. Zhao, and W. Xu, "Nonparametric regression-based failure rate model for electric power equipment using lifecycle data," *IEEE Transactions on Smart Grid*, vol. 6, no. 2, pp. 955–964, 2015.

[72] H. Firouzi, A. O. Hero, and B. Rajaratnam, "Two-stage sampling, prediction and adaptive regression via correlation screening," *IEEE Transactions on Information Theory*, vol. 63, no. 1, pp. 698–714, 2017.

[73] H. Liao and J. Sun, "Nonparametric and semi-parametric sensor recovery in multichannel condition monitoring systems," *IEEE Transactions on Automation Science and Engineering*, vol. 8, no. 4, pp. 744–753, 2011.

[74] H. Kim, M. G. Na, and G. Heo, "Application of monitoring, diagnosis, and prognosis in thermal performance analysis for nuclear power plants," *Nuclear Engineering and Technology*, vol. 46, no. 6, pp. 737–752, 2014.

[75] G. Niu and B.-S. Yang, "Dempster–shafer regression for multi-step-ahead time-series prediction towards data-driven machinery prognosis," *Mechanical systems and signal processing*, vol. 23, no. 3, pp. 740–751, 2009.

[76] H. T. Pham and B.-S. Yang, "Estimation and forecasting of machine health condition using arma/garch model," *Mechanical Systems and Signal Processing*, vol. 24, no. 2, pp. 546–558, 2010.

[77] H. T. Pham, B.-S. Yang, T. T. Nguyen *et al.*, "Machine performance degradation assessment and remaining useful life prediction using proportional hazard

model and support vector machine," *Mechanical Systems and Signal Processing*, vol. 32, pp. 320–330, 2012.

[78] D. Liu, Y. Luo, Y. Peng, X. Peng, and M. Pecht, "Lithium-ion battery remaining useful life estimation based on nonlinear ar model combined with degradation feature," in *Proc. of Annual Conf. of Prognostics and System Health Management Society*, 2012, pp. 1–7.

[79] J. Yan, M. Koc, and J. Lee, "A prognostic algorithm for machine performance assessment and its application," *Production Planning & Control*, vol. 15, no. 8, pp. 796–801, 2004.

[80] S. Liu, Y. Wang, and F. Tian, "Prognosis of underground cable via online data-driven method with field data," *Industrial Electronics, IEEE Transactions on*, vol. 62, no. 12, pp. 7786–7794, 2015.

[81] N. Gebraeel, M. Lawley, R. Liu, and V. Parmeshwaran, "Residual life predictions from vibration-based degradation signals: a neural network approach," *IEEE Transactions on industrial electronics*, vol. 51, no. 3, pp. 694–700, 2004.

[82] A. P. Vassilopoulos, E. F. Georgopoulos, and V. Dionysopoulos, "Artificial neural networks in spectrum fatigue life prediction of composite materials," *International Journal of Fatigue*, vol. 29, no. 1, pp. 20–29, 2007.

[83] A. Heng, A. C. Tan, J. Mathew, N. Montgomery, D. Banjevic, and A. K. Jardine, "Intelligent condition-based prediction of machinery reliability," *Mechanical Systems and Signal Processing*, vol. 23, no. 5, pp. 1600–1614, 2009.

[84] C. Chen, B. Zhang, and G. Vachtsevanos, "Prediction of machine health condition using neuro-fuzzy and bayesian algorithms," *IEEE Transactions on instrumentation and Measurement*, vol. 61, no. 2, pp. 297–306, 2012.

[85] Z. He, S. Wang, K. Wang, and K. Li, "Prognostic analysis based on hybrid prediction method for axial piston pump," in *Industrial Informatics (INDIN), 2012 10th IEEE International Conference on*. IEEE, 2012, pp. 688–692.

[86] G. Vachtsevanos and P. Wang, "Fault prognosis using dynamic wavelet neural networks," in *AUTOTESTCON Proceedings, 2001. IEEE Systems Readiness Technology Conference*. IEEE, 2001, pp. 857–870.

[87] A. Lorton, M. Fouladirad, and A. Grall, "A methodology for probabilistic model-based prognosis," *European Journal of Operational Research*, vol. 225, no. 3, pp. 443–454, 2013.

[88] O. Geramifard, J.-X. Xu, J.-H. Zhou, and X. Li, "A physically segmented hidden markov model approach for continuous tool condition monitoring: Diagnostics and prognostics," *IEEE Transactions on Industrial Informatics*, vol. 8, no. 4, pp. 964–973, 2012.

[89] F. Cheng, L. Qu, and W. Qiao, "Fault prognosis and remaining useful life prediction of wind turbine gearboxes using current signal analysis," *IEEE Transactions on Sustainable Energy*, 2017.

[90] A. N. Srivastava and S. Das, "Detection and prognostics on low-dimensional systems," *IEEE Transactions on Systems, Man, and Cybernetics, Part C (Applications and Reviews)*, vol. 39, no. 1, pp. 44–54, 2009.

[91] Y. Peng and M. Dong, "A hybrid approach of hmm and grey model for age-dependent health prediction of engineering assets," *Expert Systems with Applications*, vol. 38, no. 10, pp. 12 946–12 953, 2011.

[92] E. Zio, "Prognostics and health management of industrial equipment," *Diagnostics and prognostics of engineering systems: methods and techniques*, pp. 333–356, 2012.

[93] Z. Wang, C. Hu, W. Wang, X. Si, and Z. Zhou, "An off-online fuzzy modelling method for fault prognosis with an application," in *Prognostics and System Health Management (PHM), 2012 IEEE Conference on*. IEEE, 2012, pp. 1–7.

[94] M. Yu, D. Wang, M. Luo, and L. Huang, "Prognosis of hybrid systems with multiple incipient faults: augmented global analytical redundancy relations approach," *Systems, Man and Cybernetics, Part A: Systems and Humans, IEEE Transactions on*, vol. 41, no. 3, pp. 540–551, 2011.

[95] R. Kumar and S. Takai, "Decentralized prognosis of failures in discrete event systems," *Automatic Control, IEEE Transactions on*, vol. 55, no. 1, pp. 48–59, 2010.

[96] S. Takai and R. Kumar, "Inference-based decentralized prognosis in discrete event systems," *IEEE Transactions on Automatic Control*, vol. 56, no. 1, pp. 165–171, 2011.

[97] S. Takai, "Robust failure prognosis of partially observed discrete event systems," in *American Control Conference (ACC), 2012*. IEEE, 2012, pp. 6077–6082.

[98] R. K. Singleton, E. G. Strangas, and S. Aviyente, "Discovering the hidden health states in bearing vibration signals for fault prognosis," in *Industrial Electronics Society, IECON 2014-40th Annual Conference of the IEEE*. IEEE, 2014, pp. 3438–3444.

[99] W. G. Zanardelli, E. G. Strangas, H. K. Khalil, and J. M. Miller, "Wavelet-based methods for the prognosis of mechanical and electrical failures in electric motors," *Mechanical Systems and Signal Processing*, vol. 19, no. 2, pp. 411–426, 2005.

[100] D. Tobon-Mejia, K. Medjaher, N. Zerhouni, and G. Tripot, "Estimation of the remaining useful life by using wavelet packet decomposition and hmms," in *Aerospace Conference, 2011 IEEE*. IEEE, 2011, pp. 1–10.

[101] J. A. Antonino-Daviu, S. B. Lee, and E. G. Strangas, "Guest editorial special section on advanced signal and image processing techniques for electric machines and drives fault diagnosis and prognosis," *IEEE Transactions on Industrial Informatics*, vol. 13, no. 3, pp. 1257–1260, 2017.

[102] M. Ibrahim, N. Y. Steiner, S. Jemei, and D. Hissel, "Wavelet-based approach for online fuel cell remaining useful lifetime prediction," *IEEE Transactions on Industrial Electronics*, vol. 63, no. 8, pp. 5057–5068, 2016.

[103] T. Biagetti and E. Sciubba, "Automatic diagnostics and prognostics of energy conversion processes via knowledge-based systems," *Energy*, vol. 29, no. 12-15, pp. 2553–2572, 2004.

[104] B. T. Thumati, M. A. Feinstein, and S. Jagannathan, "A model-based fault detection and prognostics scheme for takagi–sugeno fuzzy systems," *IEEE Transactions on Fuzzy Systems*, vol. 22, no. 4, pp. 736–748, 2014.

[105] A. Majidian and M. Saidi, "Comparison of fuzzy logic and neural network in life prediction of boiler tubes," *International Journal of Fatigue*, vol. 29, no. 3, pp. 489–498, 2007.

[106] A. Garga, K. McClintic, R. Campbell, C.-C. Yang, M. Lebold, T. Hay, and C. Byington, "Hybrid reasoning for prognostic learning in cbm systems," in *Aerospace Conference, 2001, IEEE Proceedings.*, vol. 6. IEEE, 2001, pp. 2957–2969.

[107] Z. Liu, Q. Li, and C. Mu, "A hybrid lssvr-hmm based prognostics approach," in *Intelligent Human-Machine Systems and Cybernetics (IHMSC), 2012 4th International Conference on*, vol. 2. IEEE, 2012, pp. 275–278.

[108] J. Xu and L. Xu, "Health management based on fusion prognostics for avionics systems," *Journal of Systems Engineering and Electronics*, vol. 22, no. 3, pp. 428–436, 2011.

[109] K. Goebel, N. Eklund, and P. Bonanni, "Fusing competing prediction algorithms for prognostics," in *Aerospace Conference, 2006 IEEE*. IEEE, 2006, pp. 10–pp.

[110] B. Saha, S. Poll, K. Goebel, and J. Christophersen, "An integrated approach to battery health monitoring using bayesian regression and state estimation," in *autotestcon, 2007 IEEE*. Ieee, 2007, pp. 646–653.

[111] G. Zhang, S. Lee, N. Propes, Y. Zhao, G. Vachtsevanos, A. Thakker, and T. Galie, "A novel architecture for an integrated fault diagnostic/prognostic system," in *AAAI symposium*, 2002, pp. 25–27.

[112] D. C. Swanson, "A general prognostic tracking algorithm for predictive maintenance," in *Aerospace Conference, 2001, IEEE Proceedings.*, vol. 6. IEEE, 2001, pp. 2971–2977.

[113] L. Peel, "Data driven prognostics using a kalman filter ensemble of neural network models," in *Prognostics and Health Management, 2008. PHM 2008. International Conference on.* IEEE, 2008, pp. 1–6.

[114] N. Daroogheh, A. Baniamerian, N. Meskin, and K. Khorasani, "Prognosis and health monitoring of nonlinear systems using a hybrid scheme through integration of pfs and neural networks," *IEEE Transactions on Systems, Man, and Cybernetics: Systems*, 2017.

[115] J. Liu, W. Wang, F. Ma, Y. Yang, and C. Yang, "A data-model-fusion prognostic framework for dynamic system state forecasting," *Engineering Applications of Artificial Intelligence*, vol. 25, no. 4, pp. 814–823, 2012.

[116] C. Chen, B. Zhang, G. Vachtsevanos, and M. Orchard, "Machine condition prediction based on adaptive neuro–fuzzy and high-order particle filtering," *IEEE Transactions on Industrial Electronics*, vol. 58, no. 9, pp. 4353–4364, 2011.

[117] C. Hu, B. D. Youn, P. Wang, and J. T. Yoon, "Ensemble of data-driven prognostic algorithms for robust prediction of remaining useful life," *Reliability Engineering & System Safety*, vol. 103, pp. 120–135, 2012.

[118] M. Abbas, A. A. Ferri, M. E. Orchard, and G. J. Vachtsevanos, "An intelligent diagnostic/prognostic framework for automotive electrical systems," in *Intelligent Vehicles Symposium, 2007 IEEE.* IEEE, 2007, pp. 352–357.

[119] C. S. Byington, M. Watson, and D. Edwards, "Data-driven neural network methodology to remaining life predictions for aircraft actuator components," in *Aerospace Conference, 2004. Proceedings. 2004 IEEE*, vol. 6. IEEE, 2004, pp. 3581–3589.

[120] N. Kunst, J. Judkins, C. Lynn, and D. Goodman, "Damage propagation analysis methodology for electromechanical actuator prognostics," in *Aerospace conference, 2009 IEEE.* IEEE, 2009, pp. 1–7.

[121] B. Lamoureux, J.-R. Massé, and N. Mechbal, "An approach to the health monitoring of a pumping unit in an aircraft engine fuel system," in *Chez proceedings of first European conference of the prognostics and health management society, Dresden*, 2012.

[122] Z. Chen, "Bayesian filtering: From kalman filters to particle filters, and beyond," *Statistics*, vol. 182, no. 1, pp. 1–69, 2003.

[123] E. Balaban, A. Saxena, S. Narasimhan, I. Roychoudhury, M. Koopmans, C. Ott, and K. Goebel, "Prognostic health-management system development for electromechanical actuators," *Journal of Aerospace Information Systems*, 2015.

[124] C. S. Byington, M. Watson, D. Edwards, and P. Stoelting, "A model-based approach to prognostics and health management for flight control actuators," in *Aerospace Conference, 2004. Proceedings. 2004 IEEE*, vol. 6. IEEE, 2004, pp. 3551–3562.

[125] D. N. Nguyen, L. Dieulle, and A. Grall, "Remaining useful lifetime prognosis of controlled systems: a case of stochastically deteriorating actuator," *Mathematical Problems in Engineering*, vol. 2015, 2015.

[126] "Spoiler control system description," Tech. Rep., 01 2014, rAC-ST200-008.

[127] "Technical report, mathemtical model of mfs." Thales Canada Inc., Canada, 2014.

[128] A. Zanj, H. Karimi, A. Gholi, and M. Shafiee, "Dynamic modeling of indirect hydro-control valve–bondgraph approach," *Simulation Modelling Practice and Theory*, vol. 28, pp. 65–80, 2012.

[129] P. Maggiore, M. D. Dalla Vedova, L. Pace, and A. Desando, "Definition of parametric methods for fault analysis applied to an electromechanical servomechanism affected by multiple failures," in *Proceedings of the Second European Conference of the Prognostics and Health Management Society*, 2014, pp. 561–571.

[130] M. Kordestani, A. A. Safavi, and N. Sharafi, "Two practical performance indexes for monitoring the rhine–meuse delta water network via wavelet-based probability density function," *Neurocomputing*, vol. 177, pp. 469–477, 2016.

[131] M. M. Rahman and M. N. Uddin, "Online unbalanced rotor fault detection of an im drive based on both time and frequency domain analyses," *IEEE Transactions on Industry Applications*, 2017.

[132] J. Seshadrinath, B. Singh, and B. K. Panigrahi, "Incipient turn fault detection and condition monitoring of induction machine using analytical wavelet transform," *IEEE Transactions on Industry Applications*, vol. 50, no. 3, pp. 2235–2242, 2014.

[133] J. CusidÓCusido, L. Romeral, J. A. Ortega, J. A. Rosero, and A. G. Espinosa, "Fault detection in induction machines using power spectral density in wavelet decomposition," *IEEE Transactions on Industrial Electronics*, vol. 55, no. 2, pp. 633–643, 2008.

[134] S. G. Mallat, "A theory for multiresolution signal decomposition: the wavelet representation," *IEEE transactions on pattern analysis and machine intelligence*, vol. 11, no. 7, pp. 674–693, 1989.

[135] Q. Shen, B. Jiang, P. Shi, and C.-C. Lim, "Novel neural networks-based fault tolerant control scheme with fault alarm," *IEEE transactions on cybernetics*, vol. 44, no. 11, pp. 2190–2201, 2014.

[136] A. P. Moreno, O. L. Santiago, J. M. B. de Lazaro, and E. G. Moreno, "Comparative evaluation of classification methods used in fault diagnosis of industrial processes," *IEEE Latin America Transactions*, vol. 11, no. 2, pp. 682–689, 2013.

[137] H. Chen, G. Han, W. Yan, S. Lu, and Z. Chen, "Modeling of a switched reluctance motor under stator winding fault condition," *IEEE Transactions on Applied Superconductivity*, vol. 26, no. 4, pp. 1–6, 2016.

[138] T. de Bruin, K. Verbert, and R. Babuška, "Railway track circuit fault diagnosis using recurrent neural networks," *IEEE transactions on neural networks and learning systems*, vol. 28, no. 3, pp. 523–533, 2017.

[139] K. Salahshoor, M. S. Khoshro, and M. Kordestani, "Fault detection and diagnosis of an industrial steam turbine using a distributed configuration of adaptive neuro-fuzzy inference systems," *Simulation Modelling Practice and Theory*, vol. 19, no. 5, pp. 1280–1293, 2011.

[140] F. Ye, Z. Zhang, K. Chakrabarty, and X. Gu, "Board-level functional fault diagnosis using artificial neural networks, support-vector machines, and weighted-majority voting," *IEEE Transactions on Computer-Aided Design of Integrated Circuits and Systems*, vol. 32, no. 5, pp. 723–736, 2013.

[141] K. Salahshoor, M. Kordestani, and M. S. Khoshro, "Fault detection and diagnosis of an industrial steam turbine using fusion of svm (support vector machine) and anfis (adaptive neuro-fuzzy inference system) classifiers," *Energy*, vol. 35, no. 12, pp. 5472–5482, 2010.

[142] O. Kreibich, J. Neuzil, and R. Smid, "Quality-based multiple-sensor fusion in an industrial wireless sensor network for mcm," *IEEE Transactions on Industrial Electronics*, vol. 61, no. 9, pp. 4903–4911, 2014.

[143] X. Liu, L. Ma, and J. Mathew, "Machinery fault diagnosis based on fuzzy measure and fuzzy integral data fusion techniques," *Mechanical Systems and Signal Processing*, vol. 23, no. 3, pp. 690–700, 2009.

[144] X. Liu, "Some properties of the weighted owa operator," *IEEE Transactions on Systems, Man, and Cybernetics, Part B (Cybernetics)*, vol. 36, no. 1, pp. 118–127, 2006.

[145] V. Torra, "Owa operators in data modeling and reidentification," *IEEE Transactions on Fuzzy Systems*, vol. 12, no. 5, pp. 652–660, 2004.

[146] R. R. Yager, "Owa aggregation over a continuous interval argument with applications to decision making," *IEEE Transactions on Systems, Man, and Cybernetics, Part B (Cybernetics)*, vol. 34, no. 5, pp. 1952–1963, 2004.

[147] M. Bressel, M. Hilairet, D. Hissel, and B. O. Bouamama, "Extended kalman filter for prognostic of proton exchange membrane fuel cell," *Applied Energy*, vol. 164, pp. 220–227, 2016.

[148] D. E. Acuña and M. E. Orchard, "Particle-filtering-based failure prognosis via sigma-points: Application to lithium-ion battery state-of-charge monitoring," *Mechanical Systems and Signal Processing*, vol. 85, pp. 827–848, 2017.

[149] B. M. Wilamowski and H. Yu, "Improved computation for levenberg–marquardt training," *IEEE transactions on neural networks*, vol. 21, no. 6, pp. 930–937, 2010.

[150] J. Yu, "Machine health prognostics using the bayesian-inference-based probabilistic indication and high-order particle filtering framework," *Journal of Sound and Vibration*, vol. 358, pp. 97–110, 2015.

[151] M. Morshedizadeh, M. Kordestani, R. Carriveau, D. S. Ting, and M. Saif, "Application of imputation techniques and adaptive neuro-fuzzy inference system to predict wind turbine power production," *Energy*, 2017.

[152] ——, "Improved power curve monitoring of wind turbines," *Wind engineering*, vol. 41, no. 4, pp. 260–271, 2017.

[153] C.-W. Hsu and C.-J. Lin, "A comparison of methods for multiclass support vector machines," *IEEE transactions on Neural Networks*, vol. 13, no. 2, pp. 415–425, 2002.

[154] H. Takagi and I. Hayashi, "Nn-driven fuzzy reasoning," *International Journal of Approximate Reasoning*, vol. 5, no. 3, pp. 191–212, 1991.

[155] J. Yu, "Machine health prognostics using the bayesian-inference-based probabilistic indication and high-order particle filtering framework," *Journal of Sound and Vibration*, vol. 358, pp. 97–110, 2015.

[156] R. E. Kalman, "A new approach to linear filtering and prediction problems," *Journal of basic Engineering*, vol. 82, no. 1, pp. 35–45, 1960.

[157] R. E. Kalman and R. S. Bucy, "New results in linear filtering and prediction theory," *Journal of basic engineering*, vol. 83, no. 1, pp. 95–108, 1961.

[158] L. Ascorti, "An application of the extended kalman filter to the attitude control of a quadrotor," 2013.

[159] G. Whitmore and F. Schenkelberg, "Modelling accelerated degradation data using wiener diffusion with a time scale transformation," *Lifetime data analysis*, vol. 3, no. 1, pp. 27–45, 1997.

[160] N. Gebraeel, "Sensory-updated residual life distributions for components with exponential degradation patterns," *IEEE Transactions on Automation Science and Engineering*, vol. 3, no. 4, pp. 382–393, 2006.

[161] X. Wang, "Wiener processes with random effects for degradation data," *Journal of Multivariate Analysis*, vol. 101, no. 2, pp. 340–351, 2010.

Appendix A-Degraded Dynamic Model of Multifunctional Spoiler Systems

The degraded model is considered by injecting failures in the dynamic model of the MFS as follows:

$$X_v = \frac{K_v}{s\tau_{ehsv} + 1}(I_{cmd} + I_0 + \Delta I_0)$$

$$\frac{V_{01} + A_{bore}X_p}{\beta}\frac{dP_1}{dt} = Q_{C1} - A_{bore}\frac{dX_P}{dt} -$$

$$(C_L + \Delta C_L)(P_1 - P_2) + Q_{ANTI} + \Delta Q$$

$$\frac{V_{02} - A_{ann}X_p}{\beta}\frac{dP_2}{dt} = -Q_{C2} + A_{ann}\frac{dX_P}{dt} +$$

$$(C_L + \Delta C_L)(P_1 - P_2) - \Delta Q$$

Vita Auctoris

Mojtaba Kordestani received his Bachelors and Masters degrees from Malek Ashtar University and Tehran Azad University, Iran, in 2002 and 2008, respectively. During his graduate study, he taught various control engineering courses. He was an invited professor at Azad Tehran University in 2014. His research interests are nonlinear control, modern control systems, estimation and observer theory, fault diagnostics and fault tolerant control, intelligent control, system identification, predictive control. He is a recipient of the full grant Scholarship from Thales Company of Canada under a joint Multi university project entitled Health monitoring, failure diagnosis, and prognosis, in 2015. Currently, he is a research assistant at University of Windsor, Canada. He has authored/co-authored over 20 refereed journal and conference papers on different applications such as process control, power plants like steam turbines and wind turbines, industrial infrastructures such as large distributed water systems, aircraft industries, etc. He won Ontario Graduate Scholarship (OGS) in 2017. He has also been IEEE chair of the young professional group at University of Windsor since 2016. His new research interests include prognosis, control performance assessment, and cyber-secure control methods.

For more information, please see ($www.scholar.google.com/MojtabaKordestani$) or ($www.researchgate.net/profile/MojtabaKordestani$).

Journal Publications:

1. M. Kordestani, M. F. Samadi, M. Saif, K. Khorasani, "A New Fault Prognosis of MFS System Using Integrated Extended Kalman Filter and Bayesian Method, " IEEE Transactions on Industrial Informatics. 2018.

2. M. Kordestani, M. F. Samadi, M. Saif, K. Khorasani, "A New Fault Diagnosis of MFS System Using Integrated Articial Neural Network and Discrete Wavelet Transform methods," IEEE Sensors journal, 2018.

3. M Morshedizadeh, M Kordestani, R Carriveau, DSK Ting, M Saif, "Power Production Prediction of Wind Turbines Using Fusion of MLP and ANFIS Networks," IET Renewable Power Generation, 2018.

4. S. Soltani, M. Kordestani, P. Karimaghaee, M. Saif, "Improved Estimation for Well-Logging Problems Based on Fusion of Four Types of Kalman Filters," IEEE Transactions on Geoscience and Remote Sensing, 1-8, 2017.

5. M Morshedizadeh, M Kordestani, R Carriveau, DSK Ting, M Saif, "Application of imputation techniques and Adaptive Neuro-Fuzzy Inference System to predict wind turbine power production," Energy, 2017.

6. M Morshedizadeh, M Kordestani, R Carriveau, DSK Ting, M Saif, "Improved power curve monitoring of wind turbines," Wind engineering, 2017.

7. M Kordestani, A Safavi, N Sharafi, M, Saif, "Novel multi-agent model predictive control performance indices for monitoring of a large scale distributed water system," IEEE Systems journal, 2016.

8. M. Kordestani, A Safavi, N Sharafi, "Two practical performance indexes for monitoring the Rhine-Meuse Delta water network via wavelet-based probabil-

ity density function," Neurocomputing, Volume 177, 12 February 2016, Pages 469477.

9. S. Soltani, M. Kordestani, P. Karimaghaee, "New estimation methodologies for well logging problems via a combination of fuzzy Kalman filter and different smoothers," Journal of Petroleum Science and Engineering, 2016.

10. K. Salahshoor, M. Kordestani, "Design of an active fault tolerant control system for an industrial steam turbine," Applied Mathematical Modelling, Volume 38, Issues 56, 1 March 2014, Pages 17531774

11. K. Salahshoor, M. S. Khoshro ,M. Kordestani, " Fault detection and diagnosis of an industrial steam turbine using a distributed configuration of adaptive neuro-fuzzy inference systems," Simulation Modelling Practice and Theory 19 (2011) 12801293.

12. K. Salahshoor, M. Kordestani, M. S. Khoshro, "Fault detection and diagnosis of an industrial steam turbine using fusion of SVM (support vector machine) and ANFIS (adaptive euro-fuzzy inference system) classifiers," Energy 35 (2010) 5472-5482.

Conference Publications:

1. M. Kordestani, M, Saif, "A Data Fusion for Fault Diagnosis in Smart Grid Power Systems," Electrical and Computer Engineering (CCECE), 2017 IEEE 30th Canadian, 2017.

2. M. Kordestani, A. A. Safavi, M, Saif, "A novel method for Harmonic fault diagnosis in power quality system using harmonic wavelet," IFAC conference, Toulouse, France, 2017.

3. M. Kordestani, M. Dehghani, M, F, Samadi, M, Saif, "A non-iterative LMI based PID power system stabilizer," WAC conference, USA, 2016.

4. M. Kordestani, A. Alkhateeb, I. Rezaeian, L. Rueda, and M. Saif, "A new clustering method using wavelet based probability density functions for identifying patterns in time-series data," in 2016 IEEE EMBS International Student Conference (ISC), pp. 1-4, IEEE, 2016.

5. M. Kordestani, A. A. Safavi, "An advanced multiple model based control of an industrial steam turbine using fast version of GPC," 24th Iranian Conference on Electrical Engineering (ICEE),2016.

6. M Kordestani, AA Safavi, A Sadrzadeh,"A new method to diagnose the type and location of disturbances in fars power distribution system," 24th Iranian Conference on Electrical Engineering (ICEE), Pages 1871-1876, 2016.

7. M. Kordestani, M. S. Khoshro, A. Mirzaee, "Predictive control of large steam turbines," IEEE Asian control conference, Turkey, 23-26 June 2013.

8. K. Salahshoor, M. Kordestani, M. S. Khoshro, "Design of online soft sensors based on combined adaptive PCA and DMLP neural networks," Chinese Control and Decision Conference (CCDC), 17-19 June 2009, page(s): 3481-3486, IEEE.

9. K. Salahshoor, M. Kordestani, M. S. Khoshro, "Design of online soft sensors based on combined adaptive PCA and RBF neural networks design," Computational intelligence in control and automation, USA, March 30 2009-April 2 2009, page(s): 89-95, IEEE